SCALE-UP AND OPERATIONS OF A VERTICAL STIRRED MILL

by

Baker Francis

B.Sc., University of Dar es Salaam, 2006

A THESIS SUBMITTED IN PARTIAL FULFILLMENT OF

THE REQUIREMENTS FOR THE DEGREE OF

MASTER OF APPLIED SCIENCE

in

THE FACULTY OF GRADUATE AND POSTDOCTORAL STUDIES

(Mining Engineering)

THE UNIVERSITY OF BRITISH COLUMBIA

(Vancouver)

February 2014

Abstract

Stirred media mills are relatively new to mining industry, and several new technologies have been developed such as the VXPmill (vertical stirred mill). There is little technical understanding of optimizing and scaling-up of the VXPmill. This thesis addresses both of these issues and therefore supports commercial applications of this vertical stirred mill.

Stirred media mills are influenced by a great number of operating variables. A study was conducted to understand the influence of mill speed, feed particle size and, slurry density and rheology on the VXPmill performance. For scale-up, a study was conducted to compare the batch recycle and the pendulum testing procedures. A scale-up demonstration study was also done utilizing the pilot-scale (VXP10) mill and the full-scale (VXP2500) mill to validate the procedure.

The following are the main findings from this work:

There is an optimum tip speed such that if too high (12 m/s) results in energy losses due to mechanical friction and heat. If too low (3 m/s) there are insufficient stresses to promote breakage. The optimum tip speed was found to be about 7 m/s.

Feed particle size is an important variable when predicting the energy-size reduction relationship. A coarser feed requires more energy than a finer feed to achieve the same grind size.

The batch recycle testing procedure overestimates the energy consumption as compared to the pendulum test over a broad range of grind sizes. Therefore, it should not be used for scale up applications. However, the pendulum test can be used to predict energy requirements for scale-up.

By utilizing the VXP10 mill, the stress intensity of grinding beads and specific energy input control the grind size for the comminution of feldspars-quartz ore. At optimum stress intensity, the energy utilization is maximum.

For the effective and accurate scaling-up of stirred media mills, it is extremely important that both the pilot-scale and the full-scale mills are operated at relatively similar operating conditions, and treating similar material of the same feed particle size. However, both mills should be operated at their optimal flow rates.

Preface

The work presented in this thesis was conducted by the author. However, some assistance was provided by others as explained below:

Sample preparation and the tests on the performance of the VXP10 mill conducted at the University of British Columbia (UBC) were done by the author and assisted by fellow students.

All of the tests conducted for the determination of specific surface area for the VXP10 mill feed and ground products using the Quantachrome Autosorb-1 were conducted by the author.

The X-Ray Diffraction for the VXPmill feed sample was conducted at the University of British Columbia, in the Department of Earth, Ocean and Atmospheric Sciences, by Dr. Elisabetta Pani.

All pilot tests for the scale-up demonstration study performed at the Turk mine in Zimbabwe were conducted by the author, and the data collection for a full-scale mill was done by Bill Hines (FLSmidth site process engineer) and assisted by the Turk mine process operators. The data analysis for all of the tests conducted in this study was done by the author.

Table of contents

List of tables

List of figures

List of symbols

A	shear stress factor (Pa/NM), (Eqn. 3.2)
a_c	grinding media centrifugal acceleration (m/s^2)
a_m	molecular cross-sectional area of adsorbate (Å^2/molecule)
A_p	cross-sectional area of the stressed particle (m^2)
C	adsorption isotherm constant (Eqn. 3.9)
D	mill diameter (m)
D_s	screw diameter (m)
D_m	grinding media diameter (m)
D_d	grinding disc diameter (m)
E	specific energy (kWh/t)
E_{vb}	volume based specific energy of a single grinding bead (kJ/m^3)
F_c	centrifugal force (N)
g	acceleration due to gravity (m/s^2)
h	media height (m)
n	flow behaviour index (Eqn. 2.11)
K	ratio between vertical and horizontal media pressure (Eqn. 2.5)
k	dimensionless scaling factor (Eqn. 2.10)
k	ratio of rheometer's bob to cup diameter (Eqn. 3.3)
k	fluid consistency index (Eqn. 2.11)
L	Avogadro's constant (1/molecule) (Eqn. 3.10)
M	shear rate constant for the rheometer (s^{-1}/rad/s) (Eqn. 3.5)
n_a	amount of adsorbate adsorbed
n_m	monolayer capacity
P/P_0	relative pressure
R^2	correlation coefficient
R_1	radius of inner cylinder (m), (Eqn. 2.12)
R_2	radius of outer cylinder (m), (Eqn. 2.12)
Rc	radius of the cup fixture (m), (Eqn. 3.4)

Re_{crit}	critical Reynolds number
S_f	particle specific surface area for mill feed (m^2/g)
S_p	particle specific surface area for mill product (m^2/g)
SI_{gm}	gravitational stress intensity (NM)
SI_c	centrifugal stress intensity (NM)
SI_{total}	total stress intensity (NM)
T	Torque (NM)
V_m	grinding media volume (m^3)
V_p	volume of a particle (m^3)
V_t	mill tip speed (m/s)
V_b	peripheral velocity of the bob (m/s)

Greek letters

γ	shear rate (s^{-1})
ΔS	incremental surface area produced (m^2/g)
η	kinematic viscosity (m^2/s) (Eqn. 2.12)
η_B	Bingham viscosity (Pas)
η_C	Casson viscosity (Pas)
ρ_m	grinding media density (kg/m^3)
ρ	slurry density (kg/m^3)
τ	shear stress (Pa)
τ_{HB}	Herschel Bulkley yield stress (Pa)
τ_c	Casson yield stress (Pa)
τ_{yB}	Bingham yield stress (Pa)
τ_{yC}	Casson yield stress (Pa)
μ_p	slurry viscosity (Pas)
μ	coefficient of friction (Eqn. 2.5)
v_Θ	peripheral tangential velocity of rheometer's cup (m/s), (Eqn. 3.4)
ω	rotational velocity of rheometer's cup (rad/s), (Eqn. 3.4)

List of abbreviations

ASTM	American Society for Testing and Materials
BET	Brunauer, Emmett and Teller
Btu	British thermal unit (1 kW = 3412.1 Btu/hr)
CANNON4	Viscosity standard oil (4.8 mPas at 25°C)
CANNON44	Viscosity standard oil (74.6 mPas at 25°C)
CANNON75	Viscosity standard oil (155.8 mPas at 25°C)
CMP	Coal and Mineral Processing (the laboratory at UBC)
CZC	Zirconium oxide (type of grinding media, intrinsic SG = 6.1)
CZS	Zirconium silicate (type of grinding media, intrinsic SG = 4.2)
EF_5	Fineness grind factor (Bond's law)
EOAS	Earth Ocean and Atmospheric Sciences (department at UBC)
EU	Energy Utilization (m^2/kW) (Eqn. 2.7)
HPGR	High Pressure Grinding Roll
KMS	Knelson Milling Solutions
LCD	Liquid Crystal Display
PLC	Programmable Logic Controller
PSD	Particle Size Distribution
SG	Specific Gravity
SMD	Stirred Media Detritor
SSA	Specific Surface Area of solid sample, (m^2/g)
VXPmill	Vertical Xtra Performance mill
VXP10 mill	Vertical Xtra Performance mill with 10 liters capacity
VXP2500 mill	Vertical Xtra Performance mill with 2500 liters capacity
XRD	X- Ray Diffraction
UBC	University of British Columbia
USB	Universal Serial Bus

Acknowledgements

Much appreciation is extended to the University of Dar-es-Salaam for offering me the opportunity to undertake studies at the University of British Columbia (UBC) under the World Bank Project. Special thanks are extended to the Natural Sciences and Engineering Research Council of Canada for facilitating this research.

I would like to express my sincere gratitude to my supervisor, Dr. Bern Klein for his suggestions, guidance and willingness to assist me during the planning, execution and completion of this research work. He always spared the time to discuss with me issues related to this research. I would also like to thank Dr. Robert Hall and Dr. Daan Maijer for their constructive comments.

I am very grateful to Dr. David Rahal and Scott Reddick for the training they offered me on how to safely operate the VXP10 mill. I owe sincere and heartfelt thanks to Bill Hines (FLSmidth process engineer) who offered me a 55-kilometre span ride every day from the hotel to the Turk mine site during my stay in Bulawayo, Zimbabwe. The data collection for scale-up would not have been possible without his diligent support.

I am indebted to my colleagues, Hans Yu, Cam Bruin, Esau Erinaitwe and Jophat Engwayu. These people played a very significant role in conducting the tests successfully at UBC. It is my pleasure to thank Mrs. Sally Finora for instructing me on how to determine the BET surface area.

Finally, I wish to extend my heartfelt thanks to my beloved wife Oddelia, and my lovely children Claus and Caren, for their steadfast love, tireless prayers and encouragement. Glory be to **God**, “the fountain of life” (Psalm 36:9).

1 Introduction

1.1 Background

The world is currently experiencing unprecedented demand for minerals due to rapid economic growth in recent years. This has caused the worldwide depletion of mineral-rich reserves at an alarming rate. Ultimately, the fine-grained and refractory ore reserves which were previously considered non-economical to be mined and processed are currently becoming more economically viable due to the existing modern processing technologies (Jankovic & Sinclair, 2006). One of the acknowledged approaches used to liberate valuable minerals from the complex-refractory ores to achieve decent economical mineral recovery is “fine grinding.”

Over US$ 600 million is spent in the size reduction of copper ores throughout the world (Yerkovic et al., 1993). A study conducted by the U.S. Department of Energy identified grinding as one of the top energy-consuming processes in the U.S. mining industry. In the year 2007 the annual U.S. grinding energy consumption was 494 Trillion Btu, equivalent to 40% of the total energy consumption in the U.S. mining industry (BCS, 2007). Yerkovic et al. (1993) suggested that between 40% and 60% of the total energy consumption in size reduction process is spent in fine grinding operations.

One of the best strategies for energy savings as grinding process is concerned is the use of the proper grinding technology for a particular application. With regard to fine and ultrafine grinding applications, stirred media mills are more energy efficient than conventional milling technologies (Kwade & Stender, 1998; Jankovic, 2003). They are up to 50% more energy-efficient for such applications than the conventional ball mills (Stief et al., 1987). Therefore, the recent ore grade depletion and concomitant increase in fine-grained ore has significantly increased the demand for fine and ultrafine grinding mills (El-Shall & Somasundaran, 1984; Larson et al., 2011).

Besides being energy efficient, stirred media mills produce a ground product which is iron-free due to the use of inert ceramic grinding media (Burford & Clark, 2007). Iron-free grinding environment implies less operational issues due to less consumption of cyanide and flotation reagents in downstream processing.

Currently, there are various types of stirred media mills, both vertical and horizontal in orientation. Vertical mills include: the Tower mill (Vertimill), the Vertical Pin Stirred Mill or the Stirred Media Detritor (SMD) and the VXPmill, whereas the Netzsch/IsaMill is horizontally oriented. The mills are equipped with pins or discs mounted on a central rotating shaft. The shaft distributes mechanical energy from the motor to the charge as the discs or pins rotate with the shaft. Grinding action is influenced by the collision of grinding beads and mineral particles.

The VXPmill and the Isamill use fine grinding media and are operated at high tip speeds, making them fit for fine grinding applications (Lichter & Davey, 2002). Rahal et al. (2011a) pointed out the major advantages of the VXPmill over the Isamill, which include: leakage free bearing seal (slurry is not in contact with bearing), no design complications due to internal product separating mechanisms (ground product overflow at atmospheric pressure through a media retention screen) and, smaller footprint. Also, the VXPmill bridges the gap between the lower and the higher speed stirred media mills. Therefore, for the sake of this study only the VXPmill will be discussed.

Like other stirred media mills, the VXPmills are influenced by a significant number of operating variables. The most important ones include: mill speed, grinding media size, feed particle size, grinding media load and its specific gravity, slurry flow rate and rheology, and solids content.

Unlike the conventional ball mills, the Bond methods do not accurately predict the energy requirements for the VXP mills and other stirred media mills due to the differences in grinding mechanisms involved in the two milling technologies. Rather, the energy input-product particle size relationship forms the basis for scaling-up stirred media mills.

Figure 1.1 shows the operating principle of the VXPmill. The mill is bottom fed and discharges at the top through a media retention screen. A shaft mounted to a motor is equipped with grinding discs and spacers. When the motor is activated, the shaft spins, which then makes the grinding beads (media) collide with the ore particles. The collision makes the ore particles break down because the grinding beads are relatively heavier, tougher, larger in size and harder than the ore particles.

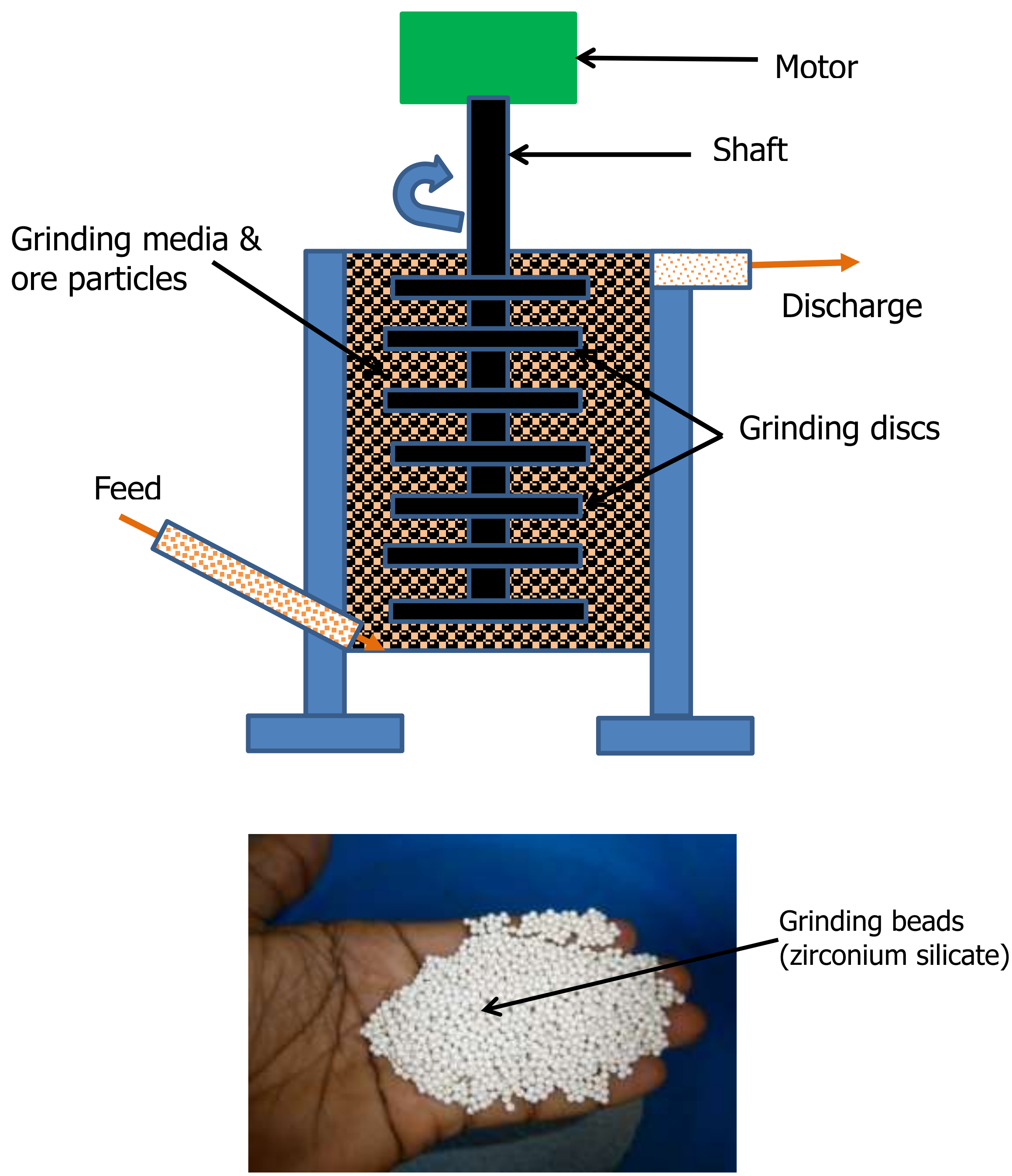

Figure 1.1 The VXPmill operating principle

1.2 Scope of work

Currently, only a few studies have been done on the analysis of the operating variables of the VXPmills. The most recent one was done by Rahal et al. (2011b). No work has been reported on scale-up demonstration for the VXPmills. The increasing demand of these mills both for the pilot and industrial scale applications has motivated the present study.

As a new technology, there was a need to develop a proper scale-up testing procedure and to provide information for the best operation of the VXPmills. The proper scale-up testing procedure makes a pilot-scale mill reflect the operation of a full-scale mill, and therefore, an accurate scale-up result is achieved. The best operation of the VXPmills gives a desired grind size with minimal energy losses; which is more desired in commercial applications.

Therefore, this study focuses on the analysis and optimization of the most important operating variables, and the scale-up demonstration for the VXPmills. The operating variables studied include: mill speed, feed particle size, solids content, and slurry rheology and flow rate. The individual effects of these variables on mill power draw and their combined effects based on the “stress intensity” of grinding media were analyzed. The test work was conducted at the Coal and Mineral Processing (CMP) laboratory, at the University of British Columbia, Vancouver, Canada, utilizing the pilot-scale VXP10 (10 litre) mill.

It is important to mention at this point that stirred media mills produce a ground product which is characterised by a higher yield stress and viscosity than the one generated by the conventional ball mills, especially at high solids content due to the strong interaction of fine particles. The yield stress and the viscosity of the ground suspensions adversely affect the comminution process for stirred media mills and, therefore, their effects were also studied in this work.

One of the most important aspects of this study was to understand the best testing procedure for the scale-up of the VXPmills (formerly the Deswik mills). And the question at hand was whether the procedure that was being used by the Deswik mills (batch recycle) was appropriate to predict the energy requirement for scale-up applications. Therefore, the batch recycle testing procedure needed to be compared with the pendulum (pass by pass basis). And, the energy input versus product particle size plots were constructed based on the two modes and the results were assessed to recommend the appropriate testing procedure for scale-up applications.

The term “scale-up” refers to the prediction of a full-scale mill motor size derived from the data (specific energy input versus product particle size) generated by a pilot-scale mill, with both mills operated at similar grinding conditions. A scale-up demonstration study was conducted at the Turk Mine in Bulawayo, Zimbabwe, utilizing the pilot-scale (VXP10) mill and the full-scale (VXP2500) mill. The scale-up demonstration was conducted using the recommended scale-up testing procedure (see the previous paragraph). Based on similar operating conditions for both mills, the full-scale (VXP2500) mill data points were plotted on the same energy-product particle size relationship with the one for the pilot-scale (VXP10) mill.

1.3 Objectives

The objectives of this research were:

1. To compare the two testing procedures of developing the specific energy input versus product particle size relationship (pendulum versus batch recycle) and to recommend the best testing procedure for scale-up applications.
2. To study the effects of various operating conditions on the specific energy input versus product particle size relationship for feldspars-quartz ore, employing the VXP10 mill.
3. To understand the effect of rheological properties of ground slurries on the specific energy input at various solids contents, grind sizes and mill tip speeds.
4. To optimize the operation of the VXPmills based on the specific energy input versus product particle size relationship, using the stress intensity of the grinding media approach.
5. To demonstrate a scale-up procedure utilizing the VXP10 and the VXP2500 mills.

2 Literature review

2.1 Process operating variables for stirred media mills

2.1.1 Introduction

Stirred media mills have proven to be the most energy efficient option for regrinding and fine grinding applications (Jankovic, 2003). Due to many operating variables in stirred mills and the way that these variables interact with each other, the complexity of the subject is apparent. These parameters include: stirrer speed, media size, media density, slurry density and flow rate, slurry rheology and media charge volume (Rahal, 1999; Jankovic, 2001; Kwade, 2010; Rahal et al., 2011b). Rahal (1999) and Rahal et al. (2011b) categorized the most significant operating variables for stirred media mills as mill configuration and process state as indicated in Figure 2.1.

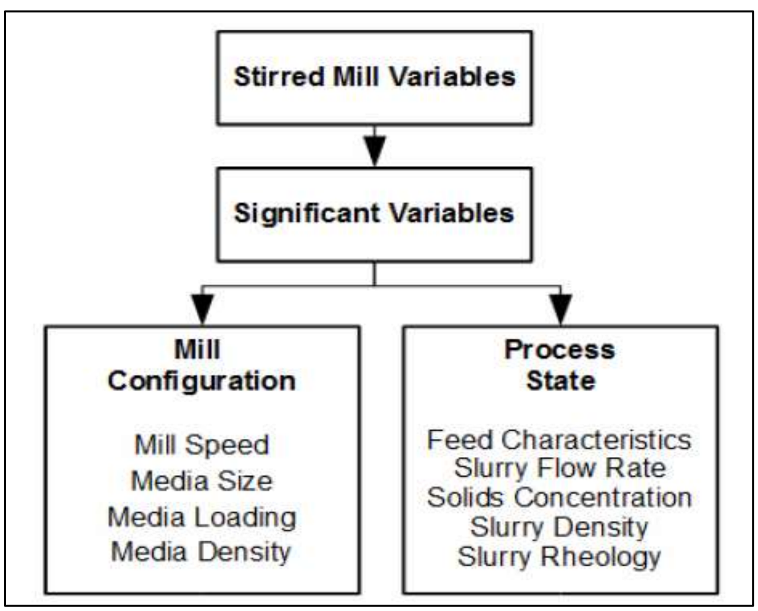

Figure 2.1 Critical mill operating variables (Rahal, 1999; Rahal et al., 2011b)

2.1.2 Critical mill operating variables

2.1.2.1 Mill speed

Mill speed is one of the most influential operating variables in the operation of stirred media mills (Jankovic, 2001, 2003; Wang et al., 2004). A study conducted by Gao et al. (1996) showed that mill speed was the dominant factor for the determination of power draw. In their study, pure dolomite was ground using a horizontal stirred mill.

Utilizing different types of stirred mills and feed materials, a number of researchers, using coal (Mankosa et al., 1989), limestone (Zheng et al., 1996) and (Jankovic, 2003), dolomite (Gao & Forssberg, 1993a), investigated the effect of stirring speed on the product size. They all concluded that at a given specific energy input, increasing stirred speed lowers the energy efficiency (utilization).

Energy inefficiency at higher stirrer speed is caused by the decrease in effective grinding volume for comminution due to a large vortex created at the centre of the mill (Mankosa et al., 1989; Wang et al., 2004). Also, at higher stirrer speeds, more energy is lost as heat and mechanical friction (Gao & Forssberg, 1993a). The extra heat and friction generated at high mill speed increases the wear rate of the grinding media and the internal grinding mill assembly especially at high media load.

However, using dolomite material, a study was conducted by Wang and Forssberg (2000) on analyzing the effect of mill speed and grinding media size on particle size distribution. They concluded that the increase in mill speed increases beads velocity, which in turn gives a finer product with narrow size distribution; which is more desired in downstream operations. Also, Gao and Forssberg (1993a) demonstrated the increase in milling rate with an increase in mill speed.

2.1.2.2 Media size

The size of the grinding media is another important variable for the operation of stirred media mills. Media selection depends on feed and desired product size. A number of researchers have studied the effect of media size on comminution in stirred media mills (Mankosa et al., 1986; Zheng et al., 1996; Becker et al., 2001; Yue & Klein, 2006).

For fine feed particle size i.e., less than 40 μm, Yue and Klein (2006) agreed with Mankosa at al. (1986) that, the optimum ratio of bead size to feed particle size is 20:1. Conversely, for coarse feed particle size (F_{50} =166 μm), Zheng et al. (1996) concluded that the best ratio is 12:1. The disparity of the optimum ratio of bead size to feed particle size for the two scenarios was possibly due to the differences in feed particle size i.e., the coarser the feed particle size, the smaller the optimum ratio. In terms of product size distribution, larger beads produced a narrower distribution (Wang & Forssberg, 2000; Yue & Klein, 2006).

Media size should be large enough to provide sufficient impact for effective comminution; this is due to the large velocity gradient executed by coarser media size (Mankosa et al., 1986; Wang & Forssberg, 2000). However, coarser grinding media is effective for coarser feed and less effective for finer feed sizes (Jankovic, 2003).

Therefore, a simple technique is to use large beads for coarser feed material and smaller beads for finer feed (Wang & Forssberg, 1997, 2007). Also, blending larger and smaller beads in the proportions is a better approach to encounter appropriate size reduction for different size fractions present in the feed. Alternatively, pre-grinding of coarse particles using larger media size before using smaller media size for fine grinding is also a good approach (Wang & Forssberg, 1997).

2.1.2.3 Media density and material

Generally, grinding media should be heavy enough to provide sufficient impact for effective and fast comminution process. However, they should be able to be stirred enough to acquire high velocity (Gao & Forssberg, 1993b). Knelson Milling Solutions (KMS) recommends the intrinsic density of the media to be more than three times the expected slurry density and the media density should be selected with the criteria based on the slurry density between 1.2 and 1.5 kg/L (Rahal et al., 2011a).

Gao et al. (2001) investigated the effect of media specific gravity on mill power draw and milling capacity for the comminution of zinc scavenger concentrate. It was observed that in order to achieve a high milling capacity, a denser medium (SG = 3.7), though less energy efficient, was a better medium than the less dense medium (SG = 2.6). A similar observation was made by Zheng et al. (1996) for the comminution of pure limestone. Another study was conducted by Gao and Forssberg (1993a) using three different types of grinding media with specific gravities 2.5, 3.7 and 5.4 to grind pure dolomite. It was concluded that the optimum media specific gravity to achieve highest energy utilization was 3.7. The denser media (SG = 5.4) was unable to be stirred up whereas the less dense media (SG = 2.5) was not heavy enough to provide intense impact for effective comminution.

Besides media density, other media considerations to be taken into account include: hardness, competency and shape of the grinding media. Competent grinding media should be well-rounded and free of flaws and cracks; media with flaws and cracks breakdown easily resulting in unacceptable high wear of grinding media (Lichter & Davey, 2006). For effective comminution, the grinding media should be harder than the mineral being ground (Krause & Pickering, 1998; Becker et al., 2001).

2.1.2.4 Media load volume

Media load is the percentage by volume of grinding media with respect to the net grinding chamber volume of the stirred media mill. At a given specific energy, higher media charge produces large product surface area and finer product size (He, 2005).

The increase in media load increases collision frequency i.e., stress events in the grinding chamber at a given mill speed. This phenomenon increases the area for particle breakage sites in the grinding chamber, but the operating torque and power increase too (Rahal et al., 2011a). However, media load should not be higher than 90%, or else media compression will result in unacceptable high media and liner wear due to excessive friction in the grinding chamber (Gao & Weller, 1993).

Using carbonate minerals (dolomite and limestone), a study was conducted by Wang and Forssberg (1997) on analyzing the effect of beads (load, size and density) on the grinding performance. They concluded that the energy utilization increases linearly with media load from 50% to 83%, particularly, for the coarse media size. Rahal et al. (2011b) observed the increase in operating torque with the increase in media load. In their observation, the increased torque was lower for less dense grinding media as compared to higher density grinding media.

2.1.2.5 Slurry density

It is quite obvious that a slurry with a high solids content will increase the throughput rate in the grinding operation. However, grinding at a lower slurry density yields a finer product with a narrower size distribution which is more desired in mineral beneficiation processes.

Utilizing a quartz ore sample, Yue and Klein (2004, 2005) observed that grinding at lower solid contents generates a narrower product size distribution. On the other hand, Mankosa et al. (1989) observed a broader and coarser size distribution at 60% solids by weight, for a coal sample. In the study, there was no significant change in energy efficiency of the stirred media mill when the solids content was changed from 20% to 50% by weight.

Using high purity limestone (96% $CaCO_3$), Zheng et al. (1996) observed that the product surface area increased with solids content from 60% to 75% by volume and decreased slightly at 80%. Also, observation through a transparent mill chamber revealed that only the media and particles were stirred intensively at the centre of the impeller while beyond the stirrer the solids were almost stagnant.

Zheng et al. (1996) concluded that the best energy efficiency for high purity limestone is at 65% by weight. Greenwood et al. (2002) suggested that typical maximum solids content is around 50% by weight without dispersant, while the maximum solids content with optimum dispersant is up to 80%.

2.1.2.6 Interaction of variables

The interaction of processing variables in stirred media mills is very strong and therefore the effect of one variable cannot be solely generalized (Jankovic, 2003). Matsuo et al. (1990) and Jankovic (2003) suggested that there is a strong interaction between optimum size of the grinding media and the mill speed. At a higher mill speed, finer media performed better which was contrary for coarser media size. Similarly, Wang and Forssberg (1997, 2000) indicated that an optimum bead to feed size ratio exists at high mill speed.

Kwade (1999, 2004) proposed that in order to achieve maximum production capacity, the mill speed should be as high as possible to achieve the highest power consumption while decreasing the media size to achieve optimum “stress energy.” The stress energy of the grinding media is the maximum energy which can be transferred to the captured particles between two colliding grinding beads (Stenger et al., 2005).

Gao and Forssberg (1993a) observed that the effect of mill speed on energy utilization diminished at 75 % by weight solids content. At such high slurry density no matter how the mill speed is increased, the slurry near the stirrer rotates synchronically with the discs leaving the rest of the mill almost stationary (Gao & Weller, 1993; Zheng et al., 1996).

2.1.3 Size reduction and grinding limit

It is important at this point to understand that regardless of the operating conditions employed, in most grinding test works; no further size reduction is experienced after a certain milling time (Knieke et al., 2009). The grinding limit is experienced because as particle size decreases, not only the number but also the size of defects, i.e., cracks and flaws, decrease, which then lowers the grinding kinetics of the ore being ground (Reem, 2011). Another explanation is that there is less chance for fine particles to be *selected* for breakage, as coarse particles are preferentially broken (Jankovic & Sinclair, 2006).

Therefore, the effect of grinding limit is expected to lower grinding kinetics regardless of the operating conditions employed for the comminution process. Additionally, rheological effects tend to impose “a viscous dampening-related grinding limit prior to the true grinding limit” (Knieke et al., 2010, p.1401), this is because the velocity of grinding beads are remarkably dampened to adversely impair energy transfer to enhance further comminution.

2.1.4 Operating variables summary

It is important to appreciate the influence of individual operating variables in the operation of stirred media mills. However, it is quite interesting to note that these variables do interact strongly with each other. Therefore, to have a good understanding of the influence of these variables, a greater number of experimental works is required.

The size reduction process slows down remarkably with the decrease in particle size regardless of the operating conditions employed in the comminution process. However, stirred media mill operating conditions can be selected to achieve the best grinding results.

2.2 Stress intensity

2.2.1 Introduction

The operation of stirred media mills is affected by a considerable number of processing operating variables. However, some of these variables and may be categorized as less significant (Jankovic, 2003). In order to reduce the number of experiments for "optimization" of stirred media mills, Kwade et al. (1996), Kwade (2004) and Jankovic (2001) demonstrated that the effect of the most influential parameters, (media size and density, slurry density, and mill tip speed), can be assessed simultaneously by the concept of stress intensity of the grinding media.

The stress intensity of the grinding media is the energy of impact and pressure acting on the captured particles between grinding beads (Jankovic, 1996). At a constant specific energy input, stress intensity determines grind size. Therefore, stress intensity is essential for selection, scale-up and optimization of stirred media mills (Jankovic, 2001, 2003). Jankovic (2001) postulated that there are two types of stress intensities which exist in stirred media mills namely, centrifugal and gravitational.

2.2.2 Centrifugal stress intensity

In stirred media mills, centrifugal acceleration plays a very significant role on comminution. Kwade et al. (1996) and Jankovic (2001) postulated that there are two zones where comminution in stirred media mills is very intense. The first zone is located near the disc and the other at the grinding chamber wall.

Near the grinding disc zone, the specific energy is directly proportional to stress intensity and inversely proportional to particle volume as described in Equation (2.1).

$$E_{vb} \propto D_d \times V_m \times (\rho_m - \rho) \times a_c \times \frac{1}{V_p} \propto {D_m}^3 (\rho_m - \rho) {v_t}^2 \times \frac{1}{V_p} = \frac{SI_m}{V_p} \quad (2.1)$$

$$SI_m = {D_m}^3 (\rho_m - \rho) {v_t}^2 \quad (2.2)$$

where;

SI_m= stress intensity of the grinding media (N),

E_{vb} = volume based specific energy of a single grinding media (kJ/m^3),

ρ_m = density of grinding media (kg/m^3),

ρ = density of slurry (kg/m^3),

v_t = mill tip speed (m/s),

D_m = diameter of grinding media (m),

D_d = grinding disc diameter (m),

v_m = volume of grinding media (m^3),

v_p = volume of particle (m^3),

a_c = grinding media centrifugal acceleration (m/s^2).

At the chamber wall

$$\frac{F_c}{A_p} \propto {V_m}^3 \times (\rho_m - \rho) \times a_c \times \frac{1}{A_p} = {D_m}^3(\rho_m - \rho){v_t}^2 \times \frac{1}{V_p} = \frac{SI_m}{V_p} \tag{2.3}$$

where;

F_c = centrifugal force (N),

A_p = particle cross section (m^2).

From Equations (2.1) and (2.3), it can be seen that the stress intensity of grinding media is a measure for force of pressure and energy acting on the captured particles between grinding beads (Kwade, 1996). Particles with more defects can be broken down easily by low stress intensities. Conversely, higher stress intensities are required to effectively break less defective particles.

2.2.3 Gravitational stress intensity

In addition to the centrifugal stress intensity, low speed vertical stirred mills experience gravitational stress intensities (Jankovic, 2001). The gravitational component depends on the media height and mill design. It becomes even more important for full-scale operations because of the high bed height of grinding media at high media load. However, the centrifugal component surpasses the effect of gravitational as mill tip speed increases.

For Pin mills, the maximum media grinding pressure due to gravitational force is described by Equation (2.4) (Jankovic, 2001).

$$SI_{gm} = {D_m}^2(\rho_m - \rho) \times g \times h \tag{2.4}$$

where;

g = acceleration due to gravity (m/s^2),

h = media height (m).

For Tower mills, the gravitational component of media grinding pressure is described by Equation (2.5) (Jankovic, 2001).

$$SI_{gm} = K{D_m}^2\left[\frac{(D - D_s)(\rho_m - \rho)}{4\mu}\right] \tag{2.5}$$

where;

K = ratio between vertical and horizontal media pressure,

μ = coefficient of friction,

D = Mill diameter,

D_s = screw diameter.

This means that Pin and Tower mills experience both gravitational and centrifugal stress intensities and the total stress intensity for these mills is described in Equation (2.6).

$$SI_{total} = SI_{gm} + SI_m \tag{2.6}$$

where;

SI_{total} = total stress intensity, SI_{gm} = gravitational stress intensity, SI_m = centrifugal stress intensity.

Since the VXPmills are operated at relatively high tip speeds as compared to Pin and Tower mills, the gravitational stress intensity is expected to be negligibly low as compared to the centrifugal stress intensity. Yet, this has to be proven experimentally by systematically adjusting the media load and mill speed, and observing the grinding performance.

2.2.4 Stress intensity and energy utilization

Kwade et al. (1996) suggested that the specific energy input and the stress intensity of grinding media are the two main variables which determine product fineness for the comminution of limestone using stirred media mills, and similar observation is expected for other materials. At a given specific energy input, a coarse grind size is obtained when the stress intensities are either relatively large or small. At higher stress intensities, much energy is lost as heat and mechanical friction. Conversely, at the lower end of stress intensities, the stresses are insufficient to effectively cause massive fracture.

However, somewhere in between the two extremes there is an optimum stress intensity to acquire a fine product size (Kwade et al., 1996; Becker, 1997; Kwade & Stender, 1998; Kwade, 1999, 2004; Jankovic, 2001, 2003; Stenger et al., 2005).This phenomenon was described by Kwade et al. (1996) using the “energy utilization” concept.

From a comminution point of view, energy utilization is defined in Equation (2.7), as the increment of surface area produced (ΔS) per unit of specific energy consumption (Gao & Forssberg, 1993a; Kwade et al., 1996; Zheng et al., 1997; He, 2005). The stress intensity of grinding media increases with energy utilization up to a maximum value (at optimum stress intensity) and beyond this stress intensity, the energy utilization drops slowly due to energy losses.

$$EU = \frac{\Delta S}{E} = \frac{10^6 \times (S_p - S_f)}{E} \tag{2.7}$$

where;

EU = Energy Utilization (m^2/kWh),

E = Specific energy (kWh/t),

S_f = Specific surface area of mill feed (m^2/g),

S_p = Specific surface area of mill product (m^2/g),

ΔS = Incremental surface area produced (m^2/g).

2.2.5 Stress intensity summary

For stirred media mills, specific energy input and stress intensity of grinding media determine grind size. Therefore, stress intensity analysis is vital for selection, optimization and scale-up of stirred media mills. Optimum stress intensity does exist in stirred media mills, it is located between the two extremes of stress intensities, where the energy utilization is maximum. Therefore, in order to achieve the best comminution results with maximum energy utilization, stirred media mills should be operated at their optimum stress intensities.

The gravitational stress intensity of the VXPmills is expected to be negligibly small as compared to the centrifugal stress intensity. This is due to the high mill tip speed these mills are operated at. However, more investigation is required to prove this hypothesis due to the significant heights of the recently designed full-scale VXPmills e.g., for the VXP2500 mill, the bed height of the grinding media is about 2 metres high (about 4 to 6 tonnes of grinding media depending on its specific gravity) when the mill is loaded with the media at 60% of the mill grinding chamber volume.

2.3 Rheology of ground mineral slurries

2.3.1 Introduction

Rheology is the science of the deformation and flow of matter (British Standards Institution, 1975). It indicates the level of inter-particle aggregation and interaction of mineral slurries (Muster & Prestidge, 1995). From rheological point of view, yield stress is the threshold stress to be achieved before the flow is initiated and viscosity is the resistance of the fluid to flow.

The rheology of mineral suspensions affects various process operations such as grinding and classification (Kawatra & Bakshi, 1996), paste flows (Pullum et al., 2006), and pressure acid leaching for nickel laterite (Motteram et al., 1997; Whittington & Muir, 2000; Klein & Hallbom, 2002). Therefore, a good understanding of rheological flow properties of mineral slurries is very important in the plant design, scale-up and optimization of mining and mineral processing units (Akroyd & Nguyen, 2003a; Muster & Prestidge, 1995).

The fine grinding of mineral slurries in stirred media mills exhibit peculiar rheological characteristics which are not present in coarse grinding operations. These characteristics include: high viscosity slurry and, aggregation and agglomeration of fine particles (Wang & Forssberg, 1997). At higher solids content (above 60% by weight), the increase in viscosity and yield stress impairs energy delivery for further comminution. This is because of the ability of thick pulp to hold grinding media together and to cause it to adhere to the mill wall (Mankosa et al., 1989; Tangsathitkulchai, 2003).

2.3.2 Rheological effects in stirred media mills

Stirred media mills are characterized by slurries with fine particles and high solids content; these slurries are prone to high viscosities and yield stresses. In such high viscous slurries, the velocity of the grinding beads is strongly “dampened” to an extent of adversely affecting grinding efficiency. Consequently, the kinetic energy of the beads is not significant enough to effect comminution and “a viscous related dampening grinding limit is reached prior the true grinding limit” (Knieke et al., 2010, p.1401).

Yue (2003) and, Yue and Klein (2004) studied the effect of yield stress on the breakage rate of quartz at 30%, 35%, and 40% solids by weight. It was concluded that an increase in yield stress reduced the particle breakage rate as solids content increased. The effect was very significant as the particle size decreased to less than 10 microns. In their study, the mill power draw increased with the increase in yield stress and apparent viscosity.

Knieke et al. (2010) investigated the effect of rheological behaviour of tin oxide suspensions (prepared using three different solvents, ethylene glycol, water and ethanol) on the grinding efficiency. It was concluded that the breakage kinetics of tin oxide was substantially reduced for ethylene glycol based suspensions as compared to water and ethanol based suspensions.

Gao and Forssberg (1993b) experienced exponential increase in yield stress after a certain milling time, whereas the viscosity remained stable. In the study, the mill had to be stopped earlier at higher solids content (75% as compared to 65% by weight) due to poor slurry flowability. The lack of flowability was a result of strong inter-particle forces which held particles together in the slurry and blocked the water which was indispensable to provide the flow. Another explanation for lack of flowability is that, water which was supposed to provide flowability was tied up due to the increase in surface area of fine particles (Mankosa et al., 1989).

Addition of dispersant has a potential of lowering and eliminating the yield stress, which then allows ultrafine grinding even at higher slurry solids content (Kapur et al., 1996; Gao & Forssberg, 1993b; Klimpel, 1999; Greenwood et al., 2002). However, when the critical solids concentration is exceeded, the addition of dispersant is no longer effective (Wang & Forssberg 1997).

2.3.3 Factors influencing slurry rheology

Rheology is influenced by particle size and shape, particle size distribution, volume fraction (solids concentration) and inter-particle forces (Klein, 1992). As more fine particles are generated in wet ultrafine grinding and at high solids concentration, significant changes in surface properties occur which then influence rheological properties of ground slurry (Gao & Forssberg, 1993b; Klimpel, 1999; Zheng et al., 1997; Yue & Klein, 2004; He et al., 2004).

2.3.3.1 Particle size

Particle size influences rheological properties remarkably. As particle size decreases the distance between adjacent particles reduces and consequently the interaction between particles increases notably. The change in viscosity with particle size is associated with four contributions, which are electroviscous, granulaviscous, aggregation and hydrodynamic (Klein, 1992). A number of studies have shown that slurry viscosity and yield stress increases as particle size decreases (Gao & Forssberg, 1993b; Mende et al., 2003; He et al., 2004; Yue & Klein, 2004; Stenger et al., 2005; Gustafsson et al., 2008).

2.3.3.2 Particle size distribution

Jeffrey and Andreas (1976) used suspensions of spherical particles to conclude that at a given volume fraction, polydisperse suspensions exhibited lower viscosities than similar monodisperse suspensions. This is because fine particles in polydisperse suspensions fill the gaps between coarse particles which increases the maximum volume fraction and ultimately lowers the viscosity (Klein, 1992; Hill & Carrington, 2006).

Using quartz slurries ground by a horizontal stirred mill, Yue and Klein (2004) deduced that at a given solids content, a narrow size distribution slurry has a higher yield stress and viscosity as compared to the one with a broad particle size distribution. Similarly, Yang et al. (2001) showed that at the same solids content, titanium dioxide suspensions with a broad particle size distribution had lower viscosity and yield stress as compared to the one with a narrow size distribution.

2.3.3.3 Solids content

The greater number of particle interactions at high solids content is responsible for the exponential increase of viscosity (Klein, 1992). Also, yield stress increases sharply as solids content increases (Avramidis & Turian, 1991).

Hill and Carrington (2006) correlated the increase in slurry viscosity with an increase in the volume fraction of solids. At high solids content, particles become more closely packed together. This sort of packing resists the free movement of particles due to strong interaction of particles.

Using dolomite slurries, Gao and Forssberg (1993b) have shown that an increase in slurry density from 65% to 75% by weight had a remarkable increase in viscosity. Similarly, Yue and

Klein (2004) showed that apparent viscosity increased when the solids content was increased from 35% to 45% by weight using quartz suspension. The increase in viscosity was even more evident as particle size decreased. Other researchers came up with similar conclusion (Tangsathikulchai & Austin, 1988; Gustafsson et al., 2008).

2.3.3.4 Particle shape

Particle shape affects the effective volume fraction due to the way different shapes align, orient and pack in a given suspension. The increase in plate and fibrous type of particles for a given slurry has a significant effect on increasing its viscosity and yield stress. This is because the effective volume fraction increases due to wide variation of aspect ratio (mean ratio of length to width/ depth of particles) (Mueller, et al., 2009; Patra et al., 2010).

A study was conducted by Patra et al. (2010) to explore how shape, size and morphology affect pulp rheology. In their study, serpentines plate type, (lizardite, 15% w/w) and fibrous type (chrysotile, 55% w/w) were deliberately added to a non-serpentine nickel ore to assess the influence of serpentines on pulp rheology. It was concluded that serpentines were responsible for a remarkable increase of yield stress. Yuan and Murray (1997) showed that tubular halloysite was the most viscous as compared to spherical halloysite. Similarly, Barnes et al. (1989) demonstrated that the rheology of fine suspensions depends on particle shape and the effect of solids content is even more pronounced for non-spherical particles.

2.3.4 Rheological flow characteristic of mineral suspensions

Depending on the shear rate applied, mineral suspensions exhibit some changes in their rheological flow properties which can influence transport and processing. In rare cases, mineral suspensions exhibit rheopectic behavior (increase in viscosity with time at a given shear rate) which may lead to operational issues such as plugging the pipes (Klein & Hallbom, 2002). Generally, mineral suspensions exhibit time dependent or independent shear-thinning behavior. Therefore, a good knowledge of rheological flow properties is essential in wet ultra-fine grinding operations.

Figure 2.2 shows the generalized rheological flow curves for mineral slurries. Newtonian fluids or suspensions have a constant viscosity, whereas the viscosity of pseudoplastic suspensions decreases with shear rate. Suspensions exhibiting dilatancy become more viscous as the shear rate is increased. Most mineral suspensions exhibit non-Newtonian fluids (Klimpel, 1999; Klein & Hallbom, 2002; Yue & Klein, 2004). He et al. (2004) suggested that ground limestone slurries exhibit a time independent Newtonian behaviour at low solids concentration and becomes increasingly non-Newtonian at high solids content.

A study conducted by Tangsathitkulchai and Austin (1988), and Tangsathitkulchai (2003) utilizing ground quartz slurries showed that, the slurry exhibited a "time-independent non-Newtonian behaviour with and without yield stress followed by Bingham plasticity which started at 30 s^{-1}" (p. 39). Klimpel (1982, 1983) suggested that the "optimum" grinding is achieved when the slurry exhibits pseudoplasticity with no yield stress.

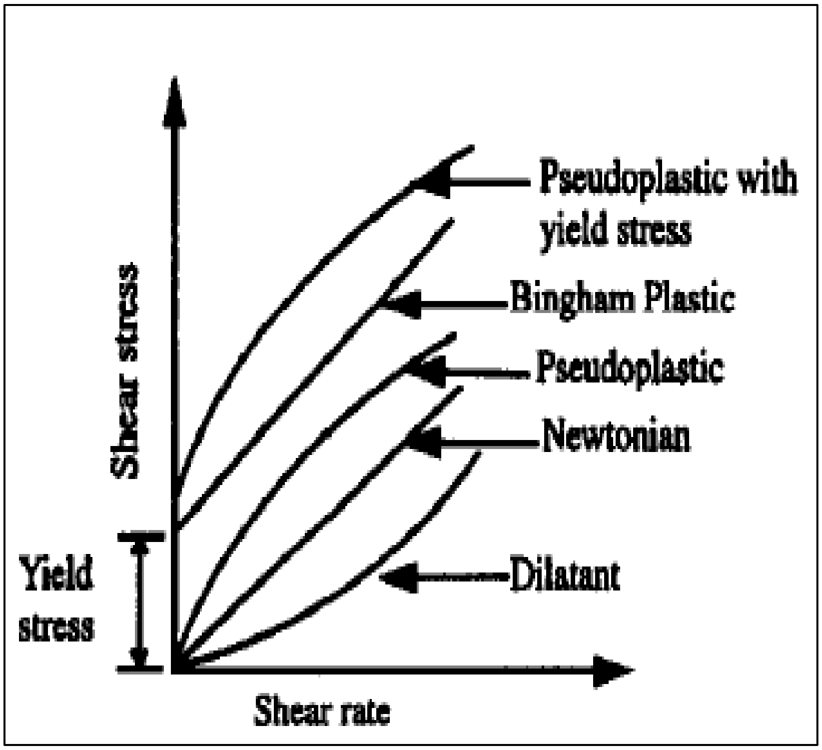

Figure 2.2 Generalized rheological flow curves for mineral slurries (Kawatra & Bakshi, 1996)

2.3.5 Rheological flow curve modeling

Empirical models of shear stress and shear rate relationship are used to describe the rheological behaviour of fluids. The criteria for the suitability of rheological model selection were well outlined by Klein (1992) and Hallbom (2008). The model should:

a. Fit the data over a wide range of shear rates,

b. Be simple with minimum number of independent constants,

c. Have easy-determined constants,

d. Have constants with meaningful physical significance.

Generally, mineral suspensions exhibit non-Newtonian behaviour. However, at very low solids content (which is not the case in a comminution circuit) they can exhibit Newtonian behaviour. The most common models used to describe the rheology of mineral suspensions are Bingham plastic, Herschel-Bulkley and Casson.

2.3.5.1 The Bingham plastic model

The Bingham plastic model is a simple two-parameter, linear rheological model shown in Equation (2.8). This model is commonly used to determine the yield stress of mineral suspensions by extrapolating a linear portion of a rheological flow curve. Gao and Forssbergy (1993b) demonstrated its application in the rheological behaviour of dolomite slurries ground using a horizontal stirred mill.

$$\tau = \tau_{yB} + \eta_B \gamma \tag{2.8}$$

where;

τ = shear stress (Pa),

τ_{yB} = Bingham yield stress (Pa),

η_B = Bingham viscosity (Pas),

γ = shear rate (s^{-1}).

With the lack of data at low shear rates, a number of fluids and suspensions can exhibit Bingham plasticity behaviour at high shear rates which tends to overestimate the yield stress (Nguyen & Boger, 1983; Yue & Klein, 2004).

2.3.5.2 The Casson model

The two-parameter Casson model is shown in Equation (2.9). The model can fit comparatively well at low shear rates when compared to the linear-Bingham model. Also, it has demonstrated good estimates of yield stress as compared to direct measurement methods (Nguyen & Boger, 1983). This model has a physical basis resulting from structural arguments and the coefficients can be determined easily (Casson, 1959; Tadros, 1980).

$$\tau^{\frac{1}{2}} = \tau_{yC}{}^{\frac{1}{2}} + (\eta_C \gamma)^{\frac{1}{2}} \qquad (2.9)$$

where;

τ = shear stress (Pa),

τ_{yc} = Casson yield stress (Pa),

η_c = Casson viscosity (Pas),

γ = shear rate (s^{-1}).

A study conducted by Ding et al. (2007) on analyzing the influence of wet ultrafine grinding on the rheological behaviour of pyrite-heptane slurry demonstrated that the Casson model was the best fit over a wide range of solids content. The Bingham model was only applicable at lower solids content. Yue and Klein (2004) demonstrated the suitability of Casson model fitting on quartz suspensions ground using a horizontal stirred mill. Similarly, Klein (1992) demonstrated that for magnetite suspensions the Casson model was the best fit compared to Bingham, Herschel Bulkley, Carreau and Cross models.

Hallbom and Klein (2004) proposed a rheological model known as “yield plastic”. It is represented by Equation (2.10). The Casson and the Bingham models are the special cases of this model (when k = 1 it represents the Bingham model and when k = 1/2 it forms the Casson model). This model has the advantage over the Herschel Bulkley model because it has physical significant coefficients (τ_{yH} and η_H) and can fit a broad range of slurries over a wide range of shear rates.

$$\tau^k = {\tau_{yH}}^k + (\eta_H \gamma)^k \tag{2.10}$$

where;

τ = shear stress (Pa),

τ_{yH} = Hallbom yield stress (Pa),

η_H = Hallbom viscosity (Pas),

γ = shear rate (s^{-1}),

k = dimensionless scaling factor.

2.3.5.3 The Herschel Bulkley model

The three-parameter Herschel Bulkley model is a simplified generalization of the Bingham plastic model to take into account for non-linearity at low shear rate. This model is mathematically represented by Equation (2.11). When n = 1 the Herschel Bulkley model becomes the Bingham model.

$$\tau = \tau_{HB} + (k\gamma)^n \tag{2.11}$$

where;

τ = shear stress (Pa),

τ_{HB} = Herschel Bulkley yield stress (Pa),

k = fluid consistency index,

γ = shear rate (s^{-1}),

n = flow behavior index.

Mangesana et al. (2008) and Kelessidis et al. (2006) demonstrated the best fitting accuracy of this model in silica sand and oil-well drilling suspensions respectively. However, using non-linear regression procedure, the Herschel Bulkley sometimes gives “meaningless negative yield stress values and imposition of the condition for positive values of the yield stress gives non-optimal solutions.” (Kelessidis et al., 2006, p. 205). Hallbom and Klein, (2009) pointed out that the Herschel Bulkley has “irrational units for the consistency coefficient $Pa.s^n$.” (p.2).

2.3.6 Rheological measurements and possible sources of error

Accurate rheological measurements of mineral slurries are of utmost importance because they give a good knowledge of the flow behaviour of slurries which helps in the design and optimization of mining and extractive processes (Akroyd, 2003a). Generally, rheological measurements are executed when a fluid sample is deformed under controlled conditions and its response is measured in terms of torque, instrument dimensions and geometrical constants (Triantafillopoulos, 1988).

Rotational and tube viscometers are the most common devices developed to measure the rheological properties of fluids. However, yield stress and time dependent properties are difficult to determine with tube viscometers. Therefore, for the sake of this work rotational viscometers and specifically concentric cylinder viscometers will be discussed. There are a number of possible sources of error on rheological measurements with regard to concentric cylinder fixtures; these include: wall slip, turbulence, temperature effects and end effects (Klein, 1992). Other considerations are particle settling and, eccentricity of bob and cup (Triantafillopoulos, 1988).

Wall slip occurs when the local solids concentration at a wall is lower than in the bulk due to the depletion of suspended particles at the wall (Barnes, 2000). This unequal distribution of solids in the suspension generates unexpectedly low shear stress because much of the shearing takes place at this depleted layer. Wall slip effect can be minimized by roughening or profiling the wall surfaces at the shearing zone (Nguyen, 1983; Klein, 1992; Barnes, 2000).

Depending on the gap size and viscosity, Taylor vortices is the three-dimensional hydrodynamic instabilities in the annular gap occurring when the speed of a rotating member (bob or cylinder) exceeds a critical shear rate (Triantafillopoulos, 1988). These hydrodynamic instabilities generate extra stresses which can be wrongly interpreted along with rheological properties of fluid. The criterion for onset of Taylor vortices is determined by Equation (2.12), (Taylor, 1923). R_1 and R_2 are the radii of the inner and outer cylinders respectively, Re_{crit} is the critical Reynolds number, V_b is the peripheral velocity of the bob, η is the kinematic viscosity of the fluid.

$$Re_{crit} = \frac{V_b(R_2 - R_1)}{\eta} > 41.3\sqrt{\left(\frac{R_2}{R_2 - R_1}\right)} \tag{2.12}$$

During rheological measurements, there is a fluid trapped at the top and bottom of the bob that creates an additional stress on top of the stress generated at the cylindrical section (Klein, 1992). End effects can be reduced by minimizing the sheared surface area, geometry arrangement so that the same shear rate is experienced at the bottom as that for the cylindrical section, adding an extra effective length in the calculation to account for additional stresses (Whorlow, 1992; Klein, 1992).

Particle bridging is encountered when a small gap is used to measure suspensions with relatively coarse particles. However, fine particles can generate large effective particle sizes when flocculated and therefore the gap size effects for flocculated fine particles should not be ignored and the largest available gaps should be used (Barnes, 2000).

In practical situations, the viscometer gap should be at least 10 times the largest particle diameter size (Whorlow, 1992; Barnes, 2000). Similarly, Klein (1992) pointed out that the gap size should be “slightly larger than 10 times the largest particle size to avoid particle bridging” and reduce hydrodynamic instabilities (p.182).

2.3.7 Rheology summary

A good knowledge of factors affecting rheology and its related rheological flow properties is extremely important in the design, optimization and scale-up of mineral processing units including wet ultra-fine grinding mills. From a rheological point of view, mineral suspensions of fine particles are prone to aggregation and agglomeration due to strong interaction of fine particles. Consequently, rheological effects limit throughput rate, lower breakage rate (Tangsathitkulchai, 2003; Yue, 2003; Yue & Klein, 2004), and produce a coarser and broader size distribution of ground product (Mankosa et al., 1989).

Regarding rheological model selection, Barnes (1999) in the paper titled *The yield stress-everything flows?* borrowed Ochham's razor philosophy, "it is inefficient to do with more what can be done with less". This is to say if the two-parameter Bingham model is the best fit, use it, if not use Casson Model or Herschel Bulkley and so on (p. 171).

2.4 Scale-up of stirred media mills

2.4.1 Introduction

The demand for energy-efficient fine grinding technology in mineral processing industry is increasing due to the need to process fine-grained complex precious and base metal ores. Currently, mineral processing industries are witnessing a dramatic increase of size of grinding chamber of stirred media mills (Kwade & Stender, 1998). Therefore, there is a need to accurately design, verify and scale-up stirred media mills to meet the demand.

Table 2.1 shows the increase of the size of grinding chamber for the VXPmills in recent years. The number after 'VXP' indicates the size of grinding chamber in litres e.g., VXP2500, the grinding chamber capacity is 2500 litres. Note that the VXP2500 mill for the Turk mine site listed in the installations outlined in Table 2.1 was the one utilized for the scale-up demonstration study in this work.

This section has reviewed the limitations of existing procedures to scale-up stirred media mills. It has also defined the signature plot and stated its limitations. Reasons for accurate direct scale-up and the common sources of error encountered during scaling up of stirred media mills are also presented.

Table 2.1 List of VXPmill stirred media mill installations (FLSmidth®, 2013)

The following is an installation list for pilot and production mills with a net volume (barrel with grinding assembly installed) of fifty litres or larger. Note that the "Deswik" label has been maintained for mills equipped with hydraulic motors rather than electric.

Location/ Site	Region	Type (#)	Install Date	Product P80 (microns)	Notes
Agrapharm & Unisun	Africa	VXP50(1)	pre 2006	Variable	Chemical Manufacturer
Pachapachi	South America	VXP50(1)	pre 2007	Variable	Silver Mine, Peru, Pilot Testing
Vubachekwe	Africa	VXP50(1)	pre 2007	Variable	Pilot Site Flotation Concentrate Regrind
Barbrook	Africa	Deswik250(1)	pre 2007	Unknown	Decommissioned
Kroondal	Africa	Deswik1000(1)	Mar-06	35	Chromite Dump Retreatment
Tantalite Resources	Africa	VXP50(1)	Jun-06	Variable	Batch Grind Tantalite Salt
Platinum Mile	Africa	Deswik2000(2)	Oct-08	25	PGM Tailings Retreatment
Altyntau	Russia/CIS	Deswik2000(3)	Mar-09	10	Gold Concentrate Regrind
Farvic	Africa	VXP250(1)	Jan-11	60	Gold Tailings and Dump Regrind
Tongon	Africa	VXP500(2)	Jul-11	10	Refractory Gold Sulfide Regrind
Springs	Africa	VXP50(1)	Jul-11	Variable	Current use Insimbi Project
Tharisa	Africa	VXP500(1)	Sep-11	20	Chrome Spiral Tails Regrind
Minera Real de Angles	Mexico	VXP50(1)	Nov-11	Variable	Pilot Testing At Company Sites
Turk	Africa	VXP2500(1)	Dec-11	20	Gold Tailings/Dump Retreatment
Minera Real de Angles	Mexico	VXP2500(3)	May-12 *	10	Pyrite Concentrate Regrind
DRDGold/ Elsburg	Africa	VXP2500(4)	Oct-12 *	19	Gold Tailings Retreatment
DRA/ Randgold	Africa	VXP2500(4)	Dec-12 *	18	Gold Concentrate/Tailings Regrind
MAK/Tsagaan Suvarga	Mongolia	VXP5000(3)	Feb-13*	27	Copper Bulk Concentrate Regrind
Bozshakol Copper Project Clay Plant	Russia/CIS	VXP5000(1)	Oct-13*	25	Copper Flotation Rougher Concentrate

2.4.2 Limitations of using the Bond method for scaling-up stirred media mills

It is customary to scale-up ball and rod mill by using standard Bond ball mill and rod mill grindability tests, respectively. One of the assumptions of the Bond test is that, material is ground from infinite feed size to 80% passing 100 microns.

The Bond method accounts for fineness using grind factor (EF_5) when 80% passing size is less than 75 microns (200 mesh). Yet it is not sufficient in determining energy input in ultrafine grinds for stirred media mills because the factor is used to correct the inefficiency of conventional ball mill on fine grinding (Lichter & Davey, 2006).

The use of the Bond method for fine grinding with stirred media mills has a disadvantage of underestimating the energy requirements due to differences in ball sizes, ball-shell interactions and trajectories (Larson et al., 2011). A scale-up procedure of the VXPmills like other stirred media mills is demonstrated by generating the energy input versus product particle size relationship referred to as a “signature plot.”

2.4.3 Signature plot definition

The common and simplest technique for scaling-up laboratory and pilot-scale stirred media mills is the use of the signature plots. Pure batch tests do not accurately reflect the actual grinding process in a full-scale operation because fresh material is not continuously added during the test work operation as in full scale operation (Larson et al., 2011).

The signature plot is a straight line plot generated when logarithm of product particle size (microns) is plotted against the logarithm of specific energy input (kWh/t). It is based on the number of passes the particles has reported to the mill grinding chamber. The slurry is pumped between the two sumps through the mill and at each pass a sample is taken for particle size analysis and the power input for the particular pass is also recorded. Typically the plot is created by passing the slurry through the mill about 5 times, generating 5 data points.

2.4.4 Limitations of signature plots

Intuitively, the signature plot can simply be extended indefinitely but in reality the plot does not predict the energy input as ground material approaches its grinding limit. Young et al. (2007) once cautioned on the awareness of the “knee” of the signature plots. Larson et al. (2011) also noted on the extrapolation limit of a signature plot to finer sizes. Furthermore, they mentioned that the plot cannot be extrapolated to zero specific energy to predict the mill feed particle size. The plot is only constructed based on the mill product particle sizes and their corresponding specific energy input, the mill feed particle size is not presented in the plot.

2.4.5 Reasons for accurate direct 1:1 scale-up and common sources of error

One of the key advantages of using the signature plots technique is accurate direct 1:1 scale-up (Weller et al., 1998; Jankovic, 2008; Larson et al., 2011). The main reasons for accurate direct 1:1 scale-up include: the use of the same type, size, and load (charge) of media, similar velocities, physics and mechanism, testing with the same slurry type and feed size for pilot as well as full-scale stirred media mills (Gao, et al., 2000; Mannheim, 2011; Larson et al., 2011) Therefore, the mimicking of the full-scale mill using the pilot-scale mill makes both mills experience the same grinding mechanisms.

Larson et al. (2011) outlined the common sources of error for the scale-up of stirred media mills, which include: the measurements of flow rate, slurry density, particle size and viscosity. Other sources of error are the use of inadequate feed testing sample and the accumulation of coarse particles in the mill due to inadequate top size breakage. These sources of error have a significant influence on the scale-up results.

2.4.6 Mill volume dimensions and flow rate

Large IsaMills can be designed based on data obtained from a 1.5-litre laboratory Isamill (Gao et al., 2000). Similarly, Weller et al. (1999) demonstrated a scale-up procedure utilizing a laboratory 4-litre Isamill to predict a motor size for a full scale size 4000-litre Isamill. It was concluded that the specific energy input-product grind size relationship formed the basis for the procedure and it is independent on the size of the mill.

A study was conducted by Weit et al. (1986) using three different mill volumes (5.5, 25.8 and 220 litres) with slurry densities between 10% and 46% by volume and flow rates ranging from 20 to 585 litres/ hour. It was concluded that specific energy consumption was the only criterion for producing a given product size. The slurry density, flow rate and mill volume had no significant influence.

However, Karbstein et al. (1996) pointed out that there is a limit in the size of laboratory stirred mills used for direct scale-up. Their study showed that under similar operating conditions, similar energy was required by three different mills of volume 1, 4 and 25 litres. Conversely, twice as much energy was required for a 0.25-litre mill and therefore based on their study, the minimum volume for direct scale-up was 1 litre.

2.4.7 Media size distribution

Due to continuous wearing of the media for full-scale operations, grinding media are added regularly (seasonal media charging) to maintain the desired media load, which means that the media size distribution is broader than that of the original charge. The mono sized media used in pilot and lab scale units does not exactly mimic the media size distribution of a full-scale mill operation (Weller et al., 1999; Lichter & Davey, 2006). Therefore, it is preferred to blend different sizes of grinding media during pilot-scale testing to reflect the media size distribution present in full-scale operation.

2.4.8 Scale-up summary

It is not appropriate to apply the Bond methods to scale-up stirred media mills. This is because of the differences in grinding mechanisms between the stirred media mills and the conventional ball mills. Apparently, the simplest scale-up technique for the stirred media mills is based on the specific energy input versus product particle size relationship known as the "signature plot." To achieve accurate scale-up results, both pilot and full-scale stirred mills should be operated at similar operating conditions.

For the pilot-scale tests, it is a good practice to blend different sizes of grinding media to reflect the media size distribution of the full-scale mills. Also, the stress intensity of grinding media should be kept constant for both mills in order to achieve constant grinding results. However, the influence of the stress intensity of grinding media on milling efficiency for relatively different mill chamber sizes is still unknown.

2.5 Literature review summary

The operation of stirred media mills is influenced by a significant number of operating variables. These variables include: mill speed, grinding media size and density, slurry density and rheology, feed size and media load. It is important to note that these variables do interact with each other very strongly. Therefore, the influence of individual variables should not be generalized. The influence of the strongest operating variables can be assessed simultaneously using the *stress intensity* of grinding media.

In stirred media mills, the stress intensity of grinding media and specific energy input control the grind size for comminution. The optimum stress intensity does exist in stirred media mills, it is located between the two extremes of stress intensities. Energy utilization is maximum at the optimum stress intensity. To achieve a given grind size, more energy is required at the lower extreme end of stress intensities because the available stresses are insufficient to generate more fractures and therefore multiple stresses are required for particles to be sufficiently broken down. On the other hand, more energy is lost as heat and mechanical friction at higher stress intensities. Therefore, a stirred media mill operated at its optimum stress intensity produces a fine grind size with minimal energy consumption.

It is also important to note that regardless of the operational conditions employed for a particular milling technology, the size reduction process slows down remarkably as particle size decreases. Not only do the number of defects (flaws and cracks) decrease, in the fine grind sizes, but also the size of defects decrease too. Moreover, the chance for fine particles to be *caught* between approaching beads during comminution is relatively minimal as compared to the one for coarse particles treated at similar operating conditions. Therefore, the grinding limit is said to be approached when the breakage kinetics drop significantly as the size of particles decrease. When the grinding limit is approached more energy is required with least size reduction.

Generally, stirred media mills are characterized by ground suspensions of fine particles. The average mean distance between particles reduce with the decrease in particle size, which means that fine particles interact very strongly with each other and hence aggregation and agglomeration is not uncommon. Consequently, stirred media mills suspensions are prone to very high viscosities and yield stresses especially at high solids content. For such high viscous suspensions, the velocity of grinding media is strongly *dampened* to adversely affect the breakage of particles.

It is inappropriate to use Bond rod or ball mill methods to scale-up stirred media mills because of differences in grinding mechanism between the two technologies. Apparently, the simplest and the most appropriate technique used for scale-up of stirred media mills is the use of the signature plot, which is a plot relating the grind size and its corresponding specific energy input. It is a direct 1:1 scale-up, based on the same operating conditions for both (pilot-scale and full-scale) mills. This means that both mills experience a similar grinding environment during comminution.

3 Experimental program

3.1 Methodology

To achieve the objectives outlined in Section 1.3, the following was done:

1. Perform tests utilizing both the batch recycle and the pendulum testing procedures using similar and different sample weights for the two tests. And, recommend the best testing procedure based on the specific energy input-product particle size relationship.
2. Conduct tests using the recommended testing procedure to understand the effect of mill speed, solids content and mill feed particle size on the VXPmill performance.
3. Conduct rheological tests for the VXPmill feed and ground suspensions produced from the tested operating conditions in order to understand the effect of rheology on the comminution process.
4. Determine the BET specific surface area of the VXPmill feed and ground products. Then, use the determined surface area to optimize the VXPmill performance using the energy utilization and the stress intensity of grinding media based on the operating conditions tested.
5. Conduct tests using the recommended testing procedure to demonstrate a scale up utilizing the VXP10 and the VXP2500 mills, both operated at similar operating conditions.

Table 3.1 indicates the typical operating conditions for the VXPmill. However, in the present study lower mill tip speeds (3 and 4 m/s) than the one outlined in Table 3.1 were attempted. Higher and lower solids content (15% and 40% v/v) than the one indicated in Table

3.1 were also attempted. This was done in order to have a broad understanding of their effects on the comminution process in stirred media mills.

The feed particle size (F_{80}) was maintained at 200 μm, although a coarser feed (F_{80} = 300 μm) was also attempted to understand the effect of feed particle size on the comminution process. Other operating variables were kept constant as described further in Section 3.2.3.2.

Table 3.1 Typical operating conditions for the VXPmills (Rahal et al., 2011a)

Operating variable	**Typical range**
Media load (%)	50 – 80 of the net grinding chamber volume
Media size (mm)	1.5 – 3.0
Flow rate	Varies depending on size reduction and the strength of the material
F_{80} (μm)	400 (max)
Mill tip speed (m/s)	10 – 12
Slurry density, solids content	(1.35 – 1.45) kg/l ≡ (42% – 50%) w/w ≡ (22% – 28%) v/v For the ore with the specific gravity of 2.6
Intrinsic media SG	More than 3 × slurry density

3.2 Analysis of process operating variables

3.2.1 Sample preparation

Fresh ore weighing about 600 kg from Barrick Veladero mine (F_{80} = 20 – 30 mm) was used in this work. The ore was crushed in two stages by the HPGR before it was fed to a laboratory cone crusher for further size reduction. The cone crusher feed and product sizes were

6 mm and 2 mm respectively. The ore was then dry ground by a laboratory rod mill, the rod mill product was sieved through a 355 µm sieve size, the undersize was fine enough for the VXPmill feed, whereas the oversize was reground further by the rod mill. The sample was then split into separate buckets using a rotary splitter. Figure 3.1 indicates a simplified flowchart of the sample preparation procedure.

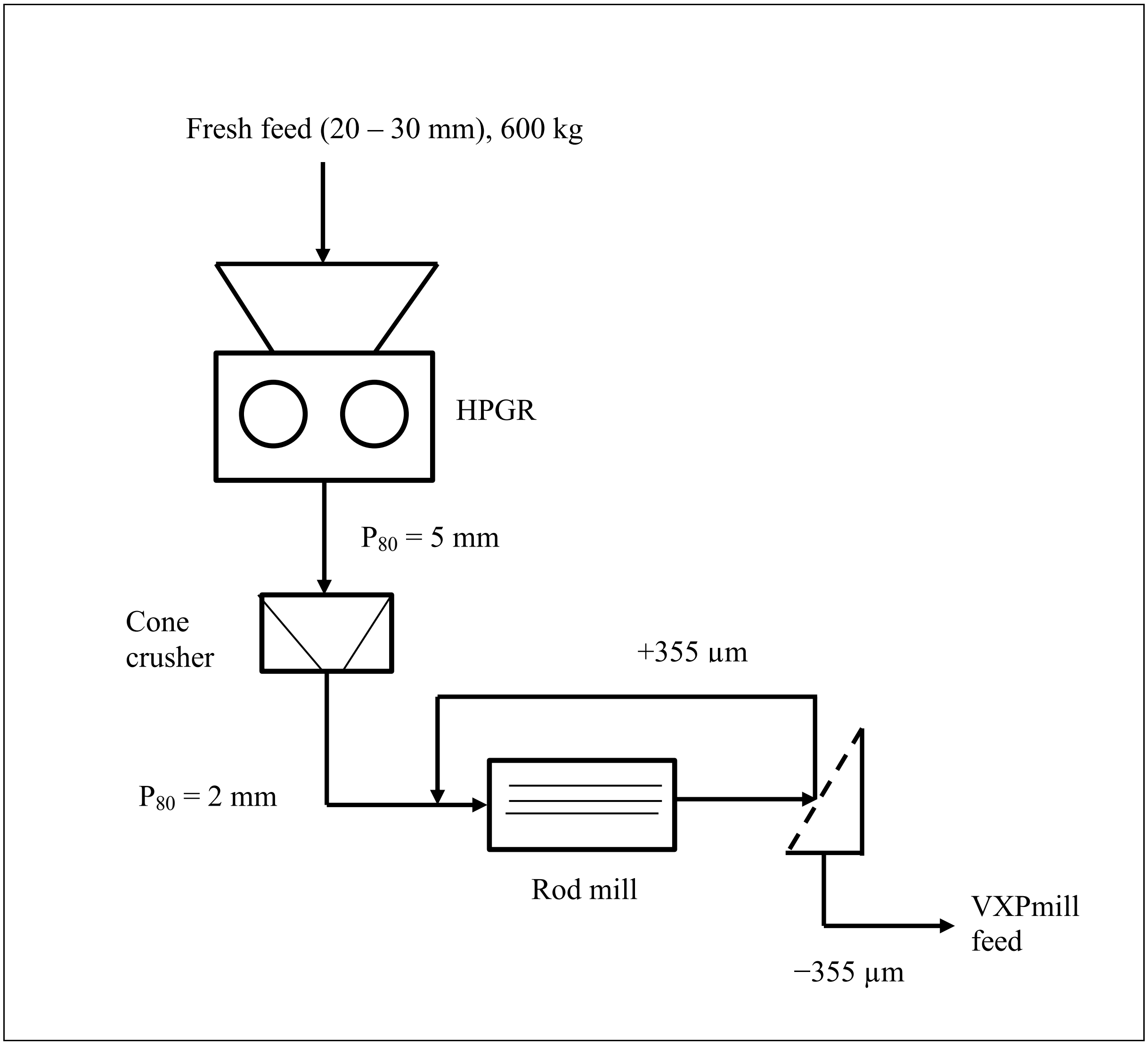

Figure 3.1 A simplified flowchart of sample preparation procedure

3.2.2 Material characterization and experimental methods

3.2.2.1 Mineral composition

The X-ray diffraction for the VXPmill feed sample was conducted and reported by Dr. Elisabetta Pani as mentioned previously in the preface of this work. The X-ray diffractometer used is regularly checked and calibrated.

The sample was reduced to the optimum grain-size range for quantitative X-ray analysis (<10 μm) by grinding under ethanol in a vibratory McCrone Micronising mill for 7 minutes. Continuous-scan X-ray powder-diffraction data were collected over a range 3 – 80° 2θ with CoKa radiation on a Bruker D8 Advance Bragg-Brentano diffractometer equipped with an Fe monochromator foil, 0.6 mm (0.3°) divergence slit, incident- and diffracted-beam Soller slits and a LynxEyeXE detector. The long fine-focus Co X-ray tube was operated at 35 kV and 40 mA, using a take-off angle of 6°.

The quantitative phase analysis of the mineral composition in the VXPmill feed is summarized in Table 3.2. The Rietveld refinement plot of the sample is shown in Figure 3.2. Results indicate that the sample was mainly composed of feldspars (potassic and plagioclase) (43.2%), quartz (23.6%), and mica group (muscovite and biotite) minerals (20%) with small proportions of pyrite (5.7%) by weight.

Table 3.2 Quantitative phase analysis (wt %) for the VXPmill feed (as reported by Dr. Elisabetta Pani, EOAS laboratory UBC)

Mineral	**Ideal Formula**	**Wt (%)**
Quartz	SiO_2	23.6
Clinochlore	$(Mg,Fe^{2+})_5Al(Si_3Al)O_{10}(OH)_8$	2.0
Kaolinite	$Al_2Si_2O_5(OH)_4$	2.4
Muscovite 2M1 - Illite	$KAl_2AlSi_3O_{10}(OH)_2$ - $K_{0.65}Al_{2.0}Al_{0.65}Si_{3.35}O_{10}(OH)_2$-	13.2
Biotite	$K(Mg,Fe^{2+})_3AlSi_3O_{10}(OH)_2$	6.8
Plagioclase	$NaAlSi_3O_8$ – $CaAlSi_2O_8$	13.1
K-feldspar	$KAlSi_3O_8$	30.1
Gypsum	$CaSO_4 \cdot 2H_2O$	0.7
Siderite	$Fe^{2+}CO_3$	1.1
Pyrite	FeS_2	5.7
Chalcopyrite	$CuFeS_2$	0.6
Rutile	TiO_2	0.8
Total		100.0

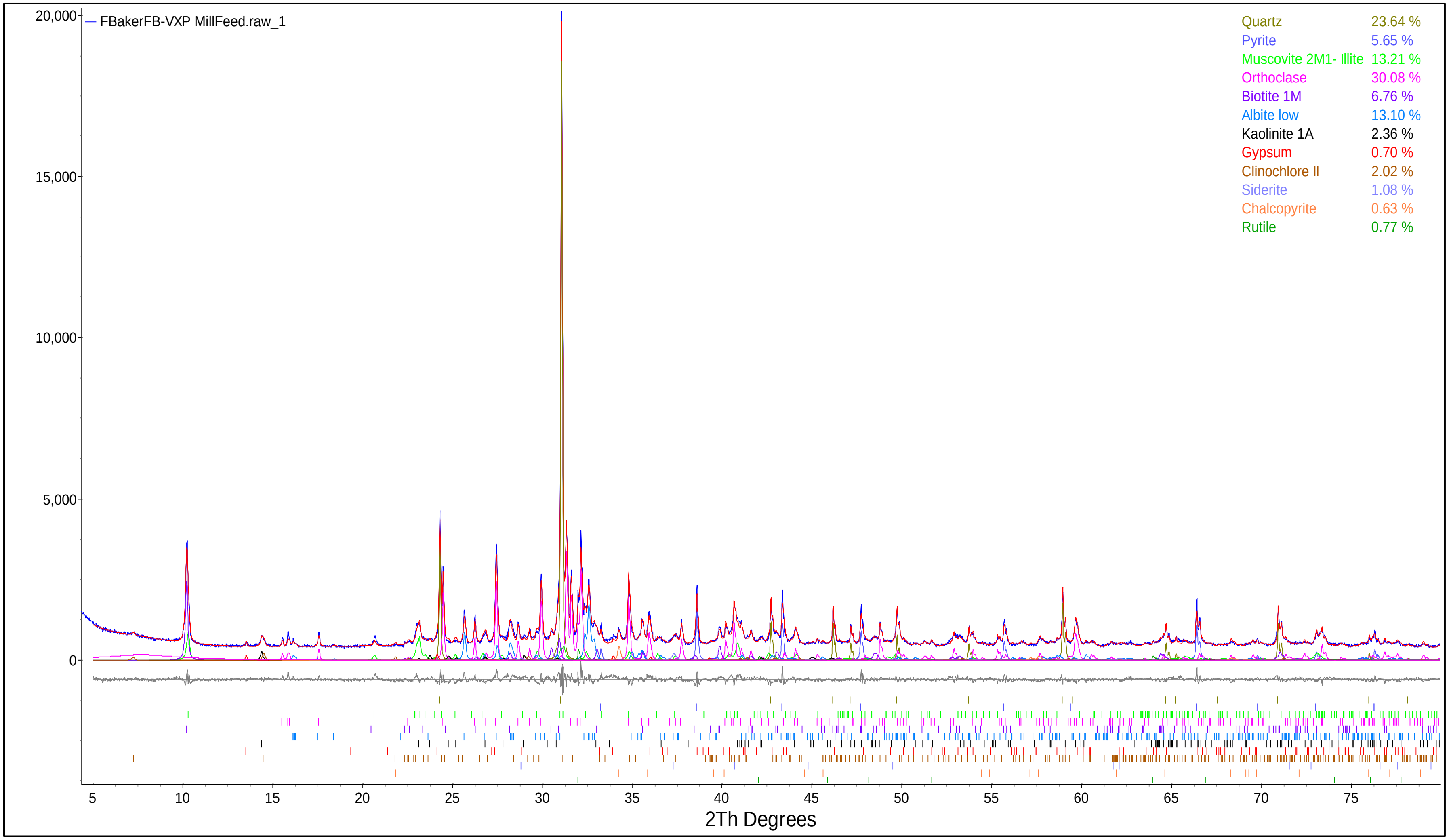

Figure 3.2 Rietveld refinement plot for the VXPmill feed (X-Ray Diffraction)

3.2.2.2 VXPmill feed particle size distribution

The particle size distributions for the HPGR feed and products are presented in Appendix A.1. Generally, for a given feed size distribution, the HPGR in an open circuit generates more fines than conventional crushers (Van der Meer & Gruendken, 2010).

Appendices A.2 and A.3 show the particle size distribution for the VXPmill feed sample utilizing laser diffraction and sieving technique respectively. The F_{80} was about 200 µm for both laser diffraction and sieving. Results for both techniques show that the particle size distribution was significantly broad. This “broadness” was possibly contributed by the presence of fines generated by the HPGR (see Appendix A.1).

3.2.2.3 Determination of ore specific gravity and moisture content

The determination of specific gravity of the ore sample was done using the ASTM D-854. A known weight of dry solid sample was transferred into a clean 2000 mL volumetric flask. Distilled water was then added to the volumetric flask until the flask was two thirds full. The slurry was thoroughly mixed by inverting the flask several times.

The slurry was gently boiled for 20 minutes to remove entrained air in the solid-water mixture. Figure 3.3 shows the slurry samples on the hot plates. Two tests were performed to check for reproducibility. The slurry was then allowed to cool down to room temperature before further addition of distilled water to a 2000 mL mark. The slurry was weighed and the mass of water was determined by subtracting the weight of the dry solids from the weight of the slurry. The volume of the solids was the difference between the volume of the flask (2000 mL) and the volume of water. The specific gravity was calculated based on the mass and the volume of solid sample. Table 3.3 presents the results for the two tests performed.

Figure 3.3 Determination of Specific Gravity of ore

Table 3.3 Data for the determination of specific gravity of ore

	Test 1	Test 2
Volume of volumetric flask (cc)	2000	2000
Weight of dry flask (g)	399.3	417.9
Weight of dry sample (cc)	358.0	358.0
Weight of flask + sample + water after boiling (g)	2619.2	2638.8
Weight of water (g)	1861.9	1862.9
Volume of water (cc)	1861.9	1862.9
Volume of solids (cc)	138.1	137.1
Solids SG	2.59	2.61

Therefore, the average specific gravity of the ore sample was 2.6.

The moisture content of the ore sample was determined by drying the sample in the oven for at least 24 hours and the net weight lost after drying was the moisture content of the sample. Results showed that it was less than 1% by weight.

3.2.2.4 The criteria for selecting grinding media type and size

Rahal et al. (2011a) recommended that in order to achieve the optimum grinding results for vertical stirred mills, the intrinsic density of grinding beads should be at least three times the expected slurry density. For the present work, the slurry density was between 1.2 and 1.6 kg/L equivalent to media density between 3.6 and 4.8 kg/L which gives an average media density of 4.2 kg/L.

Mankosa et al. (1986) and, Yue and Klein (2006) determined the optimum ratio of bead to feed size to be 20:1. However, Zheng et al. (1996) concluded that the best ratio was 12:1. For the present work, the feed size (F_{80}) was about 200 µm, and the size of grinding media used was 2.8 – 3.0 mm, thus the ratio of bead to feed size was about 15:1, which was close enough to both of the criteria recommended by the three studies.

3.2.2.5 Determination of specific gravity of grinding media

The following procedure was used to determine the specific gravity of the grinding beads (media). A known volume of water was weighed in a measuring cylinder. Grinding beads were then added gently into the measuring cylinder, the weight of grinding beads and the net volume displaced were recorded (see Figure 3.4), assuming that the volume of entrained air is negligible. The specific gravity of grinding beads was determined by Equation (3.1) and results are summarized in Table 3.4.

$$Media\ SG = \frac{Grinding\ beads\ weight\ (g)}{Net\ volume\ of\ water\ displaced\ (cc)} \tag{3.1}$$

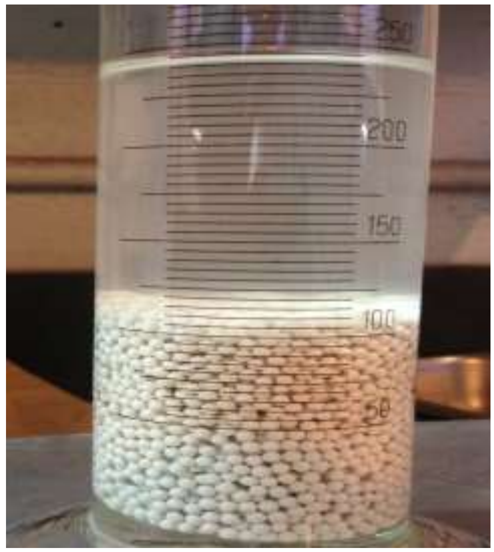

Figure 3.4 Determination of specific gravity of grinding media

Table 3.4 Data for the determination of specific gravity of grinding media

	Test 1	Test 2
Weight of water (g)	199	203
Volume of water (cc)	200	205
Weight of media + water (g)	325	367.8
Volume of media + water (cc)	230	245
Weight of Media (g)	126	164.8
Volume of media (cc)	30	40
Media SG	4.20	4.12

The measured media specific gravity was 4.2 which is in good agreement with manufacturer's specification for zirconium silicate (CZS) grinding beads.

3.2.3 Experimental plan

3.2.3.1 Batch recycle versus pendulum testing procedure

In order to understand the two testing procedures for developing a signature plot, five tests were conducted as summarized in Table 3.5. The first three tests were performed at similar operating conditions, with the only difference being test sample weight and grinding time. On the other hand, the last two experiments were performed at similar operating conditions but with equal test sample weight (25 kg) and grinding time. It should be noted that, when the first three tests indicated in Table 3.5 were performed, the sample was not entirely homogenized which is why the feed particle size was relatively low (F_{80} = 120 µm) than the expected (F_{80} = 200 µm).

Table 3.5 Experimental plan for assessing the batch recycle versus the pendulum testing procedures

Test #	Test description	Mill tip speed (m/s)	Flow rate (L/min)	Solids content (%) v/v
1	Batch recycle (F_{80} = 120 µm), 25 kg sample, 65% media load, grinding duration = 60 minutes	9.5	6.5	25
2	Batch recycle (F_{80} = 120 µm), 55 kg sample, 65% media load, grinding duration = 85 minutes	9.5	6.5	25
3	Pendulum (F_{80} = 120 µm), 40 kg sample, 65% media load, grinding duration = 45 minutes	9.5	6.5	25
4	Batch recycle (F_{80} = 200 µm), 25 kg sample, 50% media load, grinding duration = 54 minutes	10.0	10.0	15
5	Pendulum (F_{80} = 200 µm), 25 kg sample, 50% media load, grinding duration = 54 minutes	10.0	10.0	15

3.2.3.2 Analysis of process operating variables

As described in Section 2.1.1, only process state variables were studied in this work whilst keeping mill configuration variables constant except mill speed. The variables tested include: mill speed, slurry solids content and its rheological effects, and feed particle size (see Table 3.6).

Based on the criteria used in Section 3.2.2.4, grinding media size and specific gravity used were 2.8 – 3.0 mm and 4.2 respectively. For smooth operation, the media load and flow rate were selected to be 50% of the mill grinding chamber volume and 9 −10 L/min respectively. To test the effect of feed particle size on grinding performance, the sample was sieved through a 500 µm sieve size in order to get a coarse feed of F_{80} = 300 µm (see tests number 1 and 2 in Table 3.6), whereas a fine feed size (F_{80} = 200 µm) was obtained using a 355 µm sieve size.

Table 3.6 Experimental plan for analyzing the effect of operating variables on the VXPmill performance

Test No	Feed size, F_{80} (µm)	Mill tip speed (m/s)	Solids content	
			% by volume	% by weight
1	300	12	15	31
2	300	7	15	31
3	200	7	30	53
4	200	12	30	53
5	200	12	15	31
6	200	7	15	31
7	200	10	30	53
8	200	10	15	31
9	200	10	40	61
10	200	7	40	61
11	200	10	40	61
12	200	4	15	31
13	200	3	30	53
14	200	10	35	58

3.2.4 Equipment and procedure

3.2.4.1 VXP10 mill

The stirred media mill used in this work is the VXP10, shown in Figure 3.5. It is a pilot-scale vertical stirred mill designed and fabricated by FLSmidth® at Langley, British Columbia, Canada. Its net grinding chamber volume is 10 litres. It has a variable direct drive motor coupled with a shaft equipped with grinding discs and spacers to provide grinding action as the shaft rotates. Typically, the total number of grinding discs is twelve, each with a diameter of 130 mm.

The mill is bottom fed and discharges at the top through a media retention screen. The screen is fine enough to let the ground slurry pass through while retaining the grinding beads in the mill grinding chamber. The mill is equipped with two sumps with a stirrer in each sump to keep the solids suspended at all times during the test.

The mill is also equipped with a Programmable Logic Controller (PLC) and a user friendly operator station for commands during operation. Data is recorded to a flash drive during operation by logged-on command. The data recorded includes: date and time the test was performed, mill speed in revolutions per minute, slurry flow rate, inlet and outlet temperature of the slurry, mill torque, power draw and mill inlet pressure (FLSmidth, 2012).

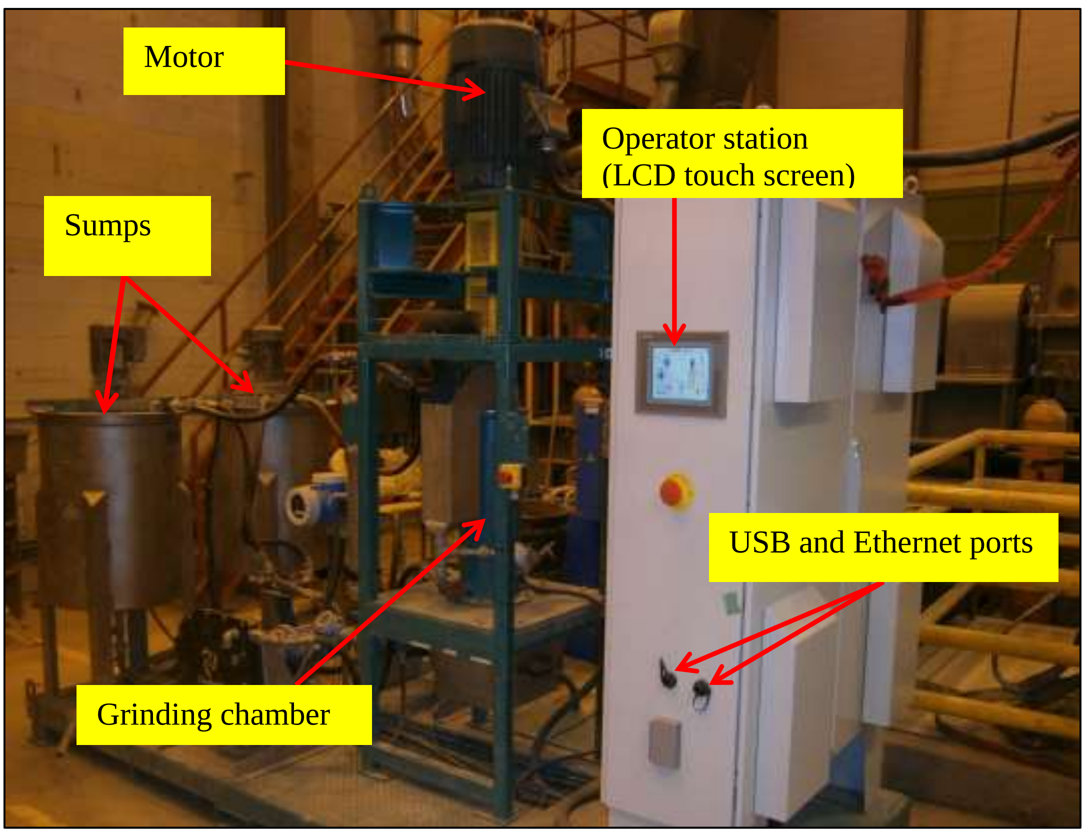

Figure 3.5 Photograph of the VXP10 mill

3.2.4.2 General grinding procedure

For both modes of testing procedure (batch recycle and pendulum) dry sample was gently mixed with tap water in a bucket using a hand mixer to prepare slurries with solids contents of 15%, 30%, and 40% by volume. The slurry was emptied in one of the sumps and the sump agitator was initiated. To ensure proper mixing, the valves were set and the feed pump was initiated to recirculate the slurry while bypassing the mill. Five minutes later, a representative feed sample for the VXPmill was collected for particle size analysis and solids content determination. The flow rate was also checked to ensure that the set point reflected the actual flow rate. A flash drive was inserted to log the data during grinding.

About 12.8 kg of media charge (50% of net grinding chamber volume) of 2.8 – 3.0 mm ceramic media (zirconium silicate) with a specific gravity of 4.2 was added to the VXPmill. The slurry was directed to the mill and at the same time, the mill speed was ramped up to the desired mill tip speed i.e., 3, 4, 7, 10 and 12 m/s.

3.2.4.3 Grinding procedures for batch recycle and pendulum

Both the batch recycle and the pendulum modes share the same procedure described previously in Section 3.2.4.2. The only difference is that in batch recycle, the mill discharge (fine particles) mixes with mill feed (coarse particles) in the same sump, whereas in the pendulum mode, the mill discharge reports to a separate sump. The experimental set up for the two modes are exemplified in Figure 3.6.

For the pendulum mode, initially one sump is full and the other is empty as indicated in Figure 3.6. Sump 1 feeds the mill and the mill discharge reports to sump 2. Therefore, the sequence is sump 1→ feed pump → mill→ discharge pump → sump 2. When sump 1 is empty, a pass is counted. Then, valves are swapped and sump 2 feeds the mill i.e., sump 2 → feed pump→ mill→ discharge pump → sump 1 and the sequence continues. At least five passes are desirable to generate a signature plot.

Depending on the mill flow rate, the grinding time for the batch recycle mode, is between 45 and 90 minutes which is equivalent to five and nine passes respectively for the pendulum mode. Due to the increased wear of grinding discs and media, longer grinding time than 90 minutes is avoided in both testing procedures. Based on the two modes described, it is expected that each mode will display its own response on the specific energy input-product particle size relationship and the best mode will be recommended for scale-up purposes.

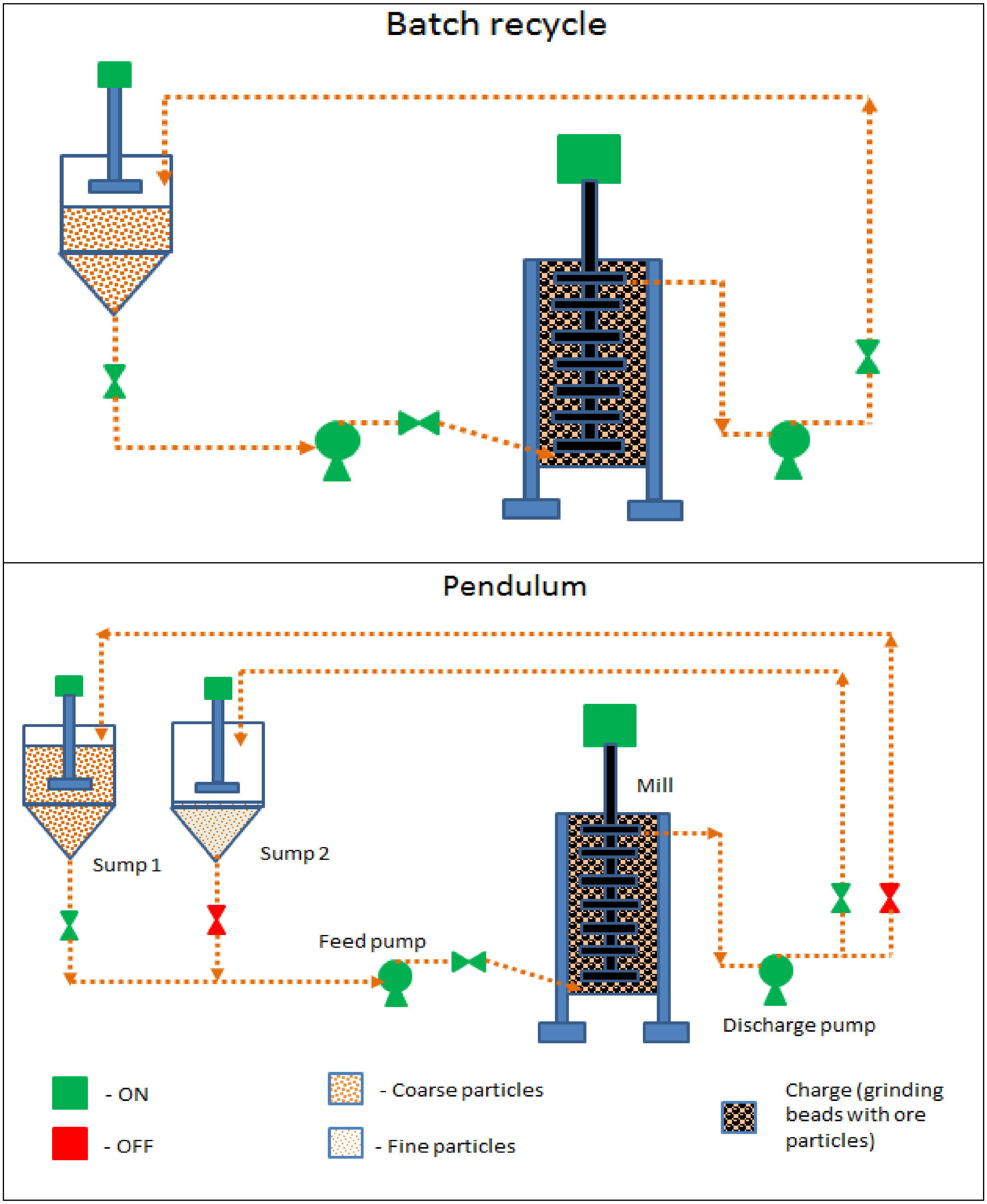

Figure 3.6 A simplified schematic view indicating operational differences between the batch recycle and the pendulum mode

3.2.4.4 Malvern the Mastersizer

The particle size analysis was carried out using the Malvern (the Mastersizer Hydro 2000S) shown in Figure 3.7, with distilled water used as a dispersant. It uses laser diffraction technique to determine the size of particles.

Laser diffraction determines particle size by employing Mie theory with an assumption that all particles are spherical. Depending on particle size, incident light is scattered at different angles. Fine particles exhibit scattering phenomena at larger angles with weaker scattering intensity. Conversely, coarse particles show scattering pattern at smaller angles with stronger scattering intensity (Mie, 1908). Therefore, by knowing the scattering angle, the relative refractive index (the ratio of refractive index of particle to that of the medium) and the wavelength of applied light, the particle diameter can be determined.

Figure 3.7 Photograph of the Malvern (the Masterizer Hydro 2000S)

3.2.4.5 Particle size analysis procedure

Prior to the determination of particle size, the glass slide of the Malvern the Mastersizer was checked and cleaned by wiping it with soft tissue paper. It was then flushed repeatedly with distilled water to remove any particles that could contaminate the sample to be analyzed. The laser was properly aligned before the measurement was initiated. The refractive index used for the analysis was that of quartz (1.54) which is almost the same as that of feldspars group minerals (1.53).

The sample collected from the VXPmill discharge at each pass was emptied in a cylinder equipped with baffles, it was then mixed properly with a desktop mixer. In order to minimize obscuration especially at high solids content, the sample was diluted with distilled water during mixing. The sample was drawn from the bottom of the mixer using an adjustable pipette. It was then emptied into the measuring cell while monitoring the obscuration to keep it within the acceptable range (by observing the obscuration bar).

Finally, the measurement was initiated. To minimize the influence of cross contamination from one sample to the other, the last pass sample was analyzed first followed by the next successive coarser sample i.e., pass 9 → pass 8 →pass 7→ and so on. The cell was flushed twice after each measurement. The measurement was repeated to check for the reproducibility.

3.3 Rheology of ground pulp

3.3.1 Equipment and experimental procedure

3.3.1.1 HAAKE viscometer and its calibration

A rheological measurement is done by measuring the torque required to deform a fluid contained in a well-defined geometry under controlled shear rate. The measured torque (T) is proportional to shear stress (τ), Equation (3.2). The constant 'A'is a shear stress factor.

$$\tau = AT \tag{3.2}$$

In the present study, the rheological measurements of the VXPmill feed and ground products were conducted employing an elongated fixture attached to a rotational viscometer. Figure 3.8 shows the HAAKE Viscotester 550 viscometer with the elongated fixture accessories used in this study. The fixture was developed by Klein (1992). The plan view dimensions of the fixture are shown in Figure 3.9. The radii dimensions were:

r_1 = 1.85 cm,

r_2 =1.95 cm,

r_3 =2.00 cm,

r_4 = 2.11 cm.

The fixture works like any other viscometric fixture, the main difference is that it minimizes the errors associated with the fast settling suspensions, this is due to its comparatively high height (see the fixture in Figure 3.8) as compared to regular fixtures. In the present study, though the specific gravity of ore used was not relatively high (SG = 2.6), the feed particle size was relatively coarse (F_{80} = 200 – 300 μm) and therefore the settling of particles was apparent.

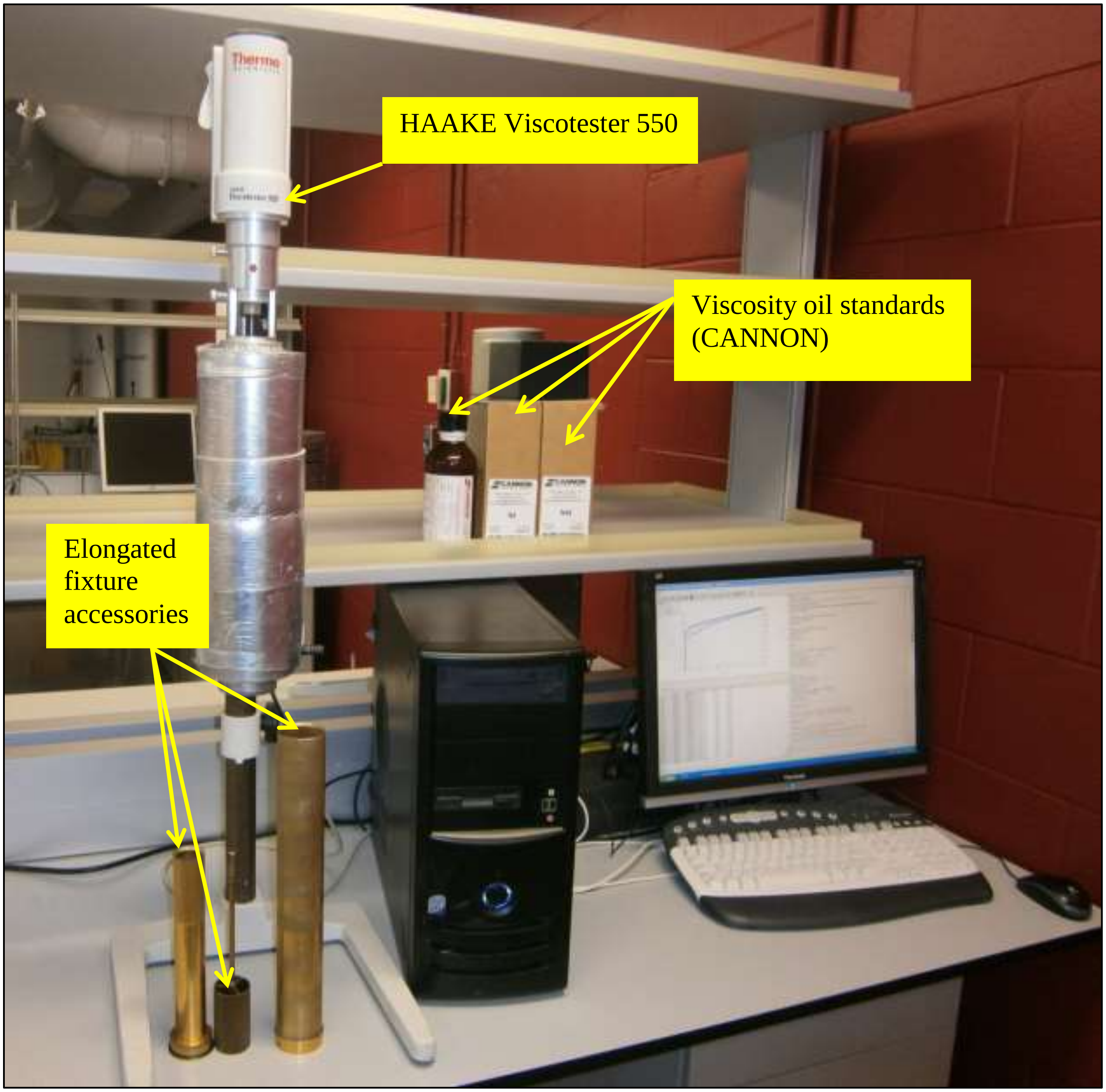

Figure 3.8 Photograph of the HAAKE Viscotester 550 with concentric elongated fixture accessories

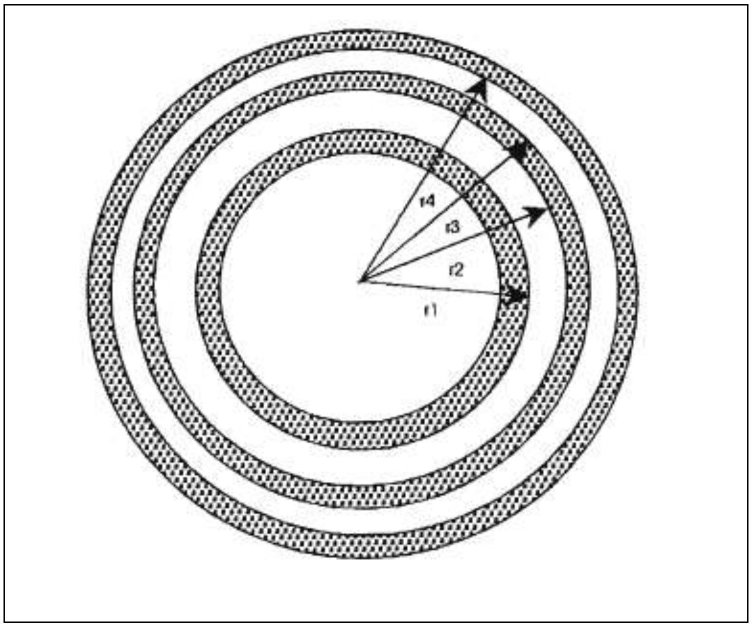

Figure 3.9 Plan view of concentric cylinder fixture dimensions (Klein, 1992)

The calibration of the viscometer was done using three standard oils, CANNON N4, CANNON N44 and CANNON N75 with viscosities 4.8, 74.6 and 155.8 mPas respectively at 25°C. Figure 3.10 indicates the rheological flow curves of the oils. The comparison between the actual and the measured viscosities is indicated in Figure 3.11. Results show that the measured and the actual viscosity values are in excellent agreement.

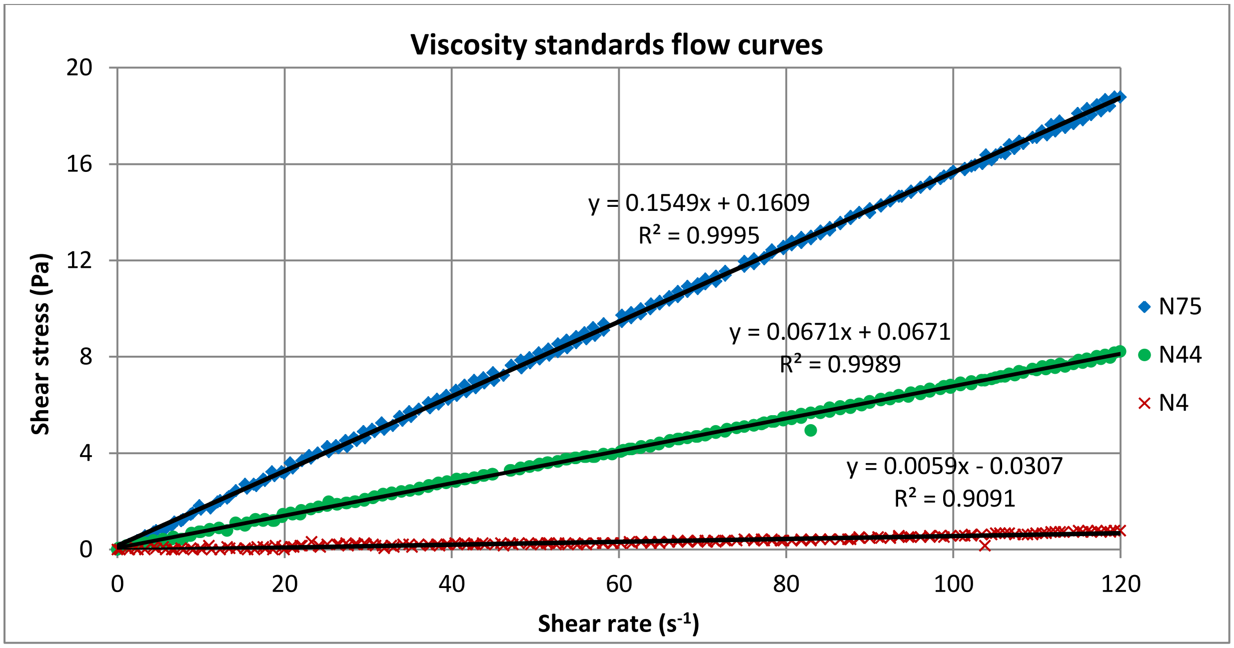

Figure 3.10 Viscosity standards flow curves

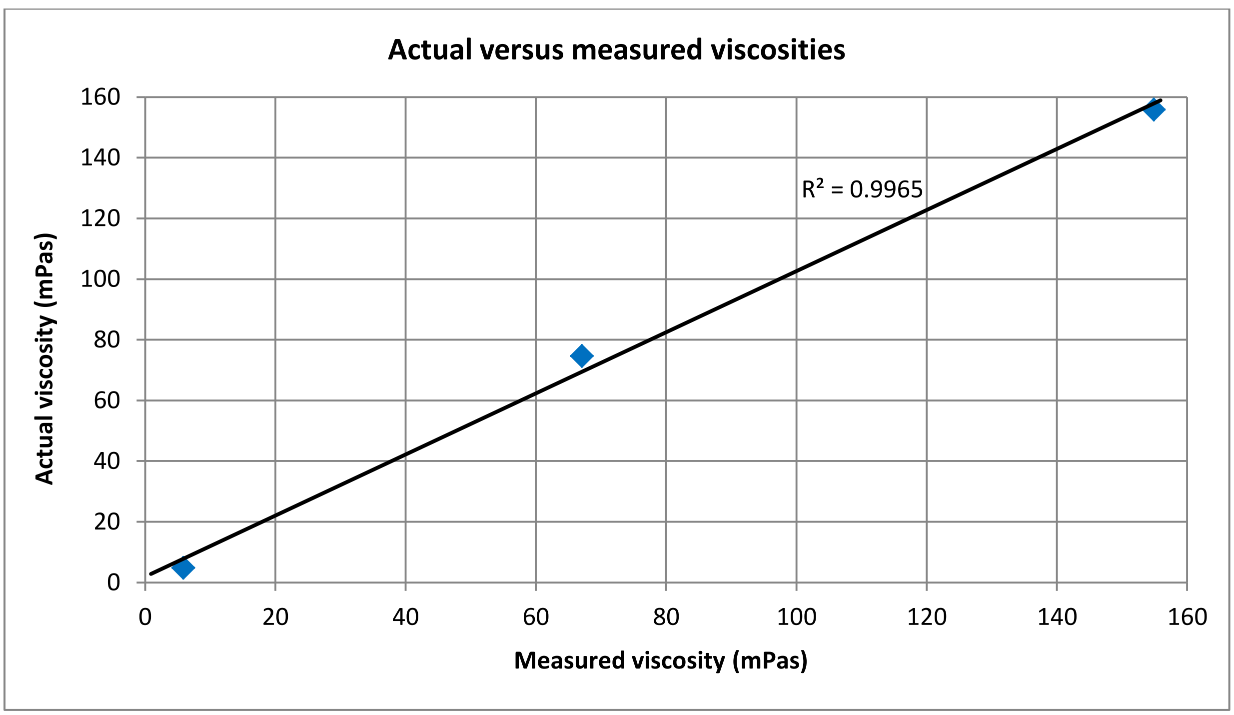

Figure 3.11 Viscosity standards (actual versus measured viscosities)

3.3.1.2 Criterion for selecting the maximum shear rate

As described in Section 2.3.6, one of the major sources of error for rheological measurements is hydrodynamic instabilities (Taylor vortices) that occur when the speed of the bob exceeds its critical speed for the suspensions under test, it is not related with the rheological properties of the suspensions. The criterion for onset of Taylor vortices was determined by Equation (3.3) (Taylor, 1923).

$$v_\theta = \frac{\dfrac{41.3\mu_p}{\rho R_c(1-k)}}{\sqrt{\dfrac{1-k}{k}}} \tag{3.3}$$

where; v_Θ is the tangential velocity in m/s, R_c is the radius of the cup, (considering the outer gap, R_c is 2.33×10^{-2}) m, k is the ratio of bob to cup diameter (considering the outer gap, k is 0.845), μ_p is the viscosity of the slurry under test, the minimum viscosity of the slurry in the present case (15% by volume) is about (13×10^{-3}) Pas.

The relation between rotational and tangential velocity is calculated by Equation (3.4). The shear rate is proportional to rotational speed as indicated by Equation (3.5) where; M is a fixture constant, related to fixture dimensions. It is calculated by Equation (3.6). Based on the radii dimensions of the elongated fixture outlined previously, the value of M is 9.867.

$$v_\theta = \omega R_c \tag{3.4}$$

$$\gamma = M\omega \tag{3.5}$$

$$M = \frac{\pi}{6}\left[\frac{{r_1}^2}{{r_2}^2 - {r_1}^2} + \frac{{r_4}^2}{{r_4}^2 - {r_3}^2}\right] \qquad (3.6)$$

The calculated shear rate for the onset of Taylor vortices at 15% solids by volume was about 120 s^{-1}. Therefore, the maximum shear rate was set at 120 s^{-1} for all rheological tests conducted in this work. However, it is expected that the shear rate for the onset of Taylor vortices is relatively higher for suspensions with 30% and 40% than the one for the 15% solids by volume.

3.3.1.3 Rheological measurements procedure

About 250 mL of VXPmill discharge sample was collected in each pass. Depending on the mill speed and grinding time, each sample collected had its own temperature at the time it was collected. To avoid the influence of temperature on rheological measurements, all samples were left to acquire ambient temperature prior to undertake the rheological measurements. Each sample was mixed by a stirrer for 2 minutes and quickly transferred to the viscometer prior to the initiation of the rheological measurements.

The viscometer reading was adjusted to zero prior to the initiation of rheological flow. The shear rate was ramped up from 0 to 120 s^{-1} in 2 minutes and ramped down from 120 to 0 s^{-1} for the other 2 minutes. During rheological flow measurements, about 100 data points of shear rate-shear stress were recorded for each ramp.

3.3.1.4 Rheological flow curve fitting

In order to determine the yield stress and the viscosity values for the suspensions, the flow curves were fitted using the Bingham, the Herschel Bulkley and the Casson models. Appendix D.1 presents rheological flow curve model fittings for the VXPmill feed and ground products (with 30% solids content by volume) when the mill was operated at a tip speed of 12 m/s, only ramp-up parts are indicated.

The Bingham model does not sufficiently fit the flow curves especially at low shear rates (see Appendix D.1 and values of R^2 shown in Appendix D.2). The model tends to overestimate the yield stress by extrapolating a linear section of the flow curve. Other researchers reported similar observations (Yue & Klein, 2004).

The Herschel Bulkley model fits very well as seen from the high values of R^2. However, the model gives “meaningless negative” yield stress values (see Appendix D2). Kelessidis et al. (2006) also reported similar observations in drilling fluids.

The Casson model fits quite well with decent values of R^2 and good estimation of yield stress. Furthermore, its coefficient has physical and meaningful significance. This observation is in good agreement with the work done by Klein (1992) using magnetite suspensions. Therefore, the Casson model was the best choice in the present study, it was then used to determine the yield stress and apparent viscosity values of the suspensions.

3.4 Determination of stress intensity of grinding media and energy utilization

3.4.1 Stress intensity

The effect of the most influential variables on the performance of stirred media mills was analyzed by employing the stress intensity approach. Since the centrifugal stress intensity is expected to be much higher than the gravitational stress intensity for the VXPmill, the total stress intensity was calculated based on Equation (3.7).

$$SI_m = D_m{}^3(\rho_m - \rho)v_t{}^2 \tag{3.7}$$

3.4.2 Energy utilization

Energy utilization is defined as the incremental surface area (ΔS) produced during comminution per unit of specific energy consumption, it is calculated using Equation (3.8).

$$EU = \frac{\Delta S}{E} = \frac{10^6 \times (S_p - S_f)}{E} \tag{3.8}$$

During the test, the energy consumption was logged to the flash drive and also manually recorded from the LCD (Liquid Crystal Display) touch screen, whereas the specific surface area of the sample was determined using the BET 11 multipoint method employing the Quantachrome Autosorb 1.

3.4.3 Experimental procedure for correlating the BET surface area with particle size

In order to observe the BET surface area-particle size correlation over a broad range of grind sizes, the samples of different grind sizes were selected. The VXPmill feed, pass 1, pass 6 and pass 9, each measuring about 250 mL of wet sample i.e., (300 g dry weight) was collected. The samples were then dried in the oven for more than 24 hours. They were rolled, homogenized and representatively split using a small riffle splitter (demonstrated in Figure 3.12 until the small representative sub-samples were obtained for the particle size analysis (Laser diffraction method) and the BET surface area determination. The BET surface area was determined using the Autosorb-1 Quantachrome shown in Figure 3.13, whereas the particle size analysis was carried out using the Malvern (the Mastersizer Hydro 2000S) shown previously in Figure 3.7.

Figure 3.12 Riffling samples for the BET surface area and particle size by laser diffraction

Figure 3.13 Photograph of the Autosorb-1 used for the BET surface area determination

Prior to undertake the tests, the Autosorb-1 was checked and calibrated. To determine the surface area, each sample was outgassed in a 6 mm bulb to remove all physisorbed species from the solid surface. The outgassed weight was obtained prior to the determination of the adsorption isotherm. Outgassing at elevated temperature was avoided in order to maintain the integrity of the sample. Therefore, the outgassing was done at ambient temperature (about 24°C) for at least 21 hours and all samples "passed" the outgassing test criteria prior to the termination of outgassing stage.

The level of liquid nitrogen in a measuring bath was checked and topped up after each test. The liquid nitrogen trap bath was also topped up after each outgassing cycle to ensure that the sample bulb was wholly immersed in liquid nitrogen. A filler rod was inserted in the bulb prior to the determination of the adsorption Isotherm. This was done to reduce the dead volume during determination of the adsorption isotherm.

The amount of pure nitrogen gas (99.99% purity) adsorbed on the solid surface at equilibrium pressure was determined after successive introduction of nitrogen gas from 0.05 to 0.3 in 0.025 mm Hg increments i.e., (BET 11 multipoint). The adsorption measurements were performed at 77K (at the boiling point of liquid nitrogen).The volume of gas required to form a monolayer was determined by plotting the relative pressure (P/P_0) and the adsorbed volume of nitrogen at equilibrium pressure. The BET (Brunauer-Emmett-Teller) surface area was then calculated based on Equations (3.9) and (3.10) (Brunauer et al., 1938).

$$\frac{P}{n_a(P_0 - P)} = \frac{1}{n_m C} + \frac{(C-1)}{n_m C} \times \frac{P}{P_0} \tag{3.9}$$

$$SSA\ BET = n_m \times L \times a_m \tag{3.10}$$

where;

SSA BET = BET specific surface area,

n_a = amount of adsorbate adsorbed, n_m = monolayer capacity,

a_m = molecular cross-sectional area of adsorbate, C = constant depending on isotherm shape, P/P_0 = relative pressure, L = Avogadro’s constant.

3.4.4 The correlation between the BET surface area and particle size

The relation between the specific surface area (BET multipoint) of the sample and its particle size by laser diffraction is presented in Figure 3.14 (see the data in Appendix E). For the tested samples, it shows that the specific surface area increases with the decrease in particle size and this relationship follows the power law. One of the possible reasons for the high surface area of the VXPmill feed sample is because of large proportions of fine particles in the sample as indicated in Appendices A.2 and A.3.

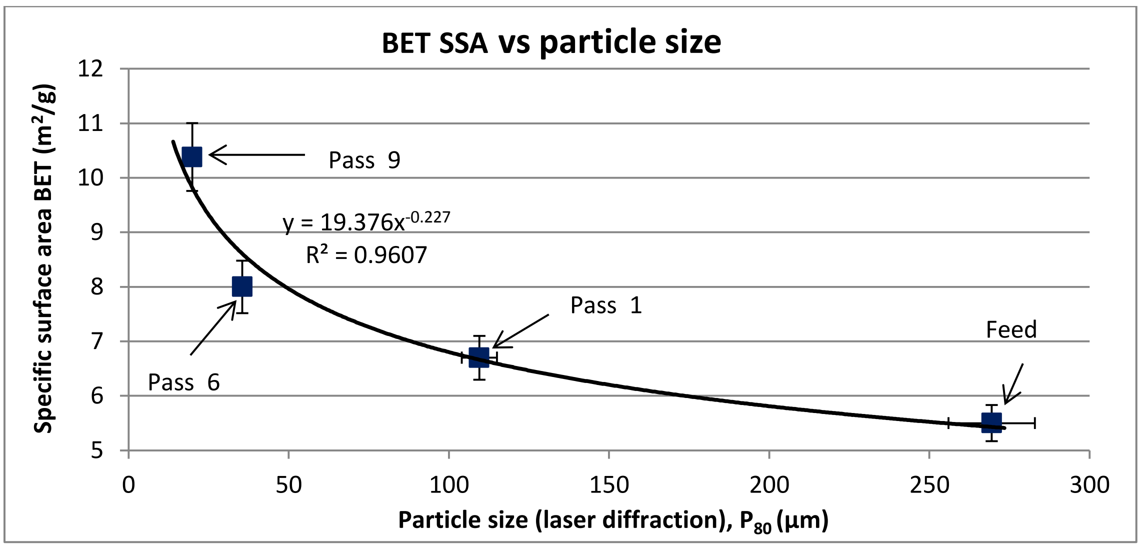

Figure 3.14 The BET specific surface area versus the particle size (Laser diffraction)

Therefore, the surface areas for all the samples in this work were calculated based on Equation (3.11) (power law relationship between surface area and particle size), and then the energy utilization was calculated using Equation (3.8).

$$BET\ SSA = 19.376 * {P_{80}}^{-0.227} \tag{3.11}$$

4 Results and discussion

4.1 Batch recycle versus pendulum tests

The specific energy input-product particle size relationship for both the batch recycle and the pendulum modes of operation is shown in Figure 4.1. All three tests were operated at similar operating conditions except test sample weight and grinding time as described in Section 3.2.3.1 (see tests number 1, 2, and 3 in Table 3.5).

Since a single sump is employed for the batch recycle test, the mill feed and discharge mix together in the sump. And therefore, the residence time distribution for each individual particle is different from the other. This means that all particles are not broken down uniformly as they report to the mill grinding chamber. The inconsistency of breakage of particles in the batch recycle test leads to more energy requirement. Moreover, with an increase in the number of particles, the chance for all particles to be broken down uniformly is even less, which is why the 55 kg sample required more energy than the 40 kg.

Conversely, the utilization of two sumps for the pendulum test (one sump for the mill feed and the other for the mill discharge) for a given pass number makes the residence time distribution for all particles to be similar. This means that at a given pass number, all particles are uniformly broken down each time they report to the mill grinding chamber, hence less energy requirement.

However, as particle size decreases, the number and size of defects decrease too, which is why the trends for both modes approach one another in the fine grind sizes. A similar observation was revealed when equal test sample weight (25 kg) was used for both testing modes as indicated in Figure 4.2. It can also be observed that at the end of the test, finer grind sizes were obtained for the two batch recycle tests than the one for the pendulum (see Figure 4.1), this is because the batch recycle tests had relatively longer grinding time than the pendulum (85 and 60 minutes versus 45 minutes); whereas in Figure 4.2 the grinding time for both testing modes was 54 minutes, eventually, the same grind size was obtained at the end of the test for both testing modes.

General observations show that under similar operating conditions, the batch recycle mode requires more mill power draw by up to 3 to 4 times the one required by the pendulum mode over a broad range of grind sizes. Also, the pendulum mode is not very sensitive to sample weight as compared to the batch recycle mode. However, more sample weight is desired in order to acquire a steady-state for the comminution in the pendulum mode.

Therefore, the batch recycle mode is not suitable for scale-up purposes. Instead, the pendulum mode should be used because all particles are uniformly broken down each time they report to the mill grinding chamber. This mimics the breakage mechanism existing in full-scale operation.

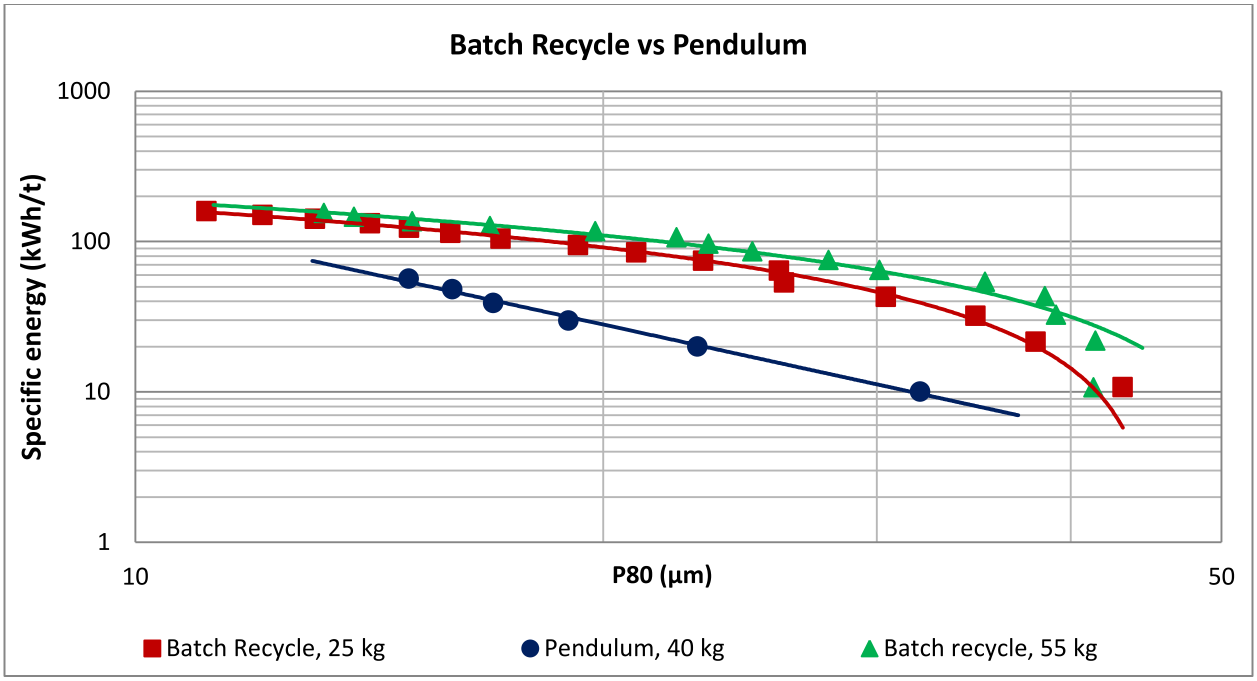

Figure 4.1 Batch recycle versus pendulum for different sample weights

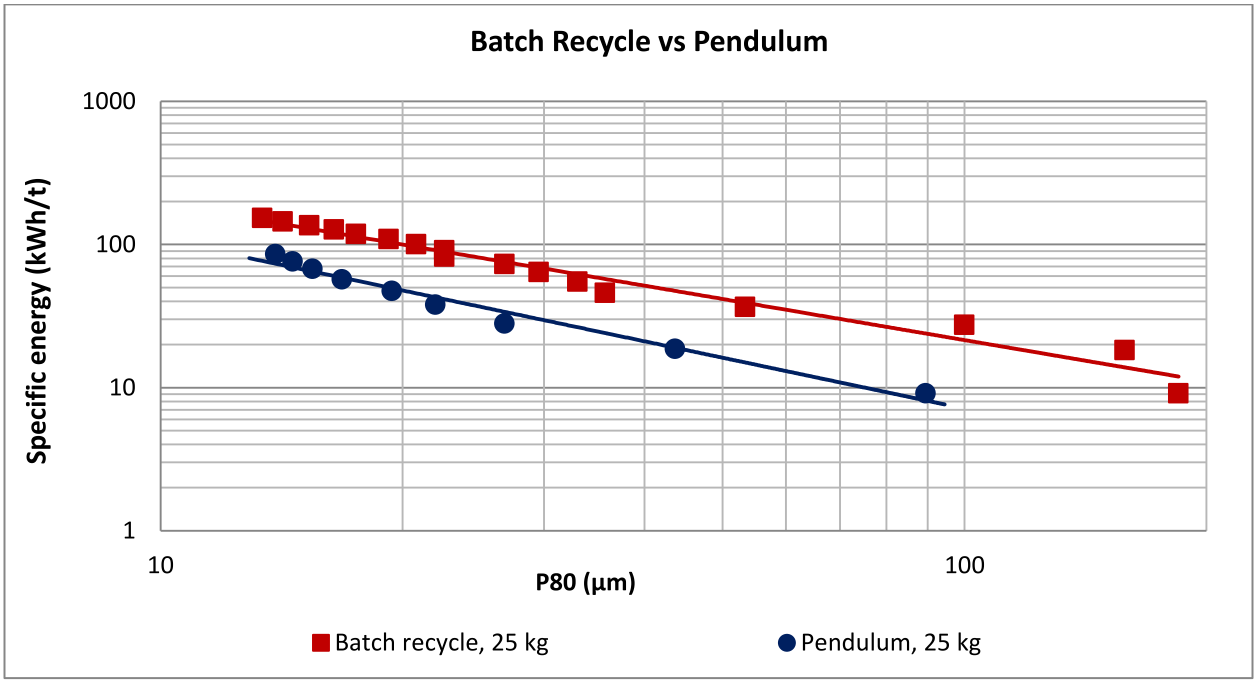

Figure 4.2 Batch recycle versus pendulum for the same sample weight

4.2 Analysis of process operating variables

4.2.1 Effect of mill speed and solids content on size reduction

The size reduction ratio is defined as the ratio of mill feed particle size at a given pass number to its corresponding product particle size at the same pass number. Figure 4.3 shows the effect of mill tip speed on size reduction ratio at 15% and 30% v/v solids content.

In the coarse fraction grind sizes, the size reduction ratio increases with the increase in mill speed and the decrease in solids content. At very low mill speeds i.e., 3 and 4 m/s, the stress intensities of grinding media are not sufficient to effectively break down particles and hence minimal size reduction ratios are attained over a broad range of grind sizes (see Figure 4.3). As mill speed increases from 7 to 12 m/s, the stress intensity of grinding media increases too, and consequently particles are sufficiently broken down. For low solids content (15% v/v), the chance for particles to be selected for comminution is higher as compared to the one for high solids content (30% v/v), that is why the size reduction ratio increases as solids content decreases. Similar observation was made for 40% v/v solids content.

However, in the fine fraction grind sizes, the size reduction ratio decreases with the decrease in particle size, and the effects of mill speed and solids content on size reduction disappear as reduction ratio approaches 1, since the grinding limit is said to be approached. The existence of the grinding limit indicates that as particle size decreases, the number and size of flaws and cracks decrease too, which means less propagation of cracks and eventually less breakage of particles (Reem, 2011).

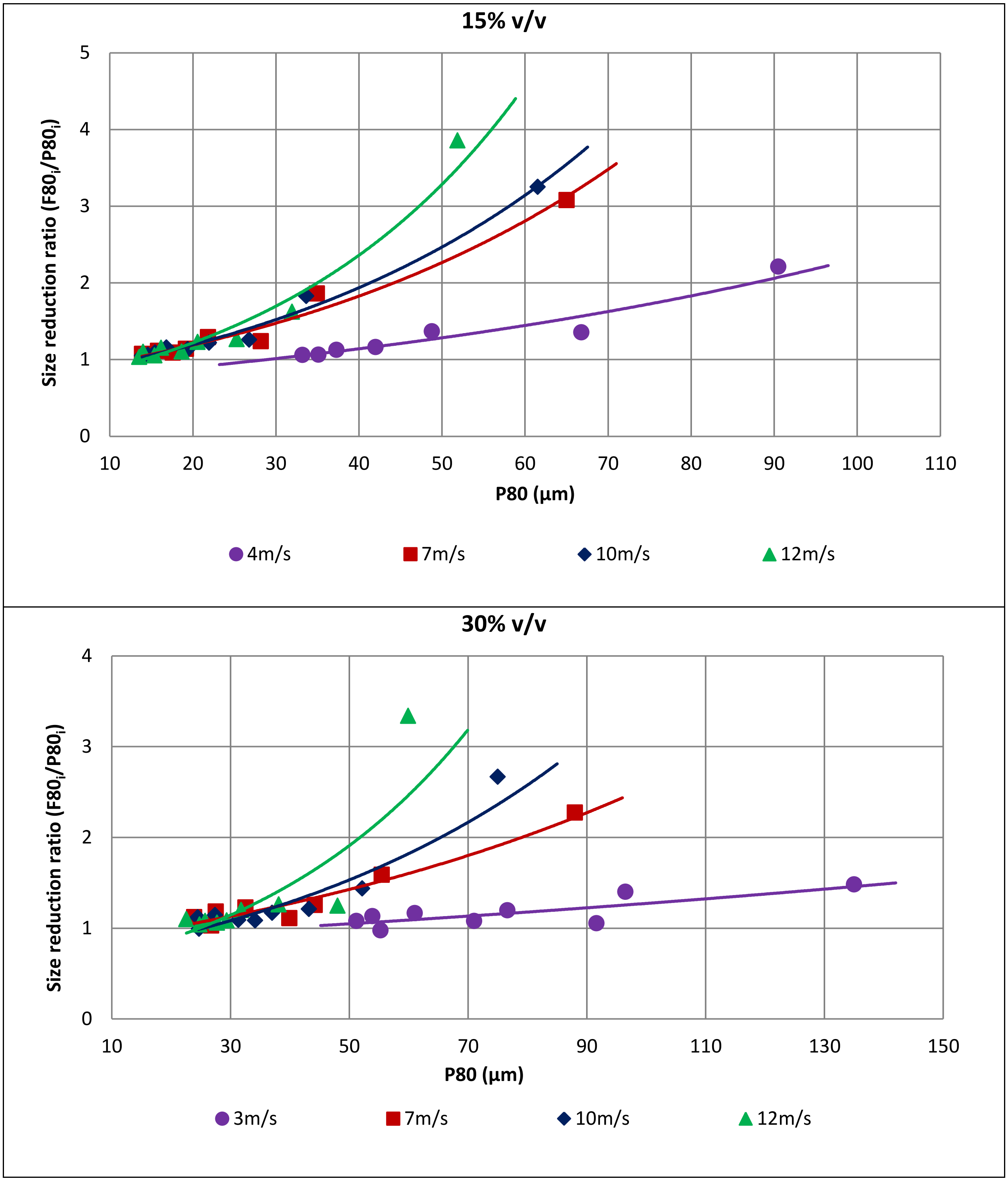

Figure 4.3 Effect of mill speed on size reduction

4.2.2 Effect of mill speed on energy consumption

Mill speed is one of the strongest variables influencing the comminution process for stirred media mills. The effect of mill speed on energy consumption at fixed solids content is presented in Figure 4.4. The general trends indicate that at a given specific energy input, increasing mill speed from 7 to 12 m/s lowers grinding efficiency over a broad range of grind sizes. However, at relatively lower mill speeds i.e., 3 and 4 m/s, grinding efficiency decreases dramatically in the fine grind sizes.

Grinding inefficiency at higher mill speed is caused by the energy losses due to mechanical friction and heat. Another explanation for energy inefficiency at high mill speed is the decrease in effective volume for comminution due to the formation of a large vortex generated at the centre of the mill. Similar observations were presented by other researchers (Gao & Forssberg, 1993a; Mankosa et al., 1989; Wang et al., 2004).

Conversely, the decrease in grinding efficiency at relatively lower mill tip speed in the fine grind sizes was due to lower energy transfer for effective comminution as a result of lower kinetic energy of the grinding beads. Therefore, multiple stresses are required to break down the particles effectively to fine grind sizes, hence more energy requirement.

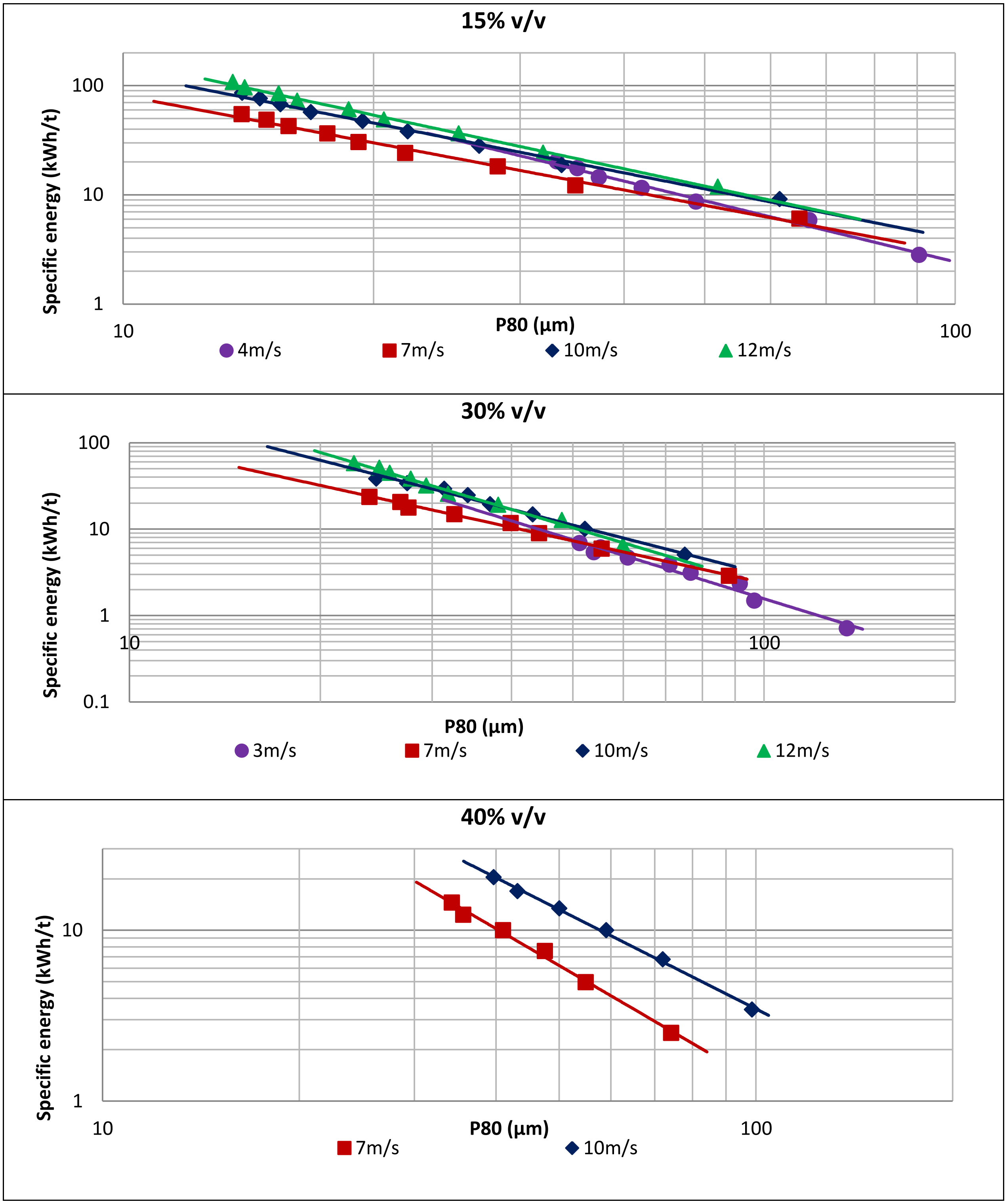

Figure 4.4 Effect of mill speed on energy consumption

4.2.3 Effect of feed particle size on energy consumption

The effect of feed particle size on energy consumption at 15% solids by volume for 7 and 12 m/s mill tip speeds is shown in Figure 4.5. A coarser feed required more stress events i.e., more energy requirement to achieve the same grind size as a finer feed. For this case, in order to achieve 30 µm grind size, up to 30% more energy was required for the coarser feed size as compared to the finer feed. The coarser and the finer feed particle size curves approach one another due to the existence of grinding limit in the fine grind sizes.

Since the same media size was used for both feed sizes, the ratio of bead to feed particle size for the coarse feed size (F_{80} = 300 µm, bead size = 2.8 – 3.0 mm) was about10:1; which was relatively lower than the optimum ratio described Section 3.2.2.4. Conversely, for the fine feed size (F_{80} = 200 µm, bead size = 2.8 – 3.0 mm) the ratio was about 15:1; which is close to the optimum ratio. Therefore, the size of grinding media used was unable to break down the coarse feed top size particles due to insufficient impact and ultimately, more stress events were required (more energy consumption) for the particles to be broken down sufficiently.

In practical situation, the feed particle size for full-scale operations varies as described further in chapter five and therefore it is the best practice to blend grinding media of different sizes in proportions to encounter the feed particle size variations; a coarse media size is effective for the coarse feed particle size and a fine media size for the fine feed particle size as described previously in Section 2.1.2.2.

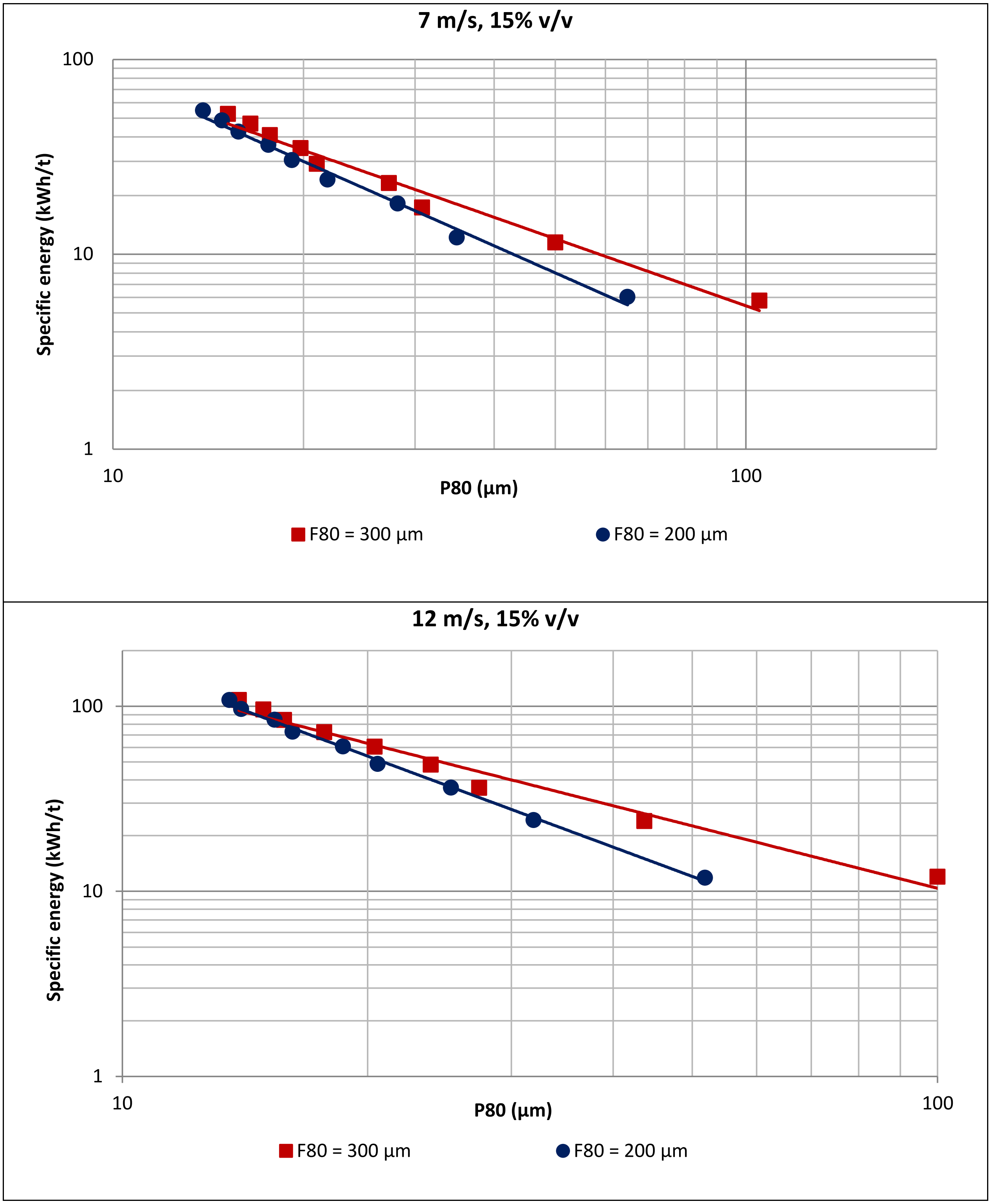

Figure 4.5 Effect of feed particle size on energy consumption

4.2.4 Effect of solids content on energy consumption

The effect of solids content of slurry on specific energy input for a given mill tip speed is presented in Figure 4.6. The effect of solids content was not very sensitive particularly at 7 m/s for the range of solids content tested. However, for higher mill tip speeds i.e., 10 and 12 m/s, grinding efficiency decreases as solids content increases particularly in the fine grind sizes.

The energy inefficiency at higher mill tip speed is possibly contributed by the interaction of rheological effect and the large vortex created at the centre of the mill particularly at higher mill tip speed. Rheological effect becomes increasingly important to adversely affect energy transfer for further comminution as solids content increases and particle size decreases. Figure 4.7 supports the observations obtained in Figure 4.6 by indicating the response of specific energy input at various solids content and grind sizes for 7 and 10 m/s mill tip speeds. Due to rheological effect, as solids content increases, the specific energy input increases particularly for fine grind sizes (see Figure 4.7).

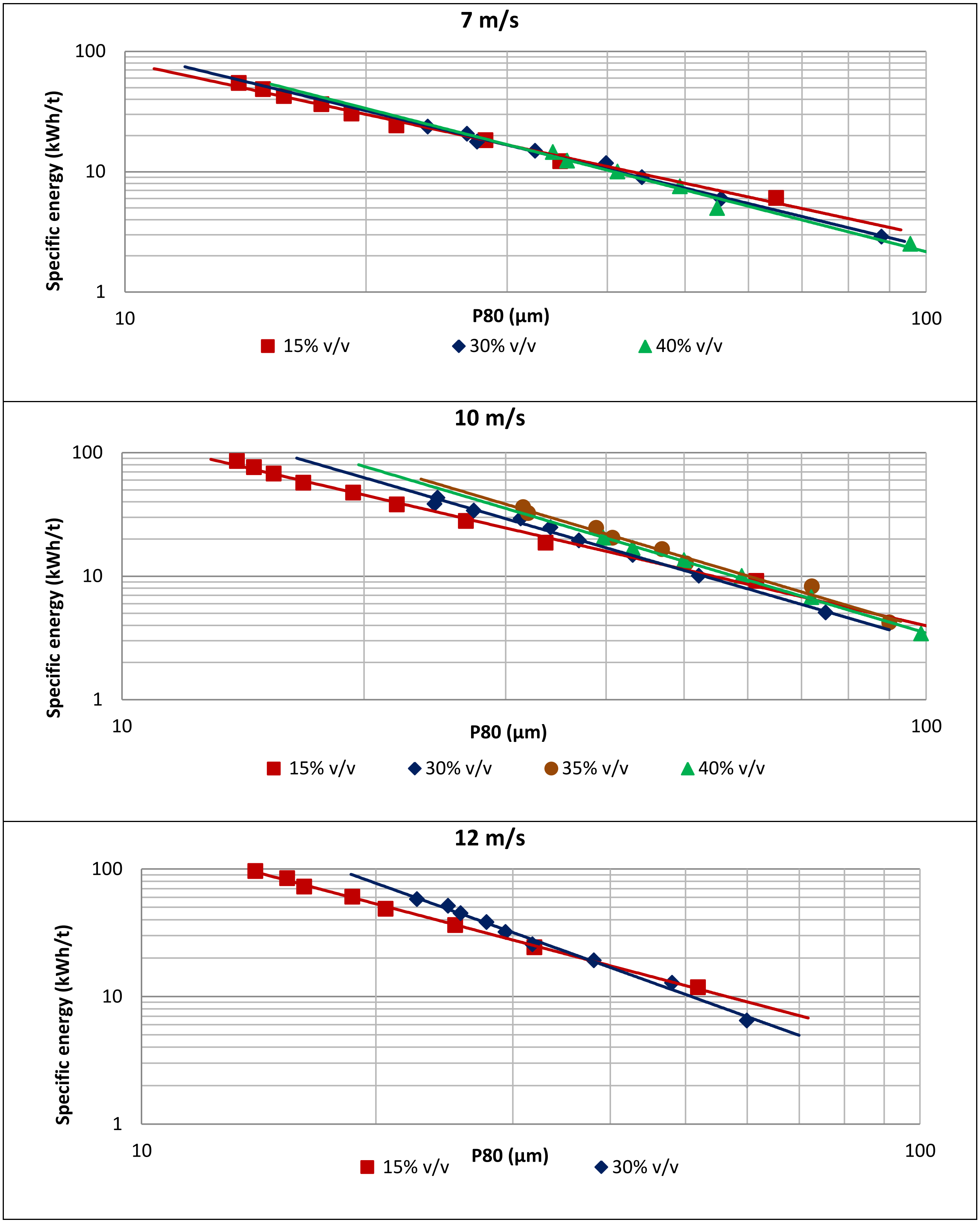

Figure 4.6 Effect of solids content on energy consumption

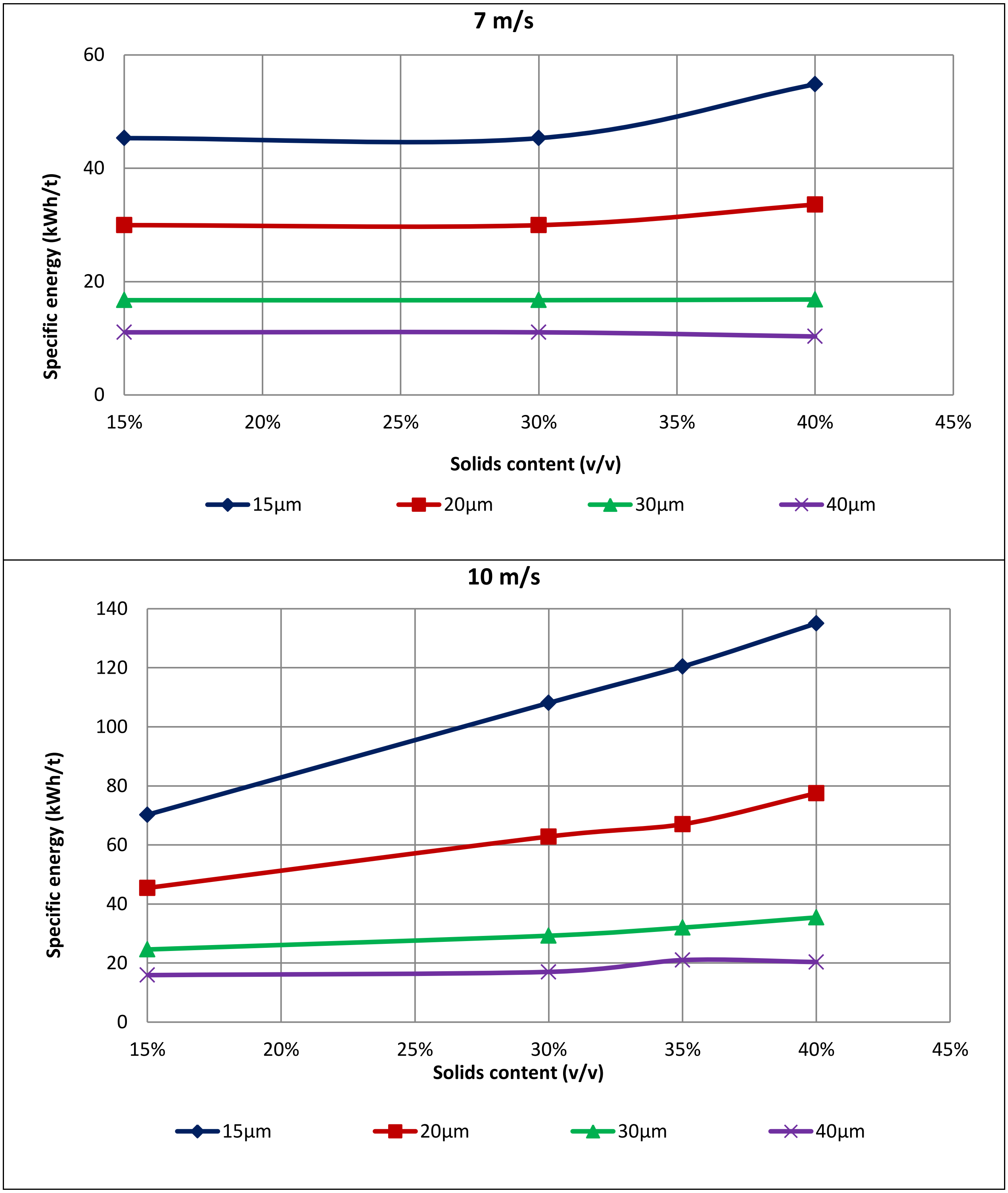

Figure 4.7 Effect of solids content on energy consumption at various grind sizes

4.2.5 Rheological effects on energy consumption

Figures 4.8 and 4.9 show the effect of apparent viscosity (at a shear rate of 100 s^{-1}) and yield stress of ground suspensions on the specific energy input for the given solids contents and mill tip speeds respectively. The energy input increases with the increase in the apparent viscosity and yield stress. This is because the kinetic energy of grinding beads is significantly reduced for particles to be broken down sufficiently as the apparent viscosity and the yield stress of ground suspensions increases.

It can also be observed that for the given mill tip speed, the increase in specific energy input is very sharp for 15% as compared to 30% and 40% v/v solids content. This is because of the high size reduction achieved at low solids content as described in Section 4.2.1; the higher the size reduction, the finer the grind size is achieved and the more the energy is required (fine particles have less number of defects). Moreover, the effects of apparent viscosity and yield stress on the specific energy input increase with the increase in mill speed, this is due to the formation of the vortex and the energy losses as described previously in Section 4.2.2.

The effect of solids content on yield stress and apparent viscosity at various grind sizes and mill tip speeds is indicated in Appendices D.3 and D.4 respectively. It shows that the yield stress and the apparent viscosity increases exponentially with solids content and the effects are more obvious as particle size decreases. Using different materials, a similar observation was made by other researchers (Tangsathikulchai & Austin, 1988; Klein, 1992; Gao & Forssberg, 1993b; Yue & Klein, 2004; He et al., 2004). At high solids content, particles are more closely packed together (high resistance of free movement of particles). Also, fine particles do interact very strongly due to strong aggregation and Van der waals attraction forces. The combined effect is the increase in viscosity and yield stress at higher solids content and finer particle sizes.

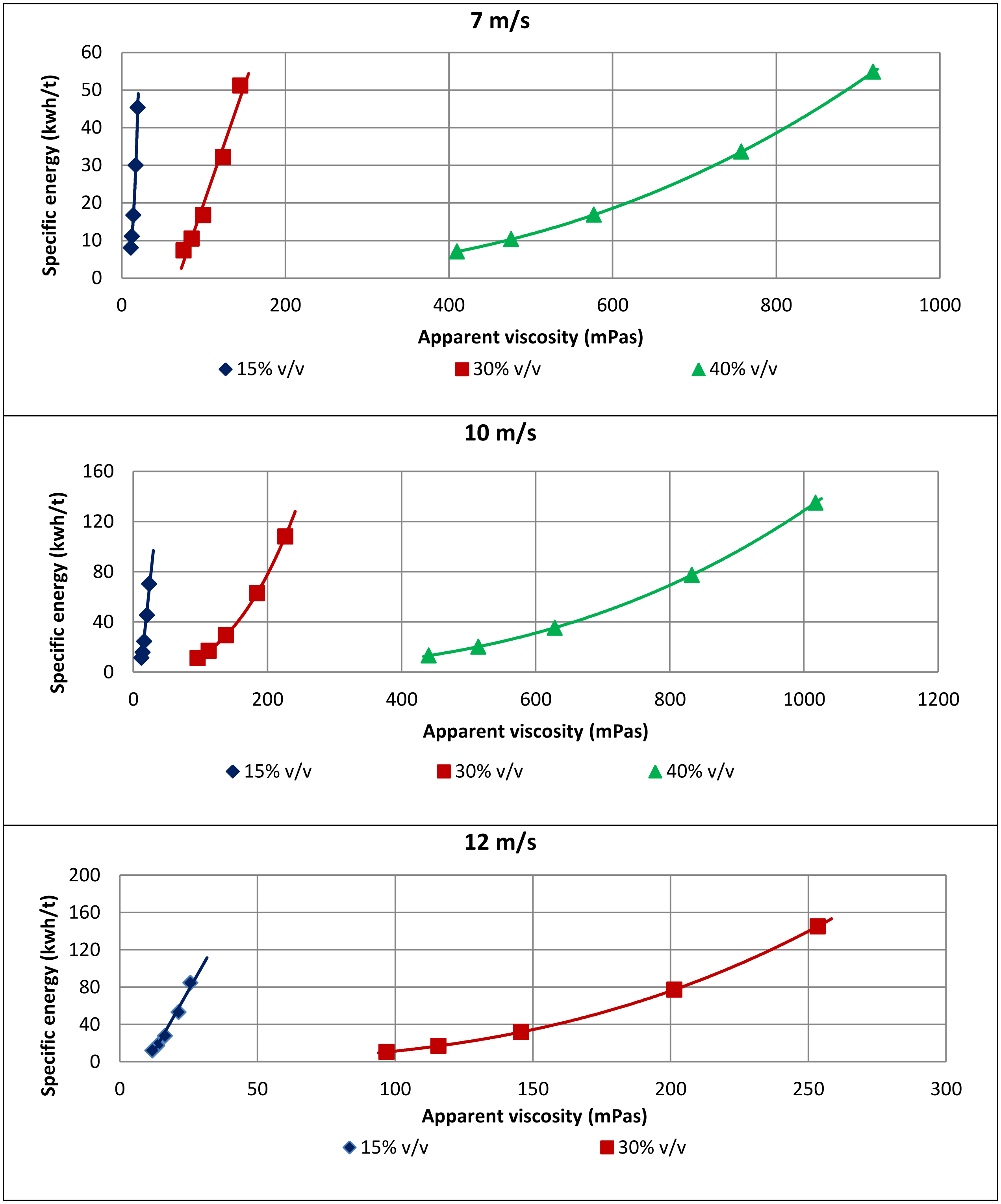

Figure 4.8 Effect of apparent viscosity (at a shear rate of 100 s^{-1}) on energy consumption

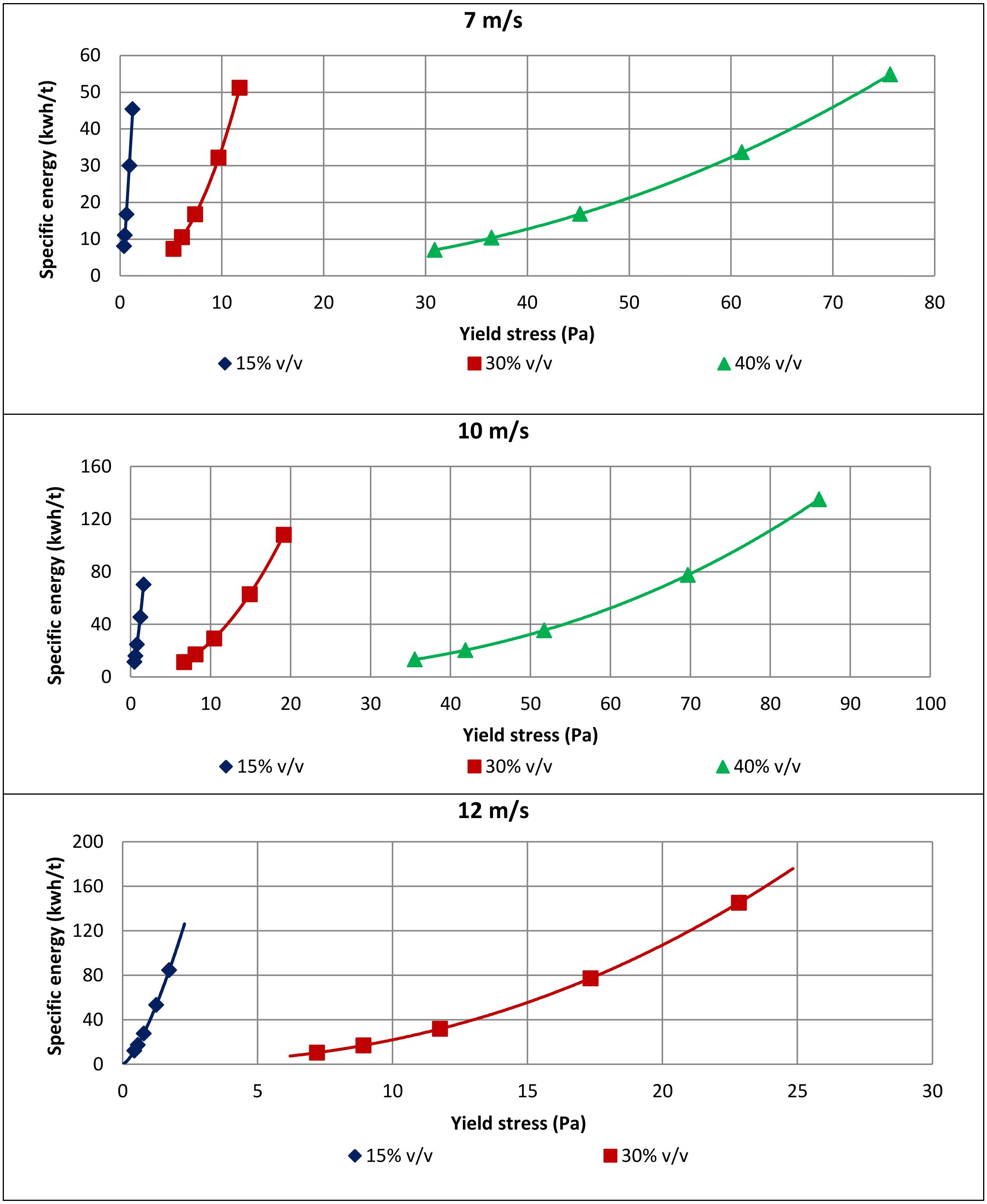

Figure 4.9 Effect of yield stress on energy consumption

4.2.6 Operational issues related to rheological effects

The operation of stirred media mills is significantly affected by the rheological effect particularly at high solids content and fine grind sizes. This is clearly indicated by the photographs in Figure 4.10 (the mill was operated at 40% solids by volume). The grinding process had to be terminated by pass 6 as compared to pass 9 for lower solids content (15% and 30% by volume). This is because the pulp became too viscous to be pumped and was unable to pass freely through a media retention screen as shown in Figure 4.10. Also, visual observations indicate that the size reduction process is expected to be significantly reduced as grinding beads disperse through such a viscous slurry. Generally, the addition of optimum amount of dispersant minimizes the operational issues related to rheological effects.

	
Front top end of mill discharge	**Back top end of mill discharge**

Figure 4.10 Plugging of the media retention screen experienced at pass 6 (40% v/v solids content, P_{80} = 40 μm)

4.3 Effect of stress intensity of grinding media on mill performance

The effect of stress intensity of grinding media on specific energy input and energy utilization for the given product (15 and 25 µm) sizes at 15% and 30% solids by volume is shown in Figure 4.11. Note that, the feed particle size was relatively constant i.e., F_{80} = 200 µm for all the tests shown in this section. At a given feed particle size, the stress intensity and specific energy input determine the grind size. It is also consistent that for both 15 and 25 µm grind sizes, high energy input is required at very low and high stress intensities, whereas the minimum energy is required between the two extremes of stress intensities (see Figure 4.11a).

At very low stress intensities, “multiple stresses” are required for the particles to be broken down sufficiently to finer grind sizes, hence more energy requirement. On the other hand, more energy is lost as heat and mechanical friction when the mill is operated at very high stress intensities. To achieve the same grind size, minimum energy is required between the two extreme ends of stress intensities; at this (optimum) stress intensity the energy input is just sufficient for breaking down particles with minimal losses and therefore the energy utilization is maximum (see Figure 4.11b). It is also important to note that, at the extreme end of higher stress intensities, no matter how much stress intensity is increased, the energy utilization do not change significantly.

The existence of the optimum stress intensity of grinding media in stirred media mills was also observed by other researchers (Kwade et al., 1996; Becker, 1997; Kwade, 1999, 2004; Jankovic, 2003). For the comminution of feldspars-quartz ore in the present study, the optimum stress intensity is about $(3.0 – 3.5) \times 10^{-3}$ NM which is translated to about 7 m/s tip speed and 15% to 30% solids by volume, the media specific gravity is 4.1 and the media size is 2.9 mm. A slight difference in stress intensity values between 15% and 30% solids by volume was due to the differences in slurry densities. However, at the lower end of stress intensities the mill tip speed was 3 m/s for 30% solids by volume against 4 m/s for 15% solids by volume.

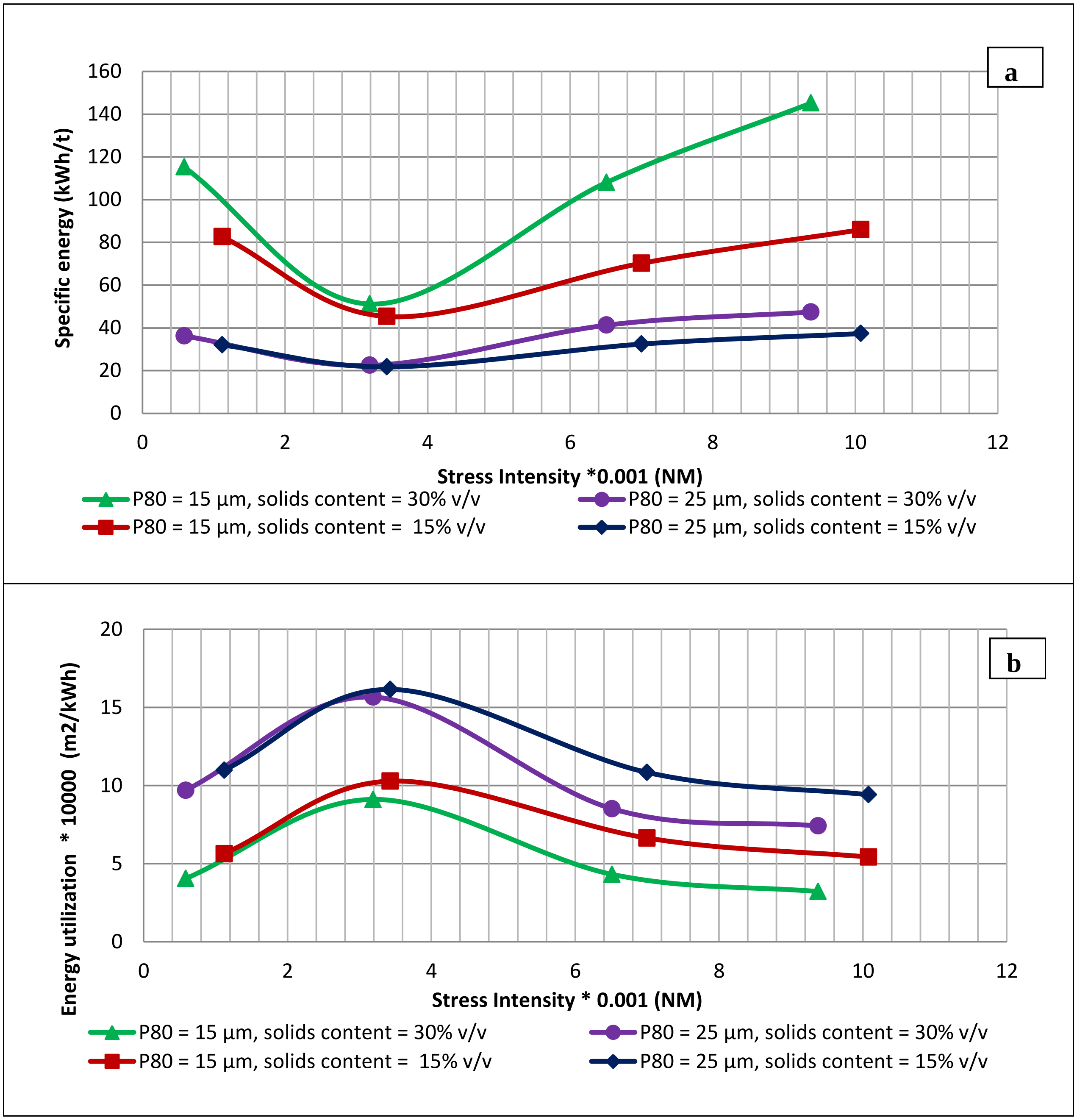

Figure 4.11 Effect of stress intensity of grinding media on mill performance

5 Scale-up demonstration study at the Turk mine

5.1 Introduction

The scale-up demonstration study was conducted at the Turk mine. Geographically, the mine is located 56 km north of Bulawayo, the second largest city of Zimbabwe after Harare, the capital city. It is situated at 19°43'S and 28°48'E as shown on the Google earth image in Figure 5.1. Mining activities have existed in this region for decades. The mine is located in Bulawayo-Bubi greenstone belt known as Bembezi gold belt (New Dawn Mining Corp, 2012).

Figure 5.1 The Turk mine geographical location (Google earth, 2013)

5.2 Mineralization

Generally, at the Turk mine, gold mineralization is mainly associated with quartz carbonates, and sulphides. Pyrite is the main sulphide mineral with small proportions of arsenopyrite and pyrrhotite (New Dawn Mining Corp, 2012). The existence of these sulphides to a lesser amount makes the ore slightly refractory. In the year 2011, the gold feed grade was about 3.5 g/t (New Dawn Mining Corp, 2012).

5.3 Processing

The ore is primary crushed using a jaw crusher and thereafter, secondary crushed using two cone crushers in parallel, one cone crusher for the intermediate fraction (+12 mm−25 mm), and the other for the coarse fraction (+25 mm). The fine crushed product (−12 mm) reports to the crusher ore bin. The crushed ore product from the bin is ground in a conventional two-staged ball milling. The grinding circuit operates in closed circuit with cyclones to produce 80% passing less than 75 µm. The cyclone overflow is thickened before it reports to the leaching circuit.

In order to increase gold liberation, the circuit was modified in the year 2011 by incorporating the VXP2500 mill between conventional ball milling and leaching circuit to achieve 95% passing 32 µm grind size (New Dawn Mining Corp, 2012). Currently, the mill is utilized to grind dump material i.e., old tailings, which has more than 1 g/t gold. The location of the VXP2500 mill in the process flowsheet is indicated by the dotted text box in Figure 5.2.

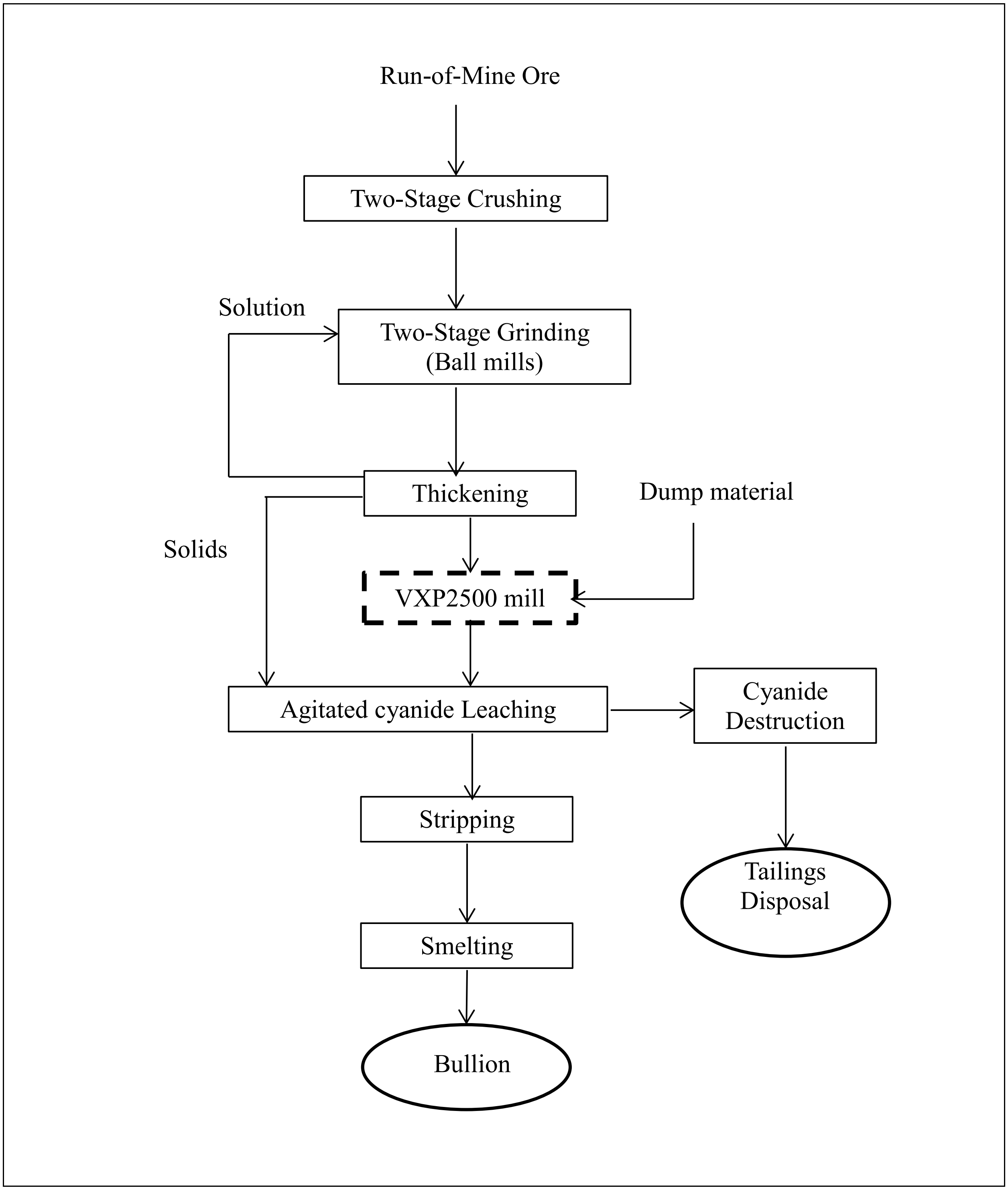

Figure 5.2 The Turk mine process flowsheet

5.4 Experimental program

5.4.1 Equipment

Figure 5.3 show the photographs of the pilot-scale (VXP10) mill and the full-scale (VXP2500) mill used for the scale-up demonstration study. The particle size analysis was carried using the Malvern (the Mastersizer hydro 2000S) as the one shown in Figure 3.7.

VXP10 mill

VXP2500 mill

Figure 5.3 Photographs of the VXPmills employed for scale-up demonstration study

5.4.2 Experimental procedure

A simplified flowsheet of the regrind mill circuit for the Turk mine is shown in Figure 5.4. Re-pulping is simply done by hosing the dump material with high pressure water to the sump, and then pumping the material to the plant. Non-ore materials (trashes) are rejected by a trash screen just before the pulp reports to the VPX2500 mill feed stock tank. Dilution water is added in the stock tank to lower the solids content to that desired for the mill feed (around 36% solids by weight). The variation of the VXPmill feed particle size and slurry density is expected because there is no automated system in place to control them.

During test work for this study, the VXP2500 mill was set to the required operating variables for the test, then the mill was allowed to run for at least 15 minutes, when the circuit stability was verified, the mill feed was sampled at inlet pipe (F) just before entering the mill and the discharge was sampled thereafter at the discharge pipe (D) a few minutes later depending on the mill flow rate. Four feed and discharge samples were taken at an interval of 15 minutes, the samples were sized and averaged to represent the particle size distribution for the test. Meanwhile, a portion of the VXP2500 mill feed was directed to fill one of the VXP10 mill sumps as indicated in Figure 5.4. In order to acquire a steady state and prevent hold up of coarse particles in the mill grinding chamber for a pilot test execution, at least 80 litres of pulp was used for each VXP10 mill test.

In order to have more data points for the analysis, some of the data used for the VXP2500 mill were recorded from a different day and time from the one a pilot test was performed provided they had similar operating conditions (media load, mill tip speed, and media size and type). A pilot study was conducted between 13th and 23rd November 2012 and data from the full-scale mill was recorded between 4th October and 23rd November 2012.

The energy input versus grind size relationship for a pilot-scale mill was generated based on the pendulum mode described in Section 3.2.4.3, whereas for a full-scale mill, the relationship was based on the continuous mode (single pass). In practice, full-scale mills are operated in a continuous mode, this is mainly done to increase the production capacity for the plant. Therefore, to demonstrate the scale-up procedure, the VXP2500 mill data points were plotted on the VXP10 mill plot (both mills operated at similar operating conditions).

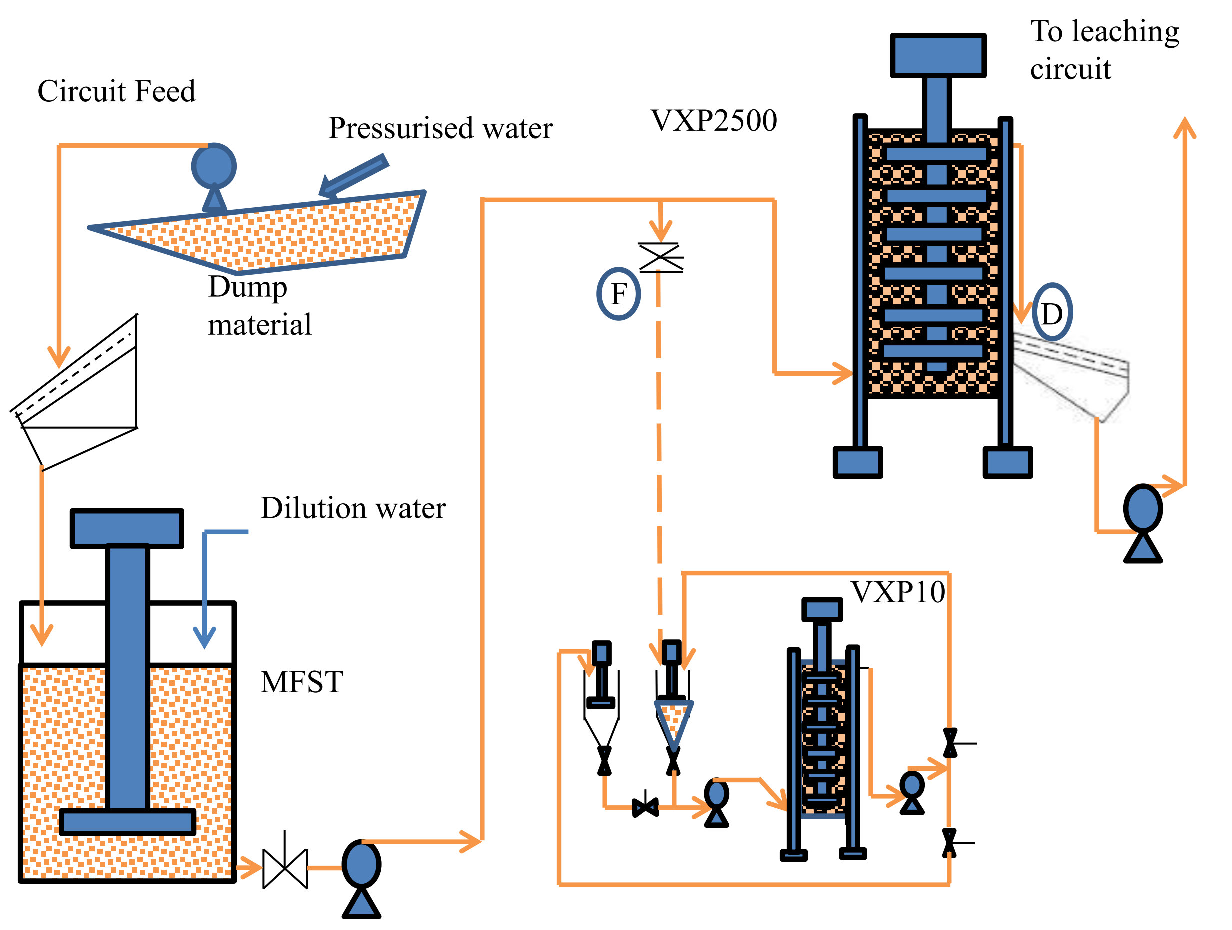

MFST = Mill Feed Stock Tank; F = Feed sampling point; D = Discharge sampling point

Figure 5.4 The Turk mine regrind circuit

The experimental conditions tested for the scale-up demonstration are summarized in Table 5.1. The data generated from the listed conditions for both mills are presented in Appendix F.

Table 5.1 Summary of experimental conditions tested for scale-up demonstration study

Test No	Media load & Type	Mill tip speed (m/s)	Media size (mm)	VXP10 mill		VXP2500 mill		
				F_{80} (µm)	Flow rate (L/min)	F_{80} (µm)	Flow rate (L/min)	Flow rate (m^3/hr)
1	65%, CZS	10	2.8 – 3.0	119	9	54.2	1250	75
						54.5	1333	80
						106.0	1250	75
						81.2	1250	75
2	40%, CZC	10	2.8 – 3.0	92.1	13	89.2	1250	75
	40%, CZC	10	2.8 – 3.0	88.1	13			
3	40%, CZC	10	2.8 – 3.0	45.3	13	40.8	500	30
5	50%, CZC	10	2.8 – 3.0	74.4	13	113.9	833	50
6	35%, CZC	10	2.8 – 3.0	38.4	9	47.9	750	45
7	35%, CZC	10	2.8 – 3.0	43.6	13	47.2	1083	65
						100.4	1667	100
8	35%, CZC	12	2.8 – 3.0	40.4	13	94.5	1083	65
						103	1083	65
						58.2	1083	65
						70.4	1083	65

5.5 Results and discussion

5.5.1 Effect of mill flow rate on grinding results

As discussed in Section 2.4.5, the scale-up of stirred media mills is direct 1:1 based on the specific energy input versus product particle size relationship (both pilot and full-scale mills operated at similar operating conditions). However, when the two mills are of very different sizes, the operating conditions vary significantly too. It is possible to fix variables such as mill tip speed and, media load and size for both mills, but it is impossible to fix mill flow rate for the two differently sized mills (10 litres vs 2500 litres). In the present study, the VXP10 mill was optimally operated between 8 and 14 L/min, lower flow rates (less than 5 L/min) were not attempted because plugging of pipes occurs for such lower flow rates. Mill flow rate should be sufficient to fluidize and keep the charge suspended at all times during comminution. On the other hand, the VXP2500 mill was operated between 500 and1667 L/min.

The effect of mill flow rate on grinding results for both mills is presented in Figure 5.5. For a given feed particle size, grinding residence time increases by lowering the mill flow rate and consequently, the finer grind size is achieved, but at the expense of high power consumption. For the VXP2500 mill, the specific energy input versus product particle size relationship remains constant regardless of the changes in mill flow rates (see Figure 5.5a). The mill was operated at a tip speed of 10 m/s, the media load and size were 35% of the mill grinding chamber volume and 2.8 – 3.0 mm respectively, and CZC (zirconium oxide) was the media type used (the data were collected on different days in the month of November 2012).

Due to the existence of the grinding limit in the fine grind sizes, the VXP10 mill data indicated a negligible effect of mill flow rate on the energy-product particle size relationship in the fine grind sizes. In the coarse grind sizes, the higher flow rate (13 L/min) required slightly more energy as compared to the lower flow rate, 9 L/min (see Figure 5.5b). Both tests were operated at a mill tip speed of 10 m/s, the media type and size were CZC and 2.8 – 3.0 mm respectively, the media load was 35%, and the solids content was relatively similar (38% w/w).

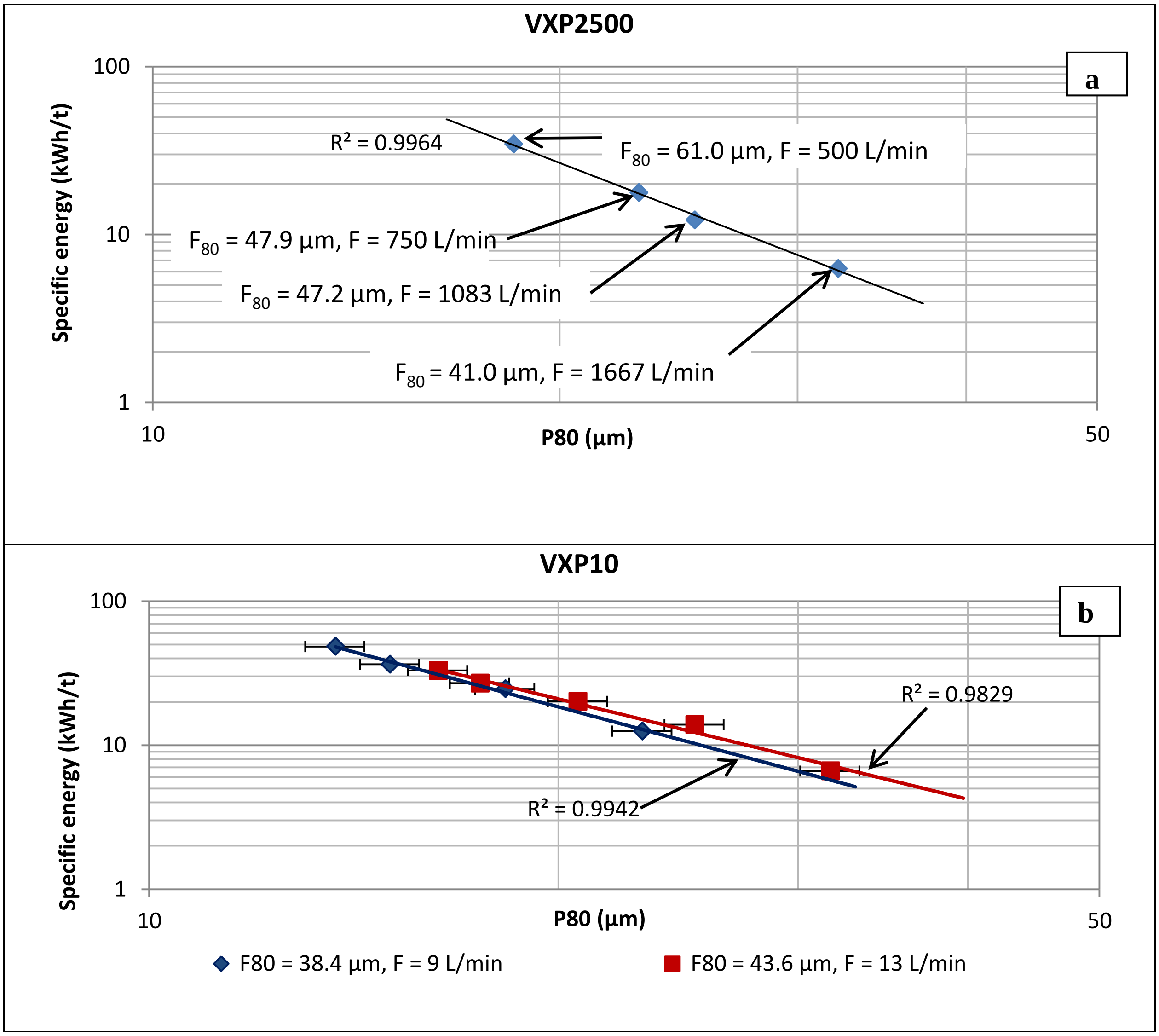

Figure 5.5 Effect of feed particle size and mill flow rate on mill performance

5.5.2 Scale-up demonstration study

Figure 5.6 demonstrates the scale-up results by utilizing the VXP2500 and the VXP10 mills. Both mills were operated at similar operating conditions and treating similar materials but of different feed particle size. Results indicate that the scale-up is exactly 1:1 when both mills treat materials of relatively the same feed sizes (see Figure 5.6a). This means that, both mills experience similar grinding environment during comminution. Similar observation was obtained when the VXP2500 mill was operated at the constant flow rate (1083 L/min), treating similar material of various feed particle sizes, while the VXP10 mill was optimally operated at 13 L/min treating the same material but of different feed particle size.

Figure 5.6b indicates that the scale-up results is as close as 1:1 when the feed particle size for both mills are relatively the same and the deviation is relatively significant when one mill treats material of relatively different feed particle size from the other mill. These observations indicate that when one mill treats material of relatively coarse feed particle size as compared to the other, it needs more “stress events” in order to achieve the same grind size as the one for the mill treating material of a fine feed particle size for the same operating conditions, and eventually more energy is required for the mill treating the coarse feed particle size. This is consistent with the results observed previously in Section 4.2.3.

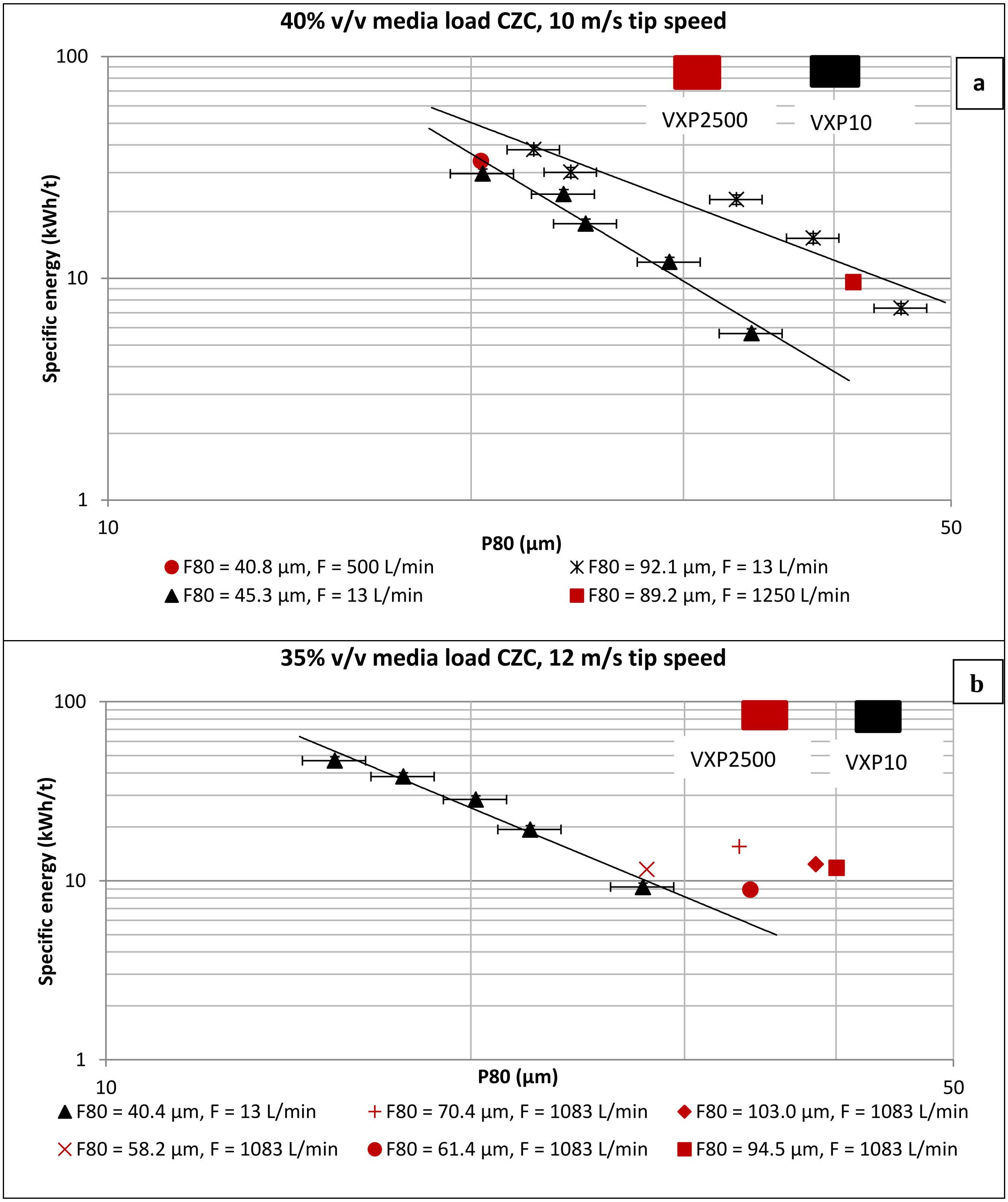

Figure 5.6 Scale-up demonstration (media size = 2.8 – 3.0 mm, media type = CZC)

Similarly, Figure 5.7 indicates that, in order to achieve accurate direct scale-up results, both pilot and full-scale mills should treat similar material of the same feed particle size. It is also interesting to note that, the effect of feed particle size on scale-up results becomes even more significant when the mill flow rate for the VXP2500 mill is relatively higher (1667 L/min) to reflect the optimal flow rate (between 8 and 13 L/min) for the VXP10 mill, (see the isolated data point i.e., F_{80} = 100.4 µm, F = 1667 L/min for the VXP2500 mill in Figure 5.7a).

It can also be observed that the effect of feed particle size on scale-up results can be minimized when both mills are operated at their optimum flow rates, as demonstrated in Figure 5.7b. Although both mills treated similar material of relatively different feed particle sizes, yet the flow rate of 833 L/min for the VXP2500 mill reflected the optimal flow rate of 13 L/min for the VXP10 mill, that is why the scale-up results was marginal.

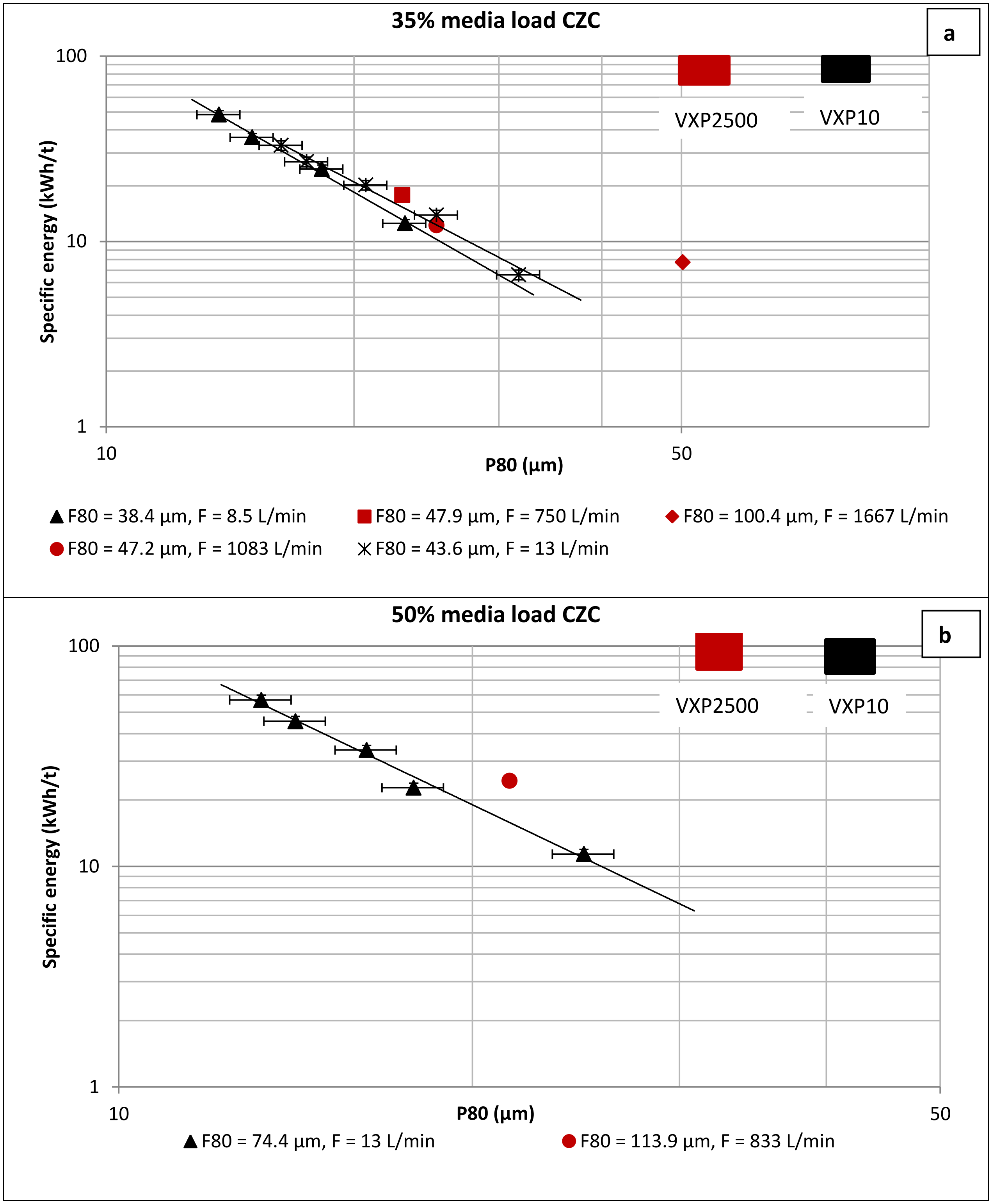

Figure 5.7 Scale-up demonstration (mill tip speed = 10 m/s, media size = 2.8 – 3.0 mm, media type = CZC)

Results presented in Figure 5.8 agree well with the previous scale-up results presented in this work. These results show that the feed particle size is one of the strongest variables for the accurate scale-up results to be achieved for the VXPmill and this is also expected for other stirred media mills. The smaller the variations of feed particle size between the two mills, the smaller the deviation of the energy input-product particle size relationship between them, i.e., the data point for the VXP10 mill with F_{80} = 119 µm is very close to the one for the VXP2500 mill with F_{80} = 106 µm and far away from the one for F_{80} = 54 µm.

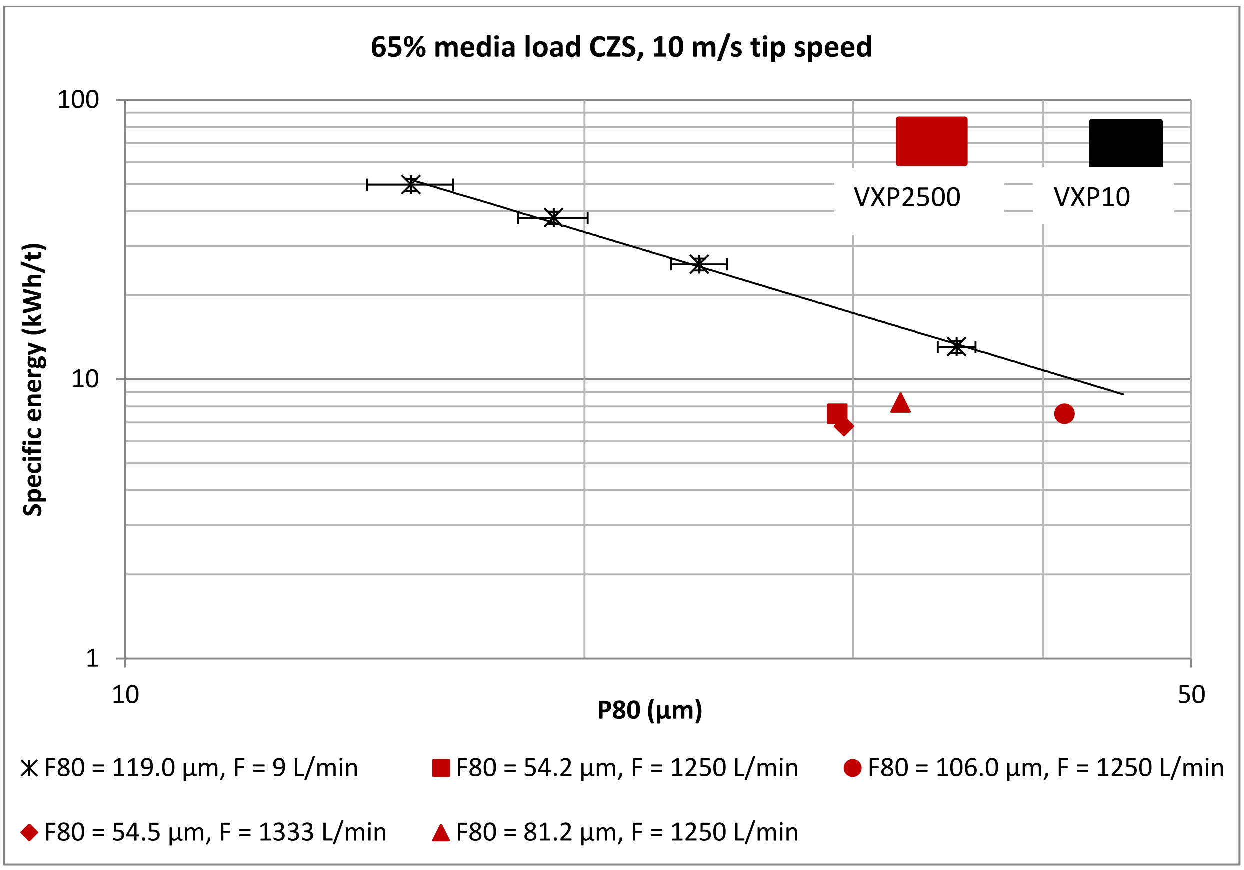

Figure 5.8 Scale-up demonstration (media size = 2.8 – 3.0 mm, media type = CZS)

Figure 5.9 shows the influence of mill speed on scale-up results. It should be noted that these results are the same as the one presented in Figure 5.6b, the major difference is that, a signature plot with 7 m/s is added to the original plot and only feed particle sizes less than F_{80} = 70 μm are shown. As the data show, the lower mill tip speed (7 m/s) is more energy efficient than the higher tip speed (12 m/s) at a given feed and grind size, and this is consistent with the results observed in Section 4.2.2.

Also, Figure 5.9 indicates that the difference in mill tip speed between the two mills can potentially affect scale-up results even though both mills treat similar material of relatively the same feed particle size. Therefore, fixing feed particle size for both mills is a necessary, but not sufficient condition for accurate scale-up results to be achieved. Other operating conditions need to be fixed as well. The more closely are the operating conditions between the two mills, the more the accurate are the scale-up results.

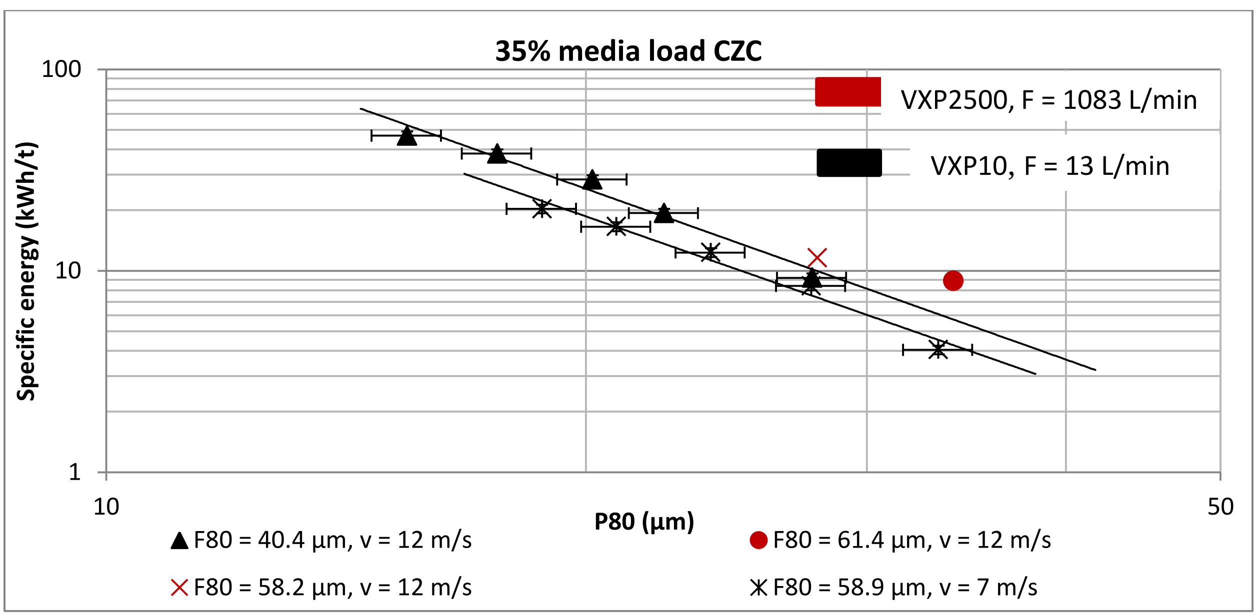

Figure 5.9 Effect of mill speed on scale-up results

Moreover, Figure 5.10 shows the specific energy input-product particle size relationship for both mills, operated at various operating conditions treating similar material of various feed particle sizes (combination of all the scale-up results presented previously in this work). It is important to note that both mills show a similar characteristic pattern, i.e., the specific energy consumption increases with the decrease in product particle size.

However, the influence of operating variables is very significant on the energy input versus product particle size relationship, as displayed by the scattered data points for both mills. Therefore, in order to achieve accurate direct scale-up results, both the pilot-scale and the full-scale mills should be operated at "similar operating conditions and treating similar material of the same feed particle size."

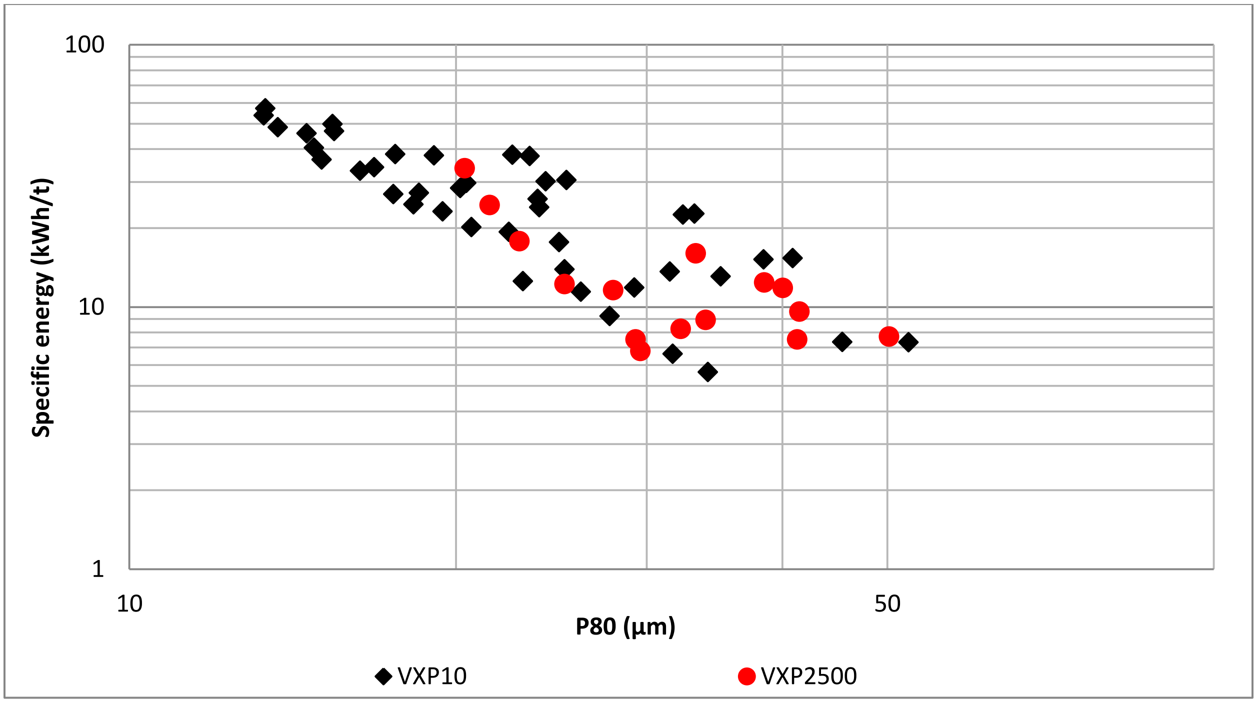

Figure 5.10 The VXP2500 and the VXP10 mills operated at various grinding conditions

6 Conclusions and recommendations

6.1 Conclusions

Based on the comparison between the two modes of testing procedure for scale-up of stirred media mills, it was concluded that:

i. For a given grind size, the batch recycle mode requires more mill power draw by up to 3 to 4 times the one required by the pendulum mode (both modes operated under similar grinding conditions). Due to the existence of grinding limit, the energy input versus product particle size plots for the two modes converge in the fine grind sizes.

ii. With an increase in the test sample weight, the energy input versus product particle size plot derived from the batch recycle test deviates significantly from the pendulum plot over a broad range of particle grind sizes. Conversely, as the test sample weight decreases, the batch recycle plot approaches the pendulum.

For the analysis of operating variables, the following was concluded:

i. In the coarse fraction grind sizes, the size reduction process increases with the increase in mill speed and the decrease in solids content. However, in the fine fraction grind sizes, the effects of mill speed and solids content diminish exponentially as reduction ratio approaches 1, since a grinding limit is said to be approached.

ii. From the energy consumption point of view, increasing mill speed lowers grinding efficiency over a broad range of grind sizes. Also, at relatively low mill tip speeds (3 and 4 m/s), grinding efficiency drops sharply in the fine grind sizes. The maximum grinding efficiency is achieved between the two extreme ends of mill speeds.

iii. The effect of feed size is critical for the energy requirement in stirred media mills. Up to 20% more energy was required for a coarse feed size (F80 = 300 µm) as compared to a finer feed size (F80 = 200 μm) to achieve P80 = 20 μm grind size (both feed sizes ground at similar operating conditions). Also, the energy difference between the two feed sizes tested decreased in the fine grind sizes due to the existence of the grinding limit.

iv. For a given feed particle size, the stress intensity of grinding media and specific energy input control the grind size for the comminution in stirred media mills. Also, there exists an optimum stress intensity between the two extreme ends of stress intensities. The energy utilization is maximum at optimum stress intensity.

v. For the comminution of feldspars-quartz ore using the VXPmill at the tested conditions, it was shown that the optimum stress intensity was about (3.0 – 3.5) $\times 10^{-3}$ NM which is translated to a mill tip speed of 7 m/s for a slurry with solids content between 15% and 30% by volume and, the media size and specific gravity of 2.9 mm and 4.1 respectively.

Based on rheological study, the following was concluded:

i. For the shear rate tested, the feldspars-quartz ore suspensions exhibited a time-independent non-Newtonian flow with characteristic shear thinning properties and evident yield stress. The Casson model proved to be the best-fit rheological flow model for the suspension.

ii. The rheological effects of ground suspensions are affected by particle size and solids content. The yield stress and viscosity of ground suspensions increase remarkably with the decrease in particle size and the increase in solids content. These effects adversely affect the operation of stirred media mills.

For the scale-up study, the following was concluded:

i. Mill feed particle size has a very strong influence on scale-up results.

ii. Keeping mill feed particle size constant in both pilot and full-scale mills is “a necessary but not sufficient” condition for accurate scale-up results to be achieved. Other operating conditions should also be fixed.
iii. Therefore, for effective and accurate scaling-up of stirred media mills, both the pilot and full-scale mills should be operated at “similar operating conditions and treating similar material of the same particle size”. It is also important that the feed flow rates for both mills are within their optimum range. Consequently, both mills experience the same grinding environment during comminution.
iv. For a given feed particle size, the higher the flow rate, the lesser the size reduction. However, the specific energy input versus product particle size relationship remains constant and it is independent of the size of the mill.

6.2 Recommendations

Based on the assessment of the two modes of testing procedure for scale-up, it was recommended that:

The pendulum testing mode should be used for scale-up purposes because all particles are uniformly broken down each time they report to the mill grinding chamber. This mimics the grinding mechanism existing in full-scale operations.

Based on the findings for the analysis of operating variables, it was recommended that:

i. More studies should be conducted to understand the effects of media size, load and type on comminution for the VXPmills, since the present study did not investigate their effects.
ii. A study should be conducted to determine the optimum size reduction ratio for a typical feed size of the VXPmill, since the present study focused mainly on the energy consumption.

iii. More investigation is required to understand the effect of bead to feed size ratio on the performance of the VXPmill.

iv. The optimum stress intensity of grinding media does exist in the comminution of feldspars-quartz ore employing the VXPmill. Other materials and grinding media type and size should be tested over a wide range of stress intensities to investigate this phenomenon.

v. When the VXPmill is operated at higher solids content (e.g., 40% solids by volume), rheological effects become so obvious to adversely affect the mill's operation for further comminution. Operational issues can possibly be minimized with the use of dispersant.

The following were recommended for the scale-up demonstration study:

i. Practically, the feed particle size for full-scale operations varies and therefore for effective size reduction, it is recommended to blend grinding media of different sizes in proportions to encounter the variations.

ii. High media load can possibly have a significant influence on scale-up results. Therefore, more investigation is required to understand the effect of gravitational stress intensity on the performance of the VXPmills and its effect on scale-up results.

iii. Freshly sized grinding media used in pilot-scale units do not reflect seasonal charged grinding media used in full-scale operations. Therefore, more studies are required to understand the influence of media size on scale-up results for the VXPmills.

iv. More investigation is required to understand the influence of internal mill configuration i.e., disk spacing and diameter on scale-up results for the VXPmills.

v. Tests should be conducted for full-scale mills to determine their optimum stress intensities.

References

Akroyd, T.J., & Nguyen, Q.D. (2003a). Continuous rheometry for industrial slurries. *Experimental Thermal and Fluid Science*, *27*(5), 507-514.

Akroyd, T.J., & Nguyen, Q.D. (2003b). Continuous on-line rheological measurements for rapid settling slurries. *Minerals Engineering*, *16*(8), 731-738.

Akroyd, T.J. (2004). *Continuous flow rheometry for settling slurries* (Doctoral dissertation, University of Adelaide, Australia).

Avramidis, K. S., & Turian, R. M. (1991). Yield stress of laterite suspensions. *Journal of colloid and interface science*, *143*(1), 54-68.

Barnes, H. A., Hutton, J. F., & Walters, K. (1989). *An introduction to rheology* (Vol. 3). Elsevier, Amsterdam, (pp. 120-124).

Barnes, H.A., (1999). The yield stress – a review or 'παντα ρει' – everything flows? *A journal for non-Newtonian fluids Mechanics*, *81*(1-2), 133-178.

Barnes, H.A. (2000). Measuring the viscosity of large-particle (and flocculated) suspensions – A note on the necessary gap size of rotational viscometers? *A journal for non-Newtonian fluids Mechanics*, *94*(2-3), 213-217.

Becker, M., Kwade, A., & Schwedes, J. (2001). Stress intensity in stirred media mills and its effect on specific energy requirement. *International Journal of Mineral Process*, *61*(3), 189-208.

BCS. (2007). Mining Industry Energy Bandwidth Study. US Department of Energy, Industrial Technologies Program. Retrieved from http://www1.eere.energy.gov/ on 02nd February 2014.

British Standards Institution, (1975). British Standard Glossary of Rheological Terms, BS 5168:1975.

Brunauer, S., Emmett, P. H., & Teller, E. (1938). *Journal of the American Chemical Society*. 60, 309-319.

Burford, B. D., & Clark, L. W. (2007). IsaMill technology used in efficient grinding circuits. In *VIII International Conference on Non-ferrous Ore Processing, Poland*.

Casson, N. (1959). A flow equation for pigment-oil suspensions of the printing ink type. *Rheology of disperse systems*, *84*, l959.

Ding, Z., Yin, Z., Liu, L., & Chen, Q. (2007). The effect of grinding parameters on the rheology of pyrite – heptane slurry in a laboratory stirred media mill. *Minerals engineering*, *20*(7), 701-709.

El-Shall, H., & Somasundaran, P. (1984). Physico-chemical aspects of grinding: a review of use of additives. *Powder Technology, 38*(3), 275-293.

FLSmidth Knelson (2012). *Stirred Mill user manual, Model VSM10*. A Division of FLSmidth ltd, Langley, British Columbia, Canada, pp. 64.

FLSmidth® (2013). *VXPmill stirred mill installation list.* FLSmidth Salt Lake City, Inc. Retrieved from www.flsmidth.com on 2nd November 2013.

Gao, M. W., & Forssberg, E. (1993a). A study on the effect of parameters in stirred ball milling. *International Journal of Mineral Processing, 37*(1-2), 45-59.

Gao, M., & Forssberg, E. (1993b). The influence of slurry rheology on ultra-fine grinding in a stirred ball mill. In *18th International Mineral Processing Congress, Sydney, CA (Conference Article), Australian* (pp. 237-244).

Gao, M.W., & Weller. K.R. (1993). Fine Grinding in Mineral Processing Using Stirred Ball mills. *Chemical Engineering in Australia*, *18*(2), 8-12.

Gao, M. W., & Weller. K.R. (1994). Comparison of Tumbling Mills and Stirred Ball Mills for Wet Grinding. *Fifth Mill Operators' conference,* (pp. 61-67). Roxby Downs, Australia: AUSIMM.

Gao, M. W., Forssberg, K. S. E., & Weller, K. R. (1996). Power predictions for a pilot scale stirred ball mill. *International Journal of Mineral Processing*, *44*, 641-652.

Gao, M., Weller, K. R., & Allum, P. (1999). Scaling-up horizontal stirred mills from a 4-litre test mill to a 4000-litre "IsaMill". In *Powder Technology Symposium, Pennsylvania State University, Pennsylvania, USA, September*.

Gao, M., Young, M. F., Cronin, B., & Harbort, G. (2001). IsaMill medium competency and its effect on milling performance. *Minerals and Metallurgical Processing (USA)*, *18*(2), 117-120.

Greenwood, R., Rowson, N., Kingman, S., & Brown, G. (2002). A new method for determining the optimum dispersant concentrationin aqueous grinding. *Powder Technology*, 123(2-3), 199-207.

Gustafsson, J., Toivakka, M., Karhu, J., & Koskinen, K.K. (2008). Rheology of settling suspensions. Rheological materials in Process industry, ReoMaT Final report, VTT Technical Research Centre of Finland.

Hallbom, D. J., & Klein, B. (2004). Flow array for nickel laterite slurry. *International Laterite Nickel Symposium 2004(as held during the 2004 TMS Annual Meeting)* (pp. 415-428).

Hallbom, D. J. (2008). *Pipe flow of homogeneous slurry* (Doctoral dissertation, University of British Columbia, Vancouver, Canada). Retrieved from https://circle.ubc.ca/ on 30th October 2013.

Hallbom, D., & Klein, B. (2009). A Physical Model for Yield Plastic Fluids. *Particulate Science and Technology*, *27*(1), 1-15.

He, M., Wang, Y., & Forssberg, E. (2004). Slurry rheology in wet ultrafine grinding of industrial minerals: a review. *Powder technology*, *147*(1-3), 94-112.

He, M. (2005). *Slurry Rheology of Limestone and its effect on wet Ultra-fine Grinding*, (Doctoral dissertation, Lulea University of Technology, Lulea, Sweden).

Hill, A., & Carrington, S. (2006). Understanding the links Between Rheology and Particle Parameters. Malvern Instruments Ltd., U.K , *American Laboratory News article*, (pp. 1-8).

Jankovic, A. (2001). Media stress intensity analysis for vertical stirred mills. *Minerals Engineering*, *14*(10), 1177-1186.

Jankovic, A. (2003). Variables affecting the fine grinding of minerals using stirred mills. *Minerals Engineering*, *16*(4), 337-345.

Jankovic, A., & Sinclair, S. (2006). The shape of product size distributions in stirred mills. *Minerals engineering*, *19*(15), 1528-1536.

Jankovic, A. (2008). A review of regrinding and fine grinding technology– the facts and myths. Metso Minerals Process Technology Australia and Asia-Pacific.

Jankovic, A., Valery, W., & La Rosa, D. (2008). Fine grinding in the Australian mining industry. Metso Minerals Process Technology Australia and Asia-Pacific.

Jeffrey, D.J., & Andreas, A. (1976). The Rheological Properties of Suspensions of Rigid Particles. Department of Chemical Engineering Stanford Engineering Stanford, California, *AIChE Journal*, *22*(3), (417-432).

Kapur, P.C., Healy, T.W., Scales, P. J., Boger, D.V., & Wilson, D. (1996). Role of dispersants in kinetics and energetics of stirred ball mill grinding. *International Journal of Mineral Processing 47*(1-2), 141-152.

Karbstein, H., Muller, F., & Polke, R. (1996). Scale-up for Grinding in Stirred Ball Mills, *Aufbereitungs-Technick*, *37*(10), 469-479.

Kawatra, S.K., & Bakshi, A.K. (1996). Online measurements of viscosity and determination of flow types for mineral suspensions. *International Journal of Mineral Processing, 47*(3), 275-283.

Kelessidis, V.C., Maglione, R., Tsamantaki, C., & Aspirtakis, Y. (2006). Optimal determination of Rheological parameters for Herscel-Bulkley drilling fluids and impact on pressure drop, velocity profiles and penetration rayes during drilling. *Journal of Petroleum Science and Engineering*, *53* (3-4), 203-224.

Klein, B. (1992). *Rheology and stability of magnetite dense media* (Doctoral dissertation, University of British Columbia, Canada). Retrieved from https://circle.ubc.ca/ on 2nd March 2013.

Klein, B., & Hallbom, D. J. (2002). Modifying the rheology of nickel laterite suspensions. *Minerals engineering*, *15*(10), 745-749.

Klimpel, R.R. (1982). Slurry rheology influence on the performance of mineral/coal grinding circuits. Part I. *Minerals Engineering*, *34*(12), 1665-1668.

Klimpel, R.R. (1983). Slurry rheology influence on the performance of mineral/coal grinding circuits. Part II. *Minerals Engineering*, *35*(1), 21-26.

Klimpel, R.R. (1999). The selection of wet grinding chemical additives based on slurry rheology control. *Powder Technology*, *105*(1-3), 430-435.

Knieke, C., Sommer, M., & Peukert, W. (2009). Identifying the apparent and true grinding limit. *Powder Technology*, *195*(1), 25-30.

Knieke, C., Steinborn, C., Romeis, S., Peukert, W., Breitung-Faes, S., & Kwade, A. (2010). Nanoparticle Production with Stirred-Media Mills: Opportunities and Limits. *Chemical Engineering & Technology*, *33*(9), 1401-1411.

Krause, C., & Pickering, M. (1998). Evaluation of ultrafine wet mineral milling using carboceramics proppant products for attrition grinding media. Colorado Springs, CO: Metso Minerals Optimization Services.

Kwade, A., Blecher, L., & Schwedes, J. (1996). Motion and stress Intensity of grinding beads in a stirred media mill. Part 2: Stress intensity and its effect on comminution. *Powder Technology*, *86*(1), 69-76.

Kwade, A., & Stender, H.H. (1998). Constant Grinding Results at Scale-Up of Stirred Media Mills. *Aufbereitungs Technik,39*(8), 373-382.

Kwade, A. (1999). Wet comminution in stirred media mills – research and its practical application. *Powder Technology*, *105*(1-3), 14-20.

Kwade, A. (2004). Mill selection and process optimization using a physical grinding model. *International Journal of Mineral Processing, 74,* S93-S101.

Kwade, A. (2010). Stress model as basis for optimization and scale-up of bead milling processes. Comminution 10, Cape Town, South Africa, April, (pp. 13-16).

Larson, M., Anderson, G., Morisson, R., & Young, M. (2011). Regrind mills: Challenges of scale-up. X-strata Technology and Julius Kruttschnitt Mineral Research Centre.

Lichter, J., & Davey, G. (2006). Advances in Comminution, *Selection and Sizing of Ultrafine and Stirred Grinding Mills*, (pp. 69-86). Denver: Society for Mining, Metallurgy and Exploration, Inc.

Mangesana, N., Chikuku, R.S., Mainza, A.N., Govender, I., Van der Westhuizen, A.P., & Narashima, M. (2008). The effect of particle sizes and solids concentration on the rheology of silica sand based suspensions. *The journal of the Southern Africa Institute of Mining and Metallurgy*, (pp. 237-243).

Mankosa, M. J., Adel, G. T., & Yoon, R.H. (1986). Effect of media size in stirred ball mill grinding of coal. *Powder technology*, *49*(1), 75-82.

Mankosa, M. J., Adel, G. T., & Yoon, R.H. (1989). Effect of operating parameters in Stirred Ball Mill Grinding of Coal. *Powder technology, 59*(4), 255-260.

Mannheim, V. (2011). Empirical and scale-up modeling in stirred ball mills. *Chemical Engineering Research and Design, 89*(4), 405-409.

Matsuo, S., Nonaka, M., & Inoue, T. (1990). *Proceedings of Second World Congress Particle Technology*, September 19 – 22, Kyoto, Japan, (pp. 599-606).

Mende, S., Stenger, F., Peukert, W., & Schwedes, J. (2003). Mechanical production and stabilization of submicron particles in stirred media mills. *Powder Technology*, *132*(1), 64-73.

Mie, G. (1908). "Beiträge zur Optik trüber Medien, speziell kolloidaler Metallösungen". *Annalen der Physik, 330*(3), 377–445.

Motteram, G., Ryan, M., & Weizenbach, R. (1997). Application of the pressure acid leach process to Western Australian nickel/cobalt laterites. *Nickel–Cobalt, 97,* 391-407.

Muster, T.H., & Prestidge, C.A. (1995). Rheological investigations of sulphide mineral slurries, *Minerals Engineering, 8*(12), 1541-1555.

New Dawn mining Corp. (2012). *Annual information form for the year ended September 30, 2012*. Retrieved from http://www.newdawnmining.com/corporate/financial-statements on October 05, 2013, (pp. 17-28).

Nguyen, Q. D., & Boger, D. V. (1983). Yield stress measurement for concentrated suspensions. *Journal of Rheology, 27*(4), 321-349.

Nguyen, Q. D. (1983). *Rheology of concentrated Bauxite residue suspensions* (Doctoral dissertation Monash University, Australia) (pp. 386).

Patra, P., Nagaraj, D.R., & Somasundaran, P. (2010). Impact of pulp rheology on selective recovery of value minerals from ores. *Proceedings of the XI International Seminar on Mineral Proceding Technology,* (pp. 1223-1231).

Pullum, L., Graham, L., Rudman, M., & Hamilton, R. (2006). High concentration suspension pumping. *Minerals engineering*, *19*(5), 471-477.

Rahal, D. (1999). The effects of a Fluorosurfactant in Fine Grinding Using a stirred Mill. MEngSc thesis, University of Queensland (JKMRC).

Rahal. D., Erasmus.D., & Major. K. (2011a). Knelson-Deswik Milling Technology: Bridging the gap between Low and High Speed Stirred Mills. *43rd Annual Meeting of the Canadian Mineral Processors*, Jan 18- 20, Ottawa, Ontario, Canada. Paper 35, (pp. 557-584).

Rahal. D., Roberts.K., & Rivett. T. (2011b). Knelson-Deswik Milling Technology: Evaluation of operating parameters. *Society of Mining, Metallurgy and Exploration Annual Meeting*, Denver, CO.

Reem, A. R. (2011). *The effect of stirred mill operation on particles breakage mechanism and their morphological features* (Doctoral dissertation, University of British Columbia, Canada). Retrieved from https://circle.ubc.ca/ on 10th December 2012.

Stenger, F., Mende, S., Schwedes, J., & Peukert, W. (2005). Nanomilling in stirred media mills. *Chemical engineering science*, *60*(16), 4557-4565.

Stief, D.E., Lawruk, W.A., & Wilson, L.J. (1987). Tower mill and its application to fine grinding. *Minerals and metallurgical processing, 4*(1), 45-50.

Tadros, T. F. (1980). Physical stability of suspension concentrates. *Advances in Colloid and Interface Science*, *12*(2), 141-261.

Tangsathitkulchai, C., & Austin, L.G. (1988). Rheology of concentrated slurries of particles of natural size distribution produced by grinding. *Powder Technology, 56*(4), 293-299.

Tangsathitkulchai, C. (2003). The effect of slurry Rheology on fine grinding in a laboratory ball mill. *International Journal of Mineral Processing*, *69*(1-4), 29-47.

Taylor, G. I. (1923). Stability of a viscous liquid contained between two rotating cylinders. *Philosophical Transactions of the Royal Society of London. Series A, Containing Papers of a Mathematical or Physical Character*, *223*, 289-343.

Triantafillopoulos, N.G. (1988). *Measurement of Fluid Rheology and Interpretation of Rheograms* (2nd ed.). Kaltec Scietific, Inc. Michigan, USA.

Van der Meer, F. P., & Gruendken, A. (2010). Flowsheet considerations for optimal use of high pressure grinding rolls. *Minerals Engineering*, *23*(9), 663-669.

Wang, Y., & Forssberg, E. (1997). Ultra-fine grinding and classification of minerals. *Comminution Practices. Society for Mining, Metallurgy and Exploration, Littleton, CO*, 203-214.

Wang, Y., & Forssberg, E. (2000). Technical note: Product size distribution in stirred media mills. *Minerals Engineering*, *13*(4), 459-465.

Wang, Y., Forssberg, E., & Sachweh, J. (2004). Dry fine comminution in a stirred media mill. MaxxMill. *International Journal of Mineral Processing*, *74*(Supplement), S65-S74.

Wang, Y., & Forssberg, E. (2007). Enhancement of energy efficiency for mechanical production of fine and ultra-fine particles in comminution. *China Particuology*, 5, (pp. 193-201).

Weit, H.,Schwedes, J., & Stehr, N. (1986). World congress Parti-cle Techology, Part 11, Niirnberg, pp. 709-724.

Whittington, B. I., & Muir, D. (2000). Pressure acid leaching of nickel laterites: a review. *Mineral Processing and Extractive Metallurgy Review*, *21*(6), 527-599.

Whorlow, R.W. (1992). Rheology techiques (2nd ed.). *Rotational viscometers*, (pp. 102-183). New York: Ellis Horwood Limited.

Yang, H. G., Li, C. Z., Gu, H. C., & Fang, T. N. (2001). Rheological behavior of titanium dioxide suspensions. *Journal of colloid and interface science*, *236*(1), 96-103.

Yerkovic, C., Menacho, J., & Gaete, L. (1993). Exploring the ultrasonic comminution of copper ores. *Minerals engineering*, *6*(6), 607-617.

Yuan, J., Murray, & H.H. (1997). The importance of crystal morphology on the viscosity of concentrated suspensions of kaolins. *Applied Clay Science,* 12(3), 209-219.

Yue, J. (2003). Rheology effects on ultrafine grinding in Stirred mills. MASc thesis. The University of British Columbia, Vancouver, Canada. Retrieved from https://circle.ubc.ca/ on 30th November 2012.

Yue, J., & Klein, B. (2004). Influence of rheology on the performance of horizontal Stirred mills. *Minerals engineering*, *17*(11-12), 1169-1177.

Yue, J., & Klein, B. (2005). Particle breakage kinetics in Horizontal Stirred mills. *Minerals Engineering*, *18*(3), 325-331.

Yue, J., & Klein, B. (2006). Advanced comminution technologies, *The effects of Bad Size on Ultrafine Grinding in a Stirred Bead mill,* part 1: (pp. 87-98). Littleton, CO:SME.

Zheng, J., Harris, C. C., & Somasundaran, P. (1996). A study on grinding and energy input in stirred media mills. *Powder Technology*, *86*(2), 171-178.

Zheng, J., Harris, C. C., & Somasundaran, P. (1997). The effect of additives on stirred media milling of limestone. *Powder technology*, *91*(3), 173-179.

Appendices

Appendix A   Particle size distribution

Appendix A.1   HPGR feed and products particle size distribution

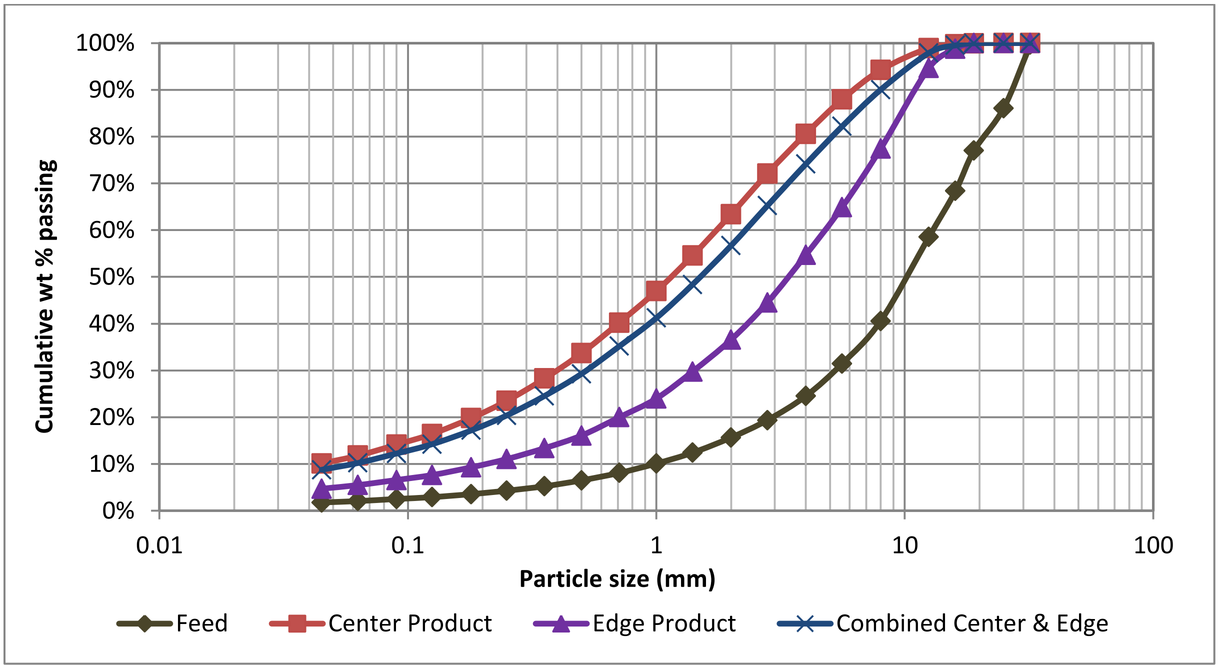

Appendix A.2 VXPmill feed particle size distribution by laser diffraction

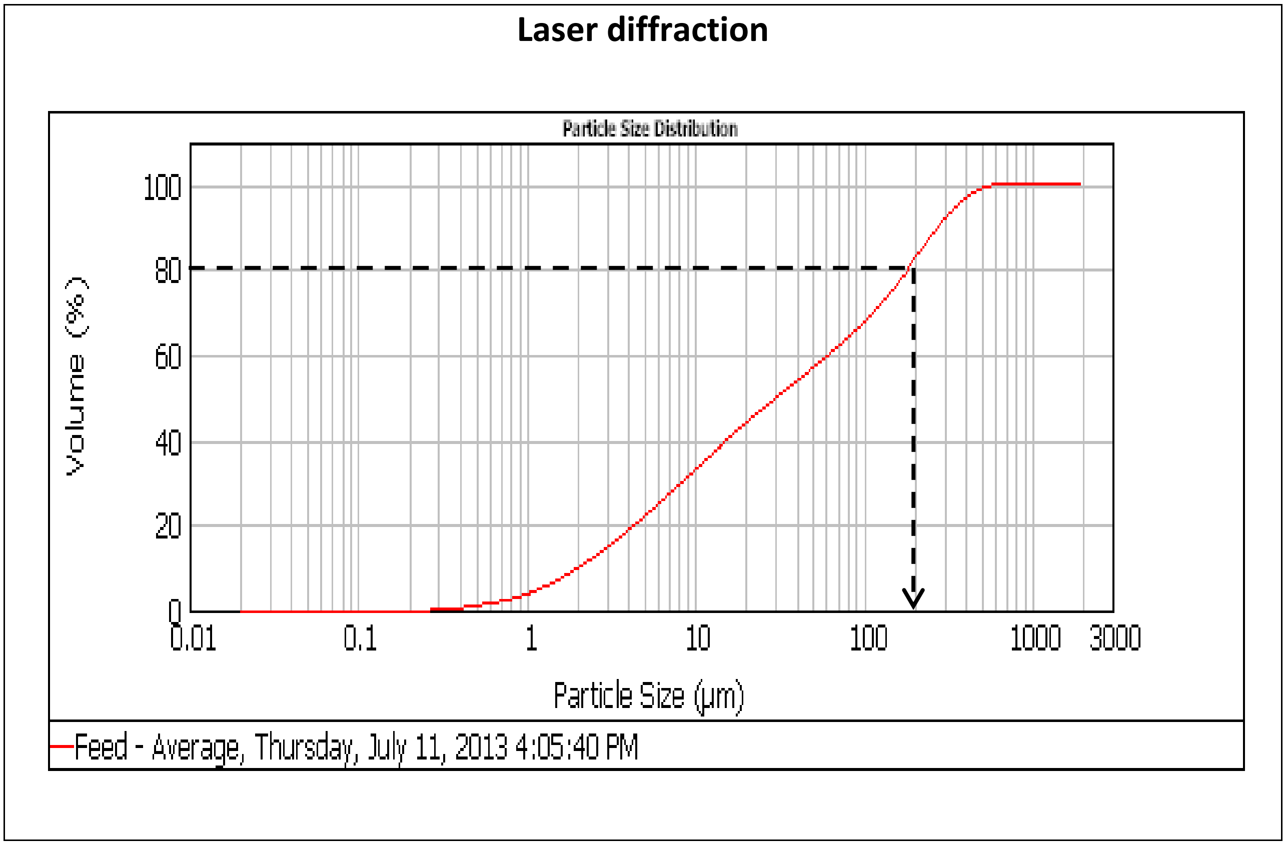

Appendix A.3 VXPmill feed particle size distribution by sieving

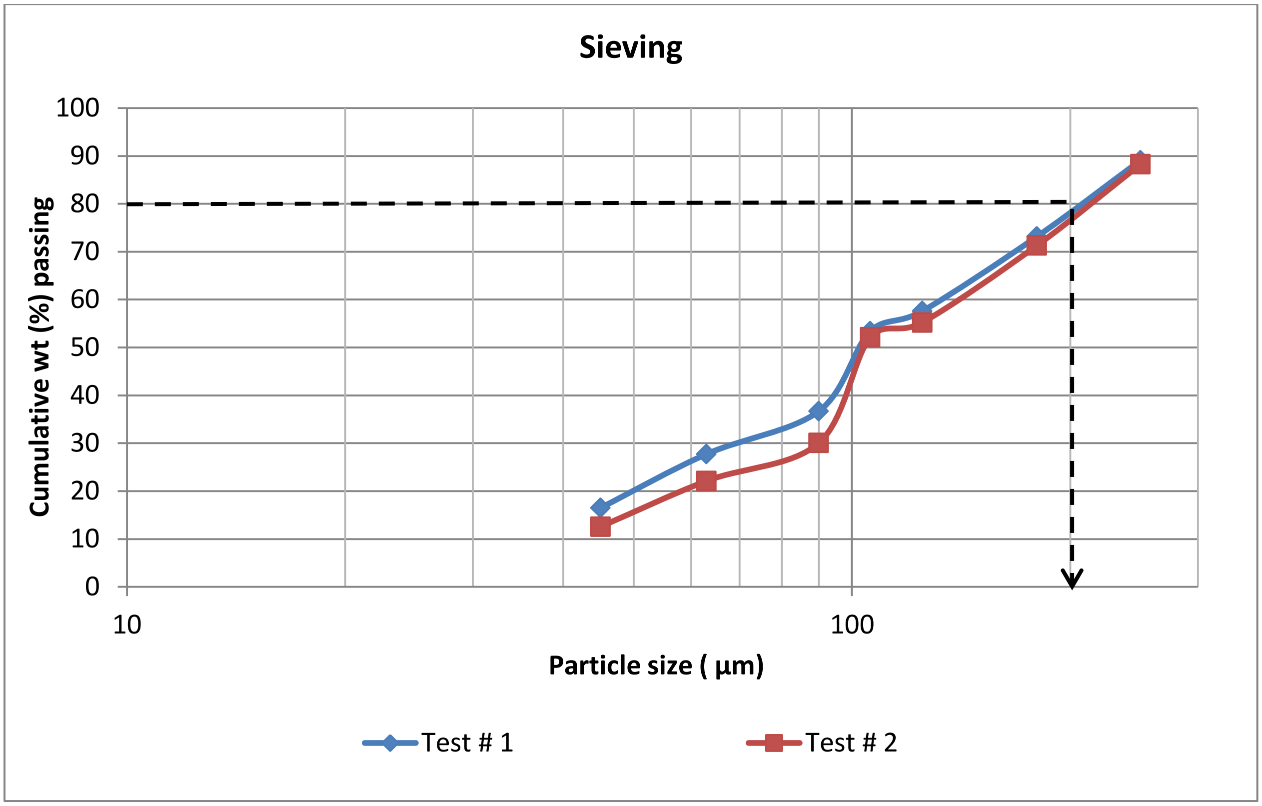

Appendix B Batch recycle versus pendulum

Appendix B.1 Pendulum, 40 kg sample weight, mill tip speed = 9.5 m/s, solids content = 30 % v/v, F_{80} = 120 µm

8th August 2012													
	Slurry density (kg/L)	Flowrate (L/min)	Mill speed (rpm)	Motor current (A)	Power (kW)	Torque (NM)	Temp out (°C)	Temp in (°C)	% solids w/w	Dry (t/h)	kWh/t	Cum kWh/t	P_{80} (µm)
Pass 1	1.4	6.4	1376	25.4	2.5	17.4	27.6	23.6	47.0	0.2	10.0	10.0	32
Pass 2	1.4	6.3	1419	25.3	2.5	16.9	31.3	26.8	47.0	0.3	10.0	20.1	23
Pass 3	1.4	6.3	1419	25.2	2.4	16.3	33.9	29.3	47.0	0.3	9.6	29.7	19
Pass 4	1.4	6.4	1419	25.1	2.4	16.0	35.9	31.4	47.0	0.3	9.3	39.1	17
Pass 5	1.4	6.5	1419	25.0	2.3	15.7	37.5	33.1	47.0	0.3	9.0	48.1	16
Pass 6	1.4	6.5	1419	24.9	2.2	15.1	38.6	34.2	47.0	0.3	8.7	56.7	15

Appendix B.2 Batch recycle, 25 kg sample weight, mill tip speed = 9.5 m/s, solids content = 30 % v/v, F_{80} = 120 µm

17th August 2012													
Time (min)	Slurry density (kg/L)	Flowrate (L/min)	Mill speed (rpm)	Motor current (A)	Power (kW)	Torque (NM)	Temp out (°C)	Temp in (°C)	% solids w/w	Dry (t/h)	kWh/t	Cum kWh/t	P_{80} (µm)
0.5	1.4	6.6	1419	25.6	2.7	18.1	28.2	25.9	46	0.3	10.7	10.7	43.2
1	1.4	6.4	1419	25.4	2.7	18.0	29.4	26.1	46	0.2	10.8	21.6	38.0
2	1.4	6.5	1419	25.5	2.6	17.7	30.5	26.5	46	0.2	10.6	32.2	34.7
4	1.4	6.4	1419	25.5	2.6	17.7	31.5	27.4	46	0.2	10.7	42.9	30.4
6	1.4	6.4	1419	25.5	2.6	17.6	32.7	28.5	46	0.2	10.6	53.5	26.2
8	1.4	6.3	1419	25.5	2.6	17.5	33.9	29.7	46	0.2	10.6	64.1	26.0
10	1.4	6.4	1419	25.4	2.6	17.3	35.1	30.8	46	0.2	10.4	74.5	23.2
12	1.4	6.4	1419	25.4	2.5	17.1	36.1	31.9	46	0.2	10.2	84.7	21.0
16	1.4	6.4	1419	25.3	2.5	16.9	37.7	33.4	46	0.2	10.1	94.8	19.3
20	1.4	6.5	1419	25.2	2.4	16.4	39.6	35.3	46	0.3	9.7	104.5	17.2
24	1.4	6.5	1419	25.1	2.4	16.1	41.2	37.0	46	0.3	9.5	114.0	15.9
28	1.4	6.5	1419	25.1	2.4	15.8	42.7	38.5	46	0.3	9.3	123.3	15.0
32	1.4	6.6	1419	25.0	2.3	15.6	44.0	39.8	46	0.3	9.1	132.4	14.2
40	1.4	6.5	1419	25.0	2.3	15.4	45.7	41.5	46	0.3	9.0	141.4	13.1
48	1.4	6.5	1419	24.9	2.3	15.3	47.7	43.3	46	0.3	9.0	150.4	12.1
60	1.4	6.6	1419	24.9	2.2	15.1	49.6	45.1	46	0.3	8.7	159.2	11.1

Appendix B.3 Batch recycle, 55 kg sample weight, mill tip speed = 9.5 m/s, solids content = 30 % v/v, F_{80} = 120 µm

23rd August 2012													
Time (min)	Slurry density (kg/L)	Flowrate (L/min)	Mill speed (rpm)	Motor current (A)	Power (kW)	Torque (NM)	Temp out (°C)	Temp in (°C)	% solids w/w	Dry (t/h)	kWh/t	Cum kWh/t	P_{80} (µm)
0.5	1.4	6.3	1419	25.3	2.5	17.1	27.0	23.3	45	0.2	10.7	10.7	41.4
1	1.4	6.3	1419	25.3	2.6	17.1	27.1	23.4	45	0.2	11.1	21.9	41.5
2	1.4	6.4	1419	25.3	2.6	17.1	27.1	23.4	45	0.2	10.8	32.6	39.1
4	1.4	6.3	1419	25.3	2.5	17.1	27.2	23.4	45	0.2	10.6	43.2	38.5
6	1.4	6.3	1419	25.3	2.5	17.1	27.2	23.4	45	0.2	10.7	54.0	35.2
8	1.4	6.3	1419	25.3	2.5	17.1	27.2	23.4	45	0.2	10.7	64.7	30.1
12	1.4	6.3	1419	25.3	2.5	17.1	27.3	23.4	45	0.2	10.7	75.4	27.9
16	1.4	6.3	1419	25.3	2.5	17.1	27.3	23.4	45	0.2	10.6	86.0	25.0
20	1.4	6.3	1419	25.3	2.5	17.1	27.3	23.4	45	0.2	10.5	96.5	23.4
24	1.4	6.4	1419	25.3	2.5	17.1	27.4	23.4	45	0.2	10.3	106.8	22.3
32	1.4	6.3	1419	25.3	2.4	17.1	27.4	23.4	45	0.2	10.2	117.0	19.8
45	1.4	6.4	1419	25.3	2.4	17.1	27.4	23.4	45	0.2	9.9	126.8	16.9
60	1.4	6.4	1419	25.3	2.3	17.1	27.5	23.4	45	0.2	9.5	136.3	15.1
75	1.4	6.5	1419	25.3	2.3	17.1	27.5	23.4	45	0.2	9.3	145.7	13.8
85	1.4	6.5	1419	25.3	2.2	17.1	27.6	23.5	45	0.2	9.2	154.9	13.2

Appendix B.4 Pendulum, 25 kg sample weight, mill tip speed = 10 m/s, solids content = 15 % v/v, F_{80} = 200 µm

10th July 2013													
	Slurry density (kg/L)	Flowrate (L/min)	Mill speed (rpm)	Motor current (A)	Power (kW)	Torque (NM)	Temp out (°C)	Temp in (°C)	% solids w/w	Dry (t/h)	kWh/t	Cum kWh/t	P_{80} (µm)
Pass 1	1.2	10	1490	24.4	2.0	12.8	25.6	23.7	31	0.2	9.1	9.1	61.5
Pass 2	1.2	10	1490	24.5	2.0	13.0	27.8	25.0	31	0.2	9.5	18.6	33.6
Pass 3	1.2	10	1490	24.4	2.0	12.9	28.9	26.6	31	0.2	9.3	28.0	26.8
Pass 4	1.1	10	1490	24.5	2.1	13.2	30.9	28.1	31	0.2	10.0	37.9	22.0
Pass 5	1.1	10	1490	24.5	2.0	12.9	31.8	29.3	31	0.2	9.5	47.4	19.4
Pass 6	1.1	10	1490	24.5	2.0	13.0	33.4	30.4	31	0.2	9.6	57.1	16.8
Pass 7	1.1	10	1490	24.5	2.0	13.1	34.0	31.4	31	0.2	10.3	67.4	15.5
Pass 8	1.2	10	1490	24.4	2.0	12.6	34.8	32.0	31	0.2	8.8	76.2	14.6
Pass 9	1.2	10	1490	24.3	2.0	12.9	35.2	33.1	31	0.2	9.3	85.5	13.9

Appendix B.5 Batch recycle, 25 kg sample weight, mill tip speed = 10 m/s, solids content = 15 % v/v, F_{80} = 200 µm

30th July 2013													
Time (min)	Slurry density (kg/L)	Flowrate (L/min)	Mill speed (rpm)	Motor current (A)	Power (kW)	Torque (NM)	Temp out (°C)	Temp in (°C)	% solids w/w	Dry (t/h)	kWh/t	Cum kWh/t	P_{80} (µm)
0.5	1.2	9.3	1490	24.4	1.9	12.5	24.3	22.6	31	0.2	9.1	9.1	184.6
1	1.2	9.3	1490	24.4	2.0	12.5	24.1	22.6	31	0.2	9.1	18.3	158.2
2	1.2	9.3	1490	24.4	1.9	12.4	24.4	23.1	31	0.2	9.2	27.4	150.0
4	1.2	9.4	1490	24.4	2.0	12.7	25.1	23.5	31	0.2	9.2	36.7	43.4
6	1.2	9.4	1490	24.4	2.0	12.6	26.0	24.3	31	0.2	9.1	45.8	35.7
8	1.2	9.4	1490	24.4	2.0	12.6	26.9	25.0	31	0.2	9.1	54.9	33.0
10	1.2	9.3	1490	24.3	1.9	12.5	27.7	25.7	31	0.2	9.1	64.0	29.5
12	1.2	9.3	1490	24.4	1.9	12.4	28.4	26.4	31	0.2	9.1	73.0	26.8
16	1.2	9.4	1490	24.4	2.0	12.6	29.3	27.3	31	0.2	9.1	82.2	22.6
20	1.2	9.5	1490	24.4	2.0	12.7	30.6	28.5	31	0.2	9.1	91.2	22.6
24	1.2	9.5	1490	24.4	2.0	12.6	31.7	29.7	31	0.2	9.0	100.3	20.8
28	1.2	9.6	1490	24.4	2.0	12.6	32.9	30.8	31	0.2	8.9	109.2	19.2
32	1.2	9.6	1490	24.4	2.0	12.7	33.9	31.8	31	0.2	8.9	118.2	17.5
36	1.2	9.6	1490	24.4	2.0	12.5	34.9	32.8	31	0.2	8.9	127.0	16.4
42	1.2	9.6	1490	24.4	2.0	12.5	36.1	33.9	31	0.2	8.8	135.9	15.3
48	1.2	9.7	1490	24.4	2.0	12.6	37.3	35.2	31	0.2	8.7	144.6	14.2
54	1.2	9.8	1490	24.4	2.0	12.5	38.4	36.2	31	0.2	8.7	153.3	13.4

Appendix C Analysis of operating variables

Appendix C.1 Mill tip speed =12 m/s, solids content = 15 % v/v, F_{80} = 300 µm

27th March 2013													
	Slurry density (kg/L)	Flowrate (L/min)	Mill speed (rpm)	Motor current (A)	Power (kW)	Torque (NM)	Temp out (°C)	Temp in (°C)	% solids w/w	Dry (t/h)	kWh/t	Cum kWh/t	P_{80} (µm)
Pass 1	1.2	10	1795	20	2.67	14.2	20.3	18.9	31	0.22	11.97	12.0	100.0
Pass 2	1.2	10	1794	20	2.67	14.2	23.0	18.9	31	0.22	11.98	23.9	43.7
Pass 3	1.2	10	1794	20	2.73	14.5	25.7	19.6	31	0.22	12.24	36.2	27.4
Pass 4	1.2	10	1794	20	2.70	14.4	27.8	22.3	31	0.22	12.09	48.3	23.9
Pass 5	1.2	10	1794	20	2.69	14.3	30.2	23.3	31	0.22	12.04	60.3	20.4
Pass 6	1.2	10	1794	20	2.67	14.2	31.5	25.7	31	0.22	11.97	72.3	17.7
Pass 7	1.2	10	1794	20	2.67	14.2	33.4	25.7	31	0.22	11.97	84.2	15.8
Pass 8	1.2	10	1794	20	2.63	14.0	34.3	25.7	31	0.22	11.77	96.0	14.9
Pass 9	1.2	10	1794	20	2.66	14.1	35.9	25.7	31	0.22	11.90	107.9	13.9

Appendix C.2 Mill tip speed = 7 m/s, solids content = 15 % v/v, F_{80} = 300 µm

28th March 2013													
	Slurry density (kg/L)	Flowrate (L/min)	Mill speed (rpm)	Motor current (A)	Power (kW)	Torque (NM)	Temp out (°C)	Temp in (°C)	% solids w/w	Dry (t/h)	kWh/t	Cum kWh/t	P_{80} (µm)
Pass 1	1.20	10	1043	24.4	1.29	11.81	20.29	19.02	31	0.22	5.77	5.77	105.0
Pass 2	1.20	10	1043	24.4	1.28	11.69	21.61	19.02	31	0.22	5.72	11.48	50.0
Pass 3	1.20	10	1043	24.4	1.31	12.00	23.14	19.02	31	0.22	5.85	17.34	30.8
Pass 4	1.20	10	1043	24.4	1.30	11.89	24.05	19.02	31	0.22	5.81	23.14	27.3
Pass 5	1.20	10	1043	24.4	1.32	12.11	25.19	19.02	31	0.22	5.91	29.05	21.0
Pass 6	1.20	10	1043	24.4	1.32	12.07	25.86	19.02	31	0.22	5.90	34.95	19.8
Pass 7	1.20	10	1043	24.4	1.30	11.89	26.79	19.02	31	0.22	5.81	40.76	17.7
Pass 8	1.20	10	1043	24.4	1.32	12.08	27.34	19.02	31	0.22	5.90	46.65	16.5
Pass 9	1.20	10	1043	24.4	1.30	11.91	27.81	19.02	31	0.22	5.82	52.47	15.2

Appendix C.3 Mill tip speed = 12 m/s, solids content = 30 % v/v, F_{80} = 200 μm

8th July 2013													
	Slurry density (kg/L)	Flowrate (L/min)	Mill speed (rpm)	Motor current (A)	Power (kW)	Torque (NM)	Temp out (°C)	Temp in (°C)	% solids w/w	Dry (t/h)	kWh/t	Cum kWh/t	P_{80} (μm)
Pass 1	1.4	10	1794	19.94	2.83	14.98	21.68	19.06	52.0	0.44	6.47	6.47	59.9
Pass 2	1.4	10	1794	19.84	2.76	14.68	23.08	19.06	52.0	0.44	6.32	12.78	48.0
Pass 3	1.4	10	1794	19.87	2.79	14.81	24.18	19.06	52.0	0.44	6.39	19.17	38.1
Pass 4	1.4	10	1794	19.87	2.80	14.84	26.25	19.06	52.0	0.44	6.40	25.57	31.8
Pass 5	1.4	10	1794	19.81	2.80	14.85	26.89	19.06	52.0	0.44	6.42	31.99	29.4
Pass 6	1.4	10	1794	19.78	2.78	14.78	28.20	19.06	52.0	0.44	6.36	38.35	27.8
Pass 7	1.4	10	1794	19.86	2.83	15.07	29.00	19.06	52.0	0.44	6.49	44.84	25.7
Pass 8	1.4	10	1794	19.78	2.79	14.83	30.01	19.06	52.0	0.44	6.40	51.24	24.8
Pass 9	1.4	10	1794	19.87	2.89	15.31	30.88	19.06	52.0	0.44	6.61	57.85	22.6

Appendix C.4 Mill tip speed = 12 m/s, solids content = 15 % v/v, F_{80} = 200 µm

8th July 2013													
	Slurry density (kg/L)	Flowrate (L/min)	Mill speed (rpm)	Motor current (A)	Power (kW)	Torque (NM)	Temp out (°C)	Temp in (°C)	% solids w/w	Dry (t/h)	kWh/t	Cum kWh/t	P_{80} (µm)
Pass 1	1.2	10	1794	19.5	2.6	13.9	23.0	19.8	31	0.2	11.8	11.8	51.9
Pass 2	1.2	10	1794	19.5	2.7	14.2	25.2	21.9	31	0.2	12.4	24.2	32.0
Pass 3	1.2	10	1794	19.4	2.7	14.1	27.6	24.7	31	0.2	12.1	36.3	25.3
Pass 4	1.2	10	1794	19.5	2.7	14.6	30.4	26.6	31	0.2	12.4	48.7	20.6
Pass 5	1.2	10	1794	19.3	2.6	14.0	31.9	28.8	31	0.2	11.8	60.5	18.7
Pass 6	1.2	10	1794	19.4	2.7	14.4	34.3	30.5	31	0.2	12.2	72.7	16.2
Pass 7	1.2	10	1794	19.3	2.6	14.0	35.4	32.2	31	0.2	11.9	84.6	15.4
Pass 8	1.2	10	1794	19.3	2.6	14.1	37.5	33.5	31	0.2	11.8	96.4	14.0
Pass 9	1.2	10	1794	19.2	2.6	14.0	38.1	35.1	31	0.2	11.6	108.0	13.5

Appendix C.5 Mill tip speed = 7 m/s, solids content = 15 % v/v, F_{80} = 200 μm

9th July 2013													
	Slurry density (kg/L)	Flow rate (L/min)	Mill speed (rpm)	Motor current (A)	Power (kW)	Torque (NM)	Temp out (°C)	Temp in (°C)	% solids w/w	Dry (t/h)	kWh/t	Cum kWh/t	P_{80} (μm)
Pass 1	1.2	10	1043	24.4	1.3	12.1	26.4	25.1	31	0.2	6.0	6.0	65.0
Pass 2	1.2	10	1043	24.4	1.3	12.3	27.4	26.1	31	0.2	6.1	12.2	34.9
Pass 3	1.2	10	1043	24.4	1.3	12.2	28.6	26.8	31	0.2	6.0	18.2	28.2
Pass 4	1.2	10	1043	24.4	1.3	12.0	29.1	27.5	31	0.2	6.0	24.2	21.8
Pass 5	1.2	10	1043	24.4	1.3	12.0	30.1	28.3	31	0.2	6.2	30.3	19.2
Pass 6	1.2	10	1043	24.4	1.3	12.0	30.6	29.0	31	0.2	6.0	36.3	17.6
Pass 7	1.2	10	1043	24.4	1.3	12.1	31.5	29.6	31	0.2	6.1	42.5	15.8
Pass 8	1.2	10	1043	24.4	1.3	12.1	31.6	30.1	31	0.2	6.0	48.5	14.9
Pass 9	1.2	10	1043	24.4	1.3	12.2	32.1	30.5	31	0.2	6.1	54.6	13.9

Appendix C.6 Mill tip speed = 10 m/s, solids content = 30 % v/v, F_{80} = 200 µm

9th July 2013													
	Slurry density (kg/L)	Flow rate (L/min)	Mill speed (rpm)	Motor current (A)	Power (kW)	Torque (NM)	Temp out (°C)	Temp in (°C)	% solids w/w	Dry (t/h)	kWh/t	Cum kWh/t	P_{80} (µm)
Pass 1	1.3	10	1490	23.5	2.0	12.9	25.1	23.1	52	0.4	5.1	5.1	75.0
Pass 2	1.3	10	1490	24.4	2.0	12.8	26.8	24.4	52	0.4	5.0	10.1	52.2
Pass 3	1.3	10	1490	24.4	2.0	12.6	28.3	25.9	52	0.4	4.7	14.8	43.2
Pass 4	1.4	10	1490	24.4	2.0	12.7	29.2	27.0	52	0.4	4.6	19.4	37.0
Pass 5	1.2	10	1490	24.4	2.0	12.8	30.1	27.8	52	0.4	5.3	24.8	34.1
Pass 6	1.4	10	1490	24.4	2.0	12.7	30.8	28.3	52	0.4	4.5	29.2	31.3
Pass 7	1.4	10	1490	24.4	2.0	12.8	31.4	29.0	52	0.4	4.7	33.9	27.4
Pass 8	1.4	10	1490	24.4	2.0	12.8	32.0	29.5	52	0.4	4.5	38.4	24.5
Pass 9	1.4	10	1490	24.2	2.0	12.9	32.6	30.7	52	0.4	4.6	43.0	24.7

Appendix C.7 Mill tip speed = 10 m/s, solids content = 15 % v/v, F_{80} = 200 μm

10th July 2013													
	Slurry density (kg/L)	Flow rate (L/min)	Mill speed (rpm)	Motor current (A)	Power (kW)	Torque (NM)	Temp out (°C)	Temp in (°C)	% solids w/w	Dry (t/h)	kWh/t	Cum kWh/t	P_{80} (μm)
Pass 1	1.2	10	1490	24.4	2.0	12.8	25.6	23.7	31	0.2	9.1	9.1	61.5
Pass 2	1.2	10	1490	24.5	2.0	13.0	27.8	25.0	31	0.2	9.5	18.6	33.6
Pass 3	1.2	10	1490	24.4	2.0	12.9	28.9	26.6	31	0.2	9.3	28.0	26.8
Pass 4	1.1	10	1490	24.5	2.1	13.2	30.9	28.1	31	0.2	10.0	37.9	22.0
Pass 5	1.1	10	1490	24.5	2.0	12.9	31.8	29.3	31	0.2	9.5	47.4	19.4
Pass 6	1.1	10	1490	24.5	2.0	13.0	33.4	30.4	31	0.2	9.6	57.1	16.8
Pass 7	1.1	10	1490	24.5	2.0	13.1	34.0	31.4	31	0.2	10.3	67.4	15.5
Pass 8	1.2	10	1490	24.4	2.0	12.6	34.8	32.0	31	0.2	8.8	76.2	14.6
Pass 9	1.2	10	1490	24.3	2.0	12.9	35.2	33.1	31	0.2	9.3	85.5	13.9

Appendix C.8 Mill tip speed = 10 m/s, solids content = 40 % v/v, F_{80} = 200 µm

11th July 2013													
	Slurry density (kg/L)	Flow rate (L/min)	Mill speed (rpm)	Motor current (A)	Power (kW)	Torque (NM)	Temp out (°C)	Temp in (°C)	% solids w/w	Dry (t/h)	kWh/t	Cum kWh/t	P_{80} (µm)
Pass 1	1.6	8.5	1490	24.2	1.8	11.5	24.6	22.6	63	0.5	3.4	3.4	98.6
Pass 2	1.6	8.5	1490	24.1	1.7	11.2	26.3	23.9	63	0.5	3.3	6.7	72.0
Pass 3	1.6	8.5	1490	24.1	1.7	11.0	27.6	24.7	63	0.5	3.3	10.0	59.0
Pass 4	1.6	8.5	1490	24.2	1.8	11.4	28.5	24.9	63	0.5	3.4	13.4	50.0
Pass 5	1.6	8.5	1490	24.2	1.8	11.5	30.0	25.0	63	0.5	3.4	16.9	43.2
Pass 6	1.6	8.5	1490	24.3	1.9	11.9	31.2	24.9	63	0.5	3.5	20.4	39.7

Appendix C.9 Mill tip speed = 7 m/s, solids content = 40 % v/v, F_{80} = 200 µm

12th July 2013													
	Slurry density (kg/L)	Flow rate (L/min)	Mill speed (rpm)	Motor current (A)	Power (kW)	Torque (NM)	Temp out (°C)	Temp in (°C)	% solids w/w	Dry (t/h)	kWh/t	Cum kWh/t	P_{80} (µm)
Pass 1	1.6	8.5	1043	24.4	1.3	12.0	23.4	22.2	63	0.5	2.5	2.5	95.6
Pass 2	1.6	8.5	1043	24.4	1.3	11.9	24.9	22.9	63	0.5	2.5	5.0	59.9
Pass 3	1.6	8.5	1043	24.5	1.3	12.4	26.2	23.5	63	0.5	2.6	7.6	49.3
Pass 4	1.6	8.5	1043	24.4	1.3	12.0	26.8	23.8	63	0.5	2.5	10.0	41.2
Pass 5	1.6	8.5	1043	24.2	1.2	10.7	27.8	24.1	63	0.5	2.2	12.3	35.6
Pass 6	1.6	8.5	1043	24.2	1.2	10.9	27.6	23.9	63	0.5	2.3	14.5	34.2

Appendix C.10 Mill tip speed = 3 m/s, solids content = 30 % v/v, F_{80} = 200 µm

2nd Sept 2013													
	Slurry density (kg/L)	Flow rate (L/min)	Mill speed (rpm)	Motor current (A)	Power (kW)	Torque (NM)	Temp out (°C)	Temp in (°C)	% solids w/w	Dry (t/h)	kWh/t	Cum kWh/t	P_{80} (µm)
Pass 1	1.4	9.0	445	23.7	0.3	6.3	23.6	23.8	52	0.4	0.7	0.7	135.0
Pass 2	1.4	8.7	445	23.7	0.3	6.4	24.1	23.8	52	0.4	0.8	1.5	96.5
Pass 3	1.4	8.5	445	23.7	0.3	6.6	24.4	23.9	52	0.4	0.8	2.3	91.6
Pass 4	1.4	8.6	445	23.7	0.3	6.4	24.3	24.1	52	0.4	0.8	3.1	76.6
Pass 5	1.4	8.8	445	23.7	0.3	6.4	24.5	24.2	52	0.4	0.8	3.9	71.0
Pass 6	1.4	8.8	445	23.7	0.3	6.4	24.8	24.3	52	0.4	0.8	4.7	61.0
Pass 7	1.4	8.9	445	23.6	0.3	6.3	25.0	24.2	52	0.4	0.7	5.4	53.9
Pass 8	1.4	8.8	445	23.6	0.3	6.3	24.7	24.2	52	0.4	0.7	6.2	55.3
Pass 9	1.4	8.6	445	23.7	0.3	6.2	24.6	24.4	52	0.4	0.8	6.9	51.2

Appendix C.11 Mill tip speed = 10 m/s, solids content = 35 % v/v, F_{80} = 200 µm

3rd Sept 2013													
	Slurry density (kg/L)	Flow rate (L/min)	Mill speed (rpm)	Motor current (A)	Power (kW)	Torque (NM)	Temp out (°C)	Temp in (°C)	% solids w/w	Dry (t/h)	kWh/t	Cum kWh/t	P_{80} (µm)
Pass 1	1.5	8.7	1488	24.3	1.9	12.1	25.4	23.5	58	0.5	4.2	4.2	90.0
Pass 2	1.5	8.8	1490	24.3	1.8	11.9	26.9	24.9	58	0.5	4.0	8.2	72.1
Pass 3	1.5	8.5	1490	24.3	1.9	12.3	28.3	25.7	58	0.4	4.4	12.7	50.3
Pass 4	1.5	9.0	1490	24.2	1.8	11.8	29.1	26.6	58	0.5	3.8	16.5	47.0
Pass 5	1.5	9.1	1490	24.3	1.9	12.0	29.8	27.2	58	0.5	4.0	20.5	40.8
Pass 6	1.5	9.0	1490	24.4	1.9	12.4	30.4	27.7	58	0.5	4.1	24.6	38.9
Pass 7	1.5	9.0	1490	24.3	1.9	12.2	31.1	28.2	58	0.5	4.0	28.6	34.5
Pass 8	1.5	9.3	1490	24.2	1.8	11.7	31.7	28.6	58	0.5	3.8	32.4	31.6
Pass 9	1.5	9.2	1490	24.3	1.8	11.6	32.3	29.1	58	0.5	3.7	36.1	30.7

Appendix D Rheological flow model fittings

Appendix D.1 Bingham, Herschel Bulkley and Casson models fitting for suspensions with 30% v/v ground at a tip speed of 12 m/s

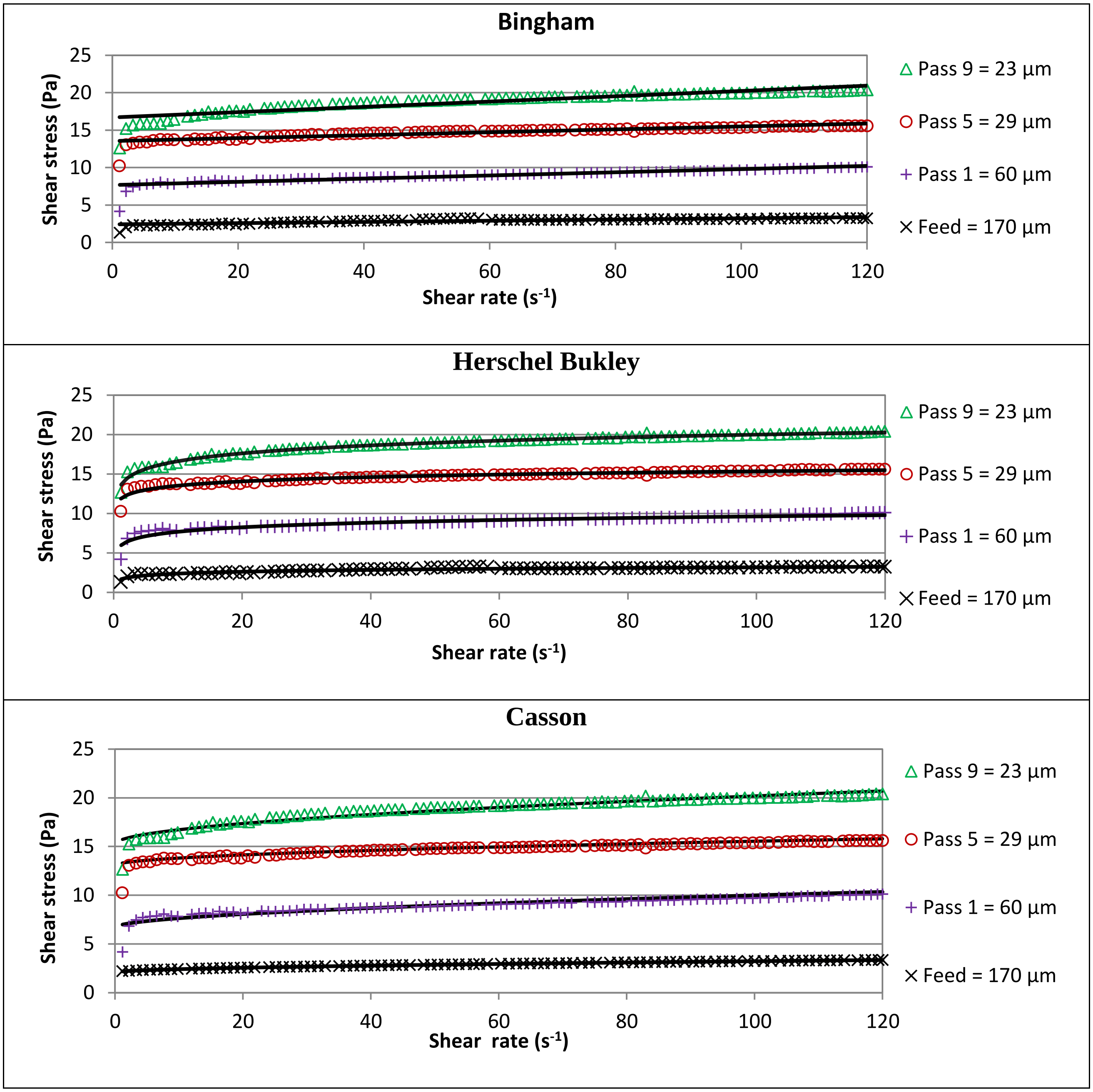

Appendix D.2 Rheological flow curves fitting parameters for suspensions with 30% v/v ground at a tip speed of 12 m/s (as calculated by HAAKE RheoWin software)

		Herschel Bulkley	Bingham	Casson
n	Pass 9	0.04	-	-
	Feed	0.008	-	-
k	Pass 9	94.4	-	-
	Feed	12.0	-	-
τ_{HB}, τ_B, τ_C (Pa)	Pass 9	−10.4	16.7	15.2
	Feed	−80.7	2.4	2.1
η_B, η_C (mPas)	Pass 9	-	35.3	3.5
	Feed	-	8.3	1.3
R^2	Pass 9	0.99	0.92	0.97
	Feed	0.86	0.69	0.76

Appendix D.3 Effect of solids content on yield stress

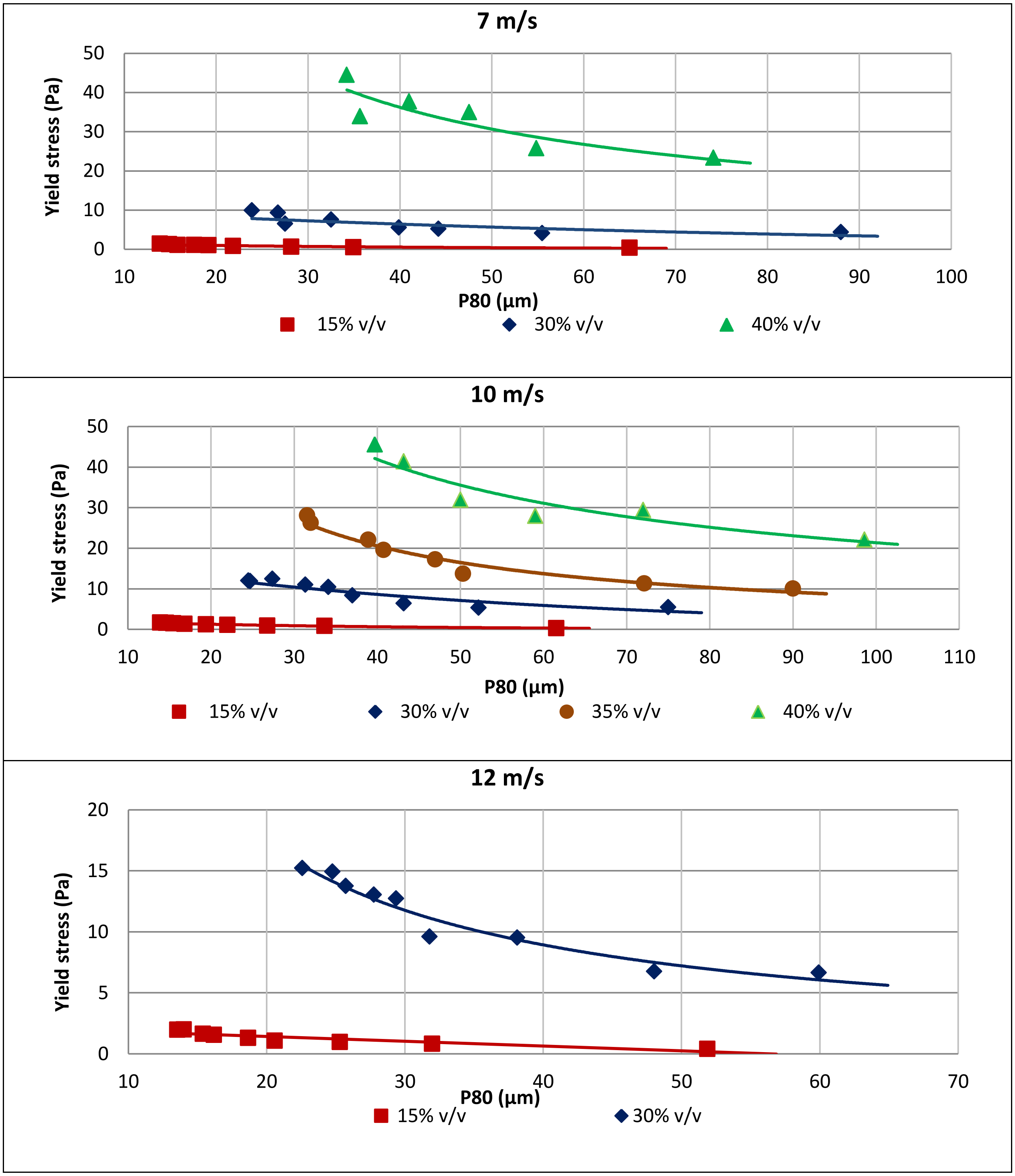

Appendix D.4 Effect of solids content on apparent viscosity (at 100 s^{-1} shear rate)

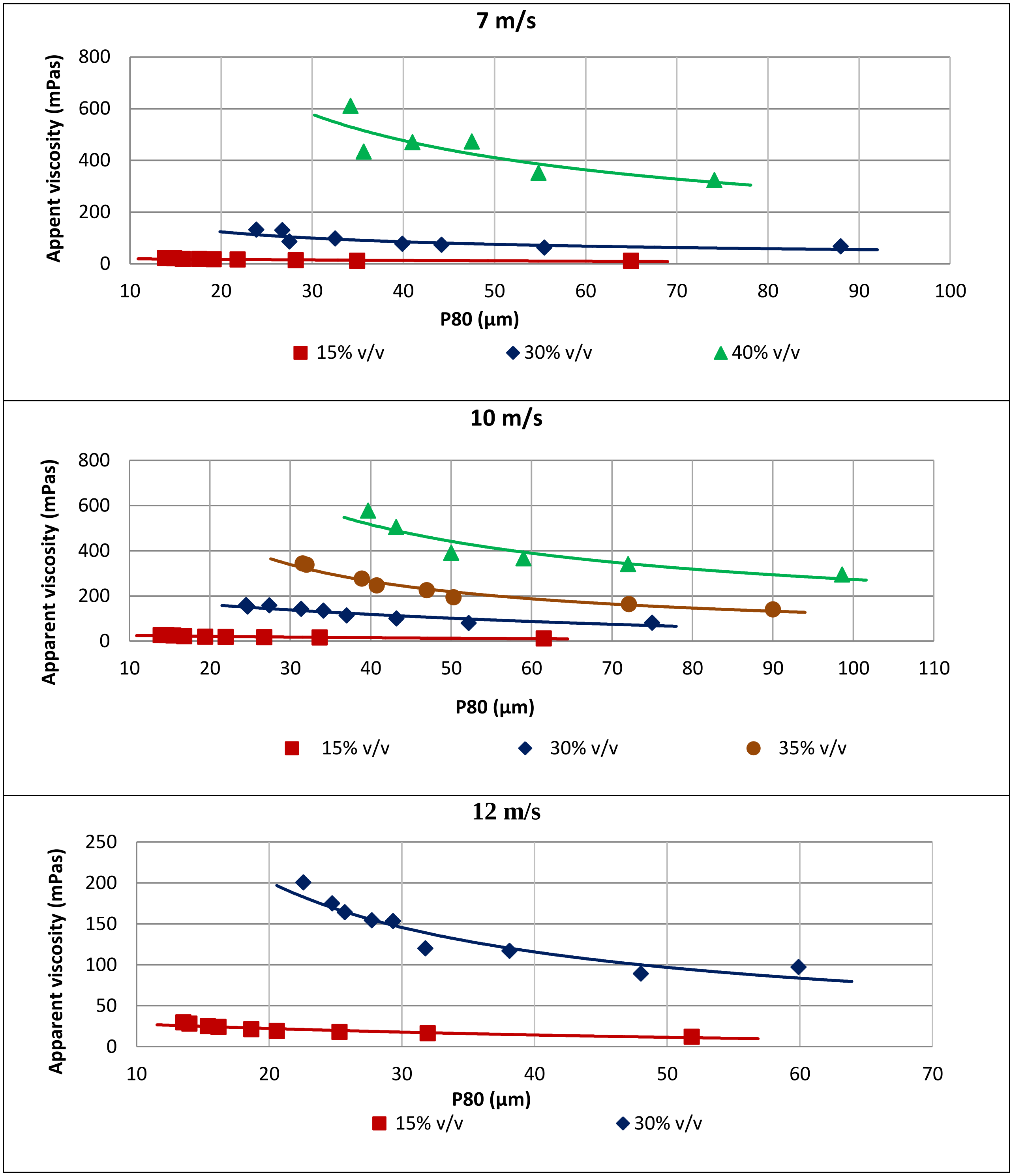

Appendix E BET surface area and particle size by laser diffraction

Appendix E.1 BET multipoint (feed)

10/22/2013

Quantachrome Instruments
Quantachrome Autosorb Automated Gas Sorption System Report
Autosorb 1 for Windows 1.52

File name:	C:\QCdata\PhysData\Baker\For BET vs Malvern\Feed.raw				
Sample ID:	Feed	Description:	Feed (6mm with rod)		
Comments:					
Operator:	Baker	Sample weight:	0.7001 g		
Analysis gas:	Nitrogen	X sect. area:	16.2 Å²/molec	Non-ideality:	6.58e-05
Adsbate (DRP):	Nitrogen	Bath Temp.:	77.30		
Outgas Temp:	24.2 °C	Outgas Time:	23.7 hrs	Analysis Time:	83.5 min
P/Po tolerance:	0	Equil. time:	3	End of run:	09/20/2013 10:50
Station #:	1	PC sw. version:	1.52	TempComp:	On

MULTIPOINT BET

P/Po	Volume [cc/g] STP	1/(W((Po/P)-1))
5.3176e-02	1.1382	3.948E+01
7.5195e-02	1.2152	5.354E+01
1.0049e-01	1.2889	6.935E+01
1.2564e-01	1.3574	8.470E+01
1.5050e-01	1.4265	9.936E+01
1.7577e-01	1.4895	1.146E+02
2.0099e-01	1.5458	1.302E+02
2.2586e-01	1.6005	1.458E+02
2.5093e-01	1.6539	1.621E+02
2.7587e-01	1.7056	1.787E+02
3.0092e-01	1.7574	1.960E+02

Area = 5.521E+00 m²/g

Slope = 6.249E+02

Y - Intercept = 5.858E+00

Correlation Coefficient = 0.999802

C = 1.077E+02

Appendix E.2 BET multipoint (pass 1)

```
10/22/2013
                                   Quantachrome Instruments
                     Quantachrome Autosorb Automated Gas Sorption System Report
                                 Autosorb 1 for Windows  1.52

File name:     C:\QCdata\PhysData\Baker\For BET vs Malvern\Pass 1.raw
Sample ID:     Pass 1            Description:   Pass 1 (6mm with rod)
Comments:
Operator:      Baker             Sample weight: 0.496 g
Analysis gas:  Nitrogen          X sect. area:  16.2 Å²/molec     Non-ideality:  6.58e-05
Adsbate (DRP): Nitrogen          Bath Temp.:    77.30
Outgas Temp:   300.0  °C         Outgas Time:   23.0  hrs         Analysis Time: 82.2 min
P/Po tolerance: 0                Equil. time:   3                 End of run:    09/15/2013 19:12
Station #:     1                 PC sw. version: 1.52             TempComp:      On

                                MULTIPOINT BET

               P/Po               Volume          1/(W((Po/P)-1))
                                [cc/g] STP

          5.1267e-02              1.3171           3.283E+01
          7.5512e-02              1.4294           4.572E+01
          1.0088e-01              1.5257           5.884E+01
          1.2584e-01              1.6138           7.137E+01
          1.5088e-01              1.6964           8.381E+01
          1.7608e-01              1.7724           9.648E+01
          2.0119e-01              1.8437           1.093E+02
          2.2603e-01              1.9146           1.220E+02
          2.5100e-01              1.9847           1.351E+02
          2.7546e-01              2.0717           1.468E+02
          3.0085e-01              2.1426           1.607E+02

                                   Area =  6.747E+00 m²/g

                                  Slope =  5.091E+02

                          Y - Intercept =  7.084E+00

                Correlation Coefficient =  0.999972

                                      C =  7.286E+01
```

Appendix E.3 BET multipoint (pass 6)

10/22/2013

Quantachrome Instruments

Quantachrome Autosorb Automated Gas Sorption System Report

Autosorb 1 for Windows 1.52

File name: C:\QCdata\PhysData\Baker\For BET vs Malvern\Pass 6.raw

Sample ID: Pass 6 Description: Pass 6, (6mm with rod)

Comments:

Operator:	Baker	Sample weight:	0.3829 g		
Analysis gas:	Nitrogen	X sect. area:	16.2 Å²/molec	Non-ideality:	6.58e-05
Adsbate (DRP):	Nitrogen	Bath Temp.:	77.30		
Outgas Temp:	22.3 °C	Outgas Time:	23.0 hrs	Analysis Time:	85.2 min
P/Po tolerance:	0	Equil. time:	3	End of run:	09/13/2013 13:12
Station #:	1	PC sw. version:	1.52	TempComp:	On

MULTIPOINT BET

P/Po	Volume [cc/g] STP	1/(W((Po/P)-1))
4.9104e-02	1.6465	2.509E+01
7.5074e-02	1.7809	3.647E+01
1.0069e-01	1.8896	4.741E+01
1.2570e-01	1.9879	5.787E+01
1.5074e-01	2.0814	6.823E+01
1.7578e-01	2.1678	7.872E+01
2.0077e-01	2.2458	8.950E+01
2.2518e-01	2.3323	9.970E+01
2.5097e-01	2.4035	1.115E+02
2.7605e-01	2.4710	1.235E+02
3.0121e-01	2.5367	1.360E+02

Area = 7.965E+00 m²/g

Slope = 4.340E+02

Y - Intercept = 3.256E+00

Correlation Coefficient = 0.999668

C = 1.343E+02

Appendix E.4 BET multipoint (pass 9)

```
10/22/2013
                                  Quantachrome Instruments
                 Quantachrome Autosorb Automated Gas Sorption System Report
                                Autosorb 1 for Windows  1.52

File name:      C:\QCdata\PhysData\Baker\For BET vs Malvern\Pass 9.raw
Sample ID:      Pass 9          Description:   Pass 9 repeat (6mm with rod)
Comments:
Operator:       Baker           Sample weight: 0.4026 g
Analysis gas:   Nitrogen        X sect. area:  16.2 Å²/molec     Non-ideality:  6.58e-05
Adsbate (DRP):  Nitrogen        Bath Temp.:    77.30
Outgas Temp:    22.4  °C        Outgas Time:   24.0  hrs         Analysis Time: 83.6 min
P/Po tolerance: 0               Equil. time:   3                 End of run:    09/15/2013 16:23
Station #:      1               PC sw. version: 1.52             TempComp:      On

                                MULTIPOINT BET

               P/Po                Volume          1/(W((Po/P)-1))
                                 [cc/g] STP

           5.3492e-02               2.1252             2.128E+01
           7.4875e-02               2.2680             2.855E+01
           1.0013e-01               2.4085             3.697E+01
           1.2530e-01               2.5353             4.521E+01
           1.5035e-01               2.6527             5.337E+01
           1.7556e-01               2.7637             6.165E+01
           2.0020e-01               2.8833             6.946E+01
           2.2559e-01               2.9887             7.799E+01
           2.5070e-01               3.0847             8.678E+01
           2.7580e-01               3.1848             9.567E+01

                                  Area =  1.038E+01 m²/g

                                 Slope =  3.318E+02

                           Y - Intercept =  3.542E+00

                 Correlation Coefficient =  0.999919

                                     C =  9.468E+01
```

Appendix E.5 Laser diffraction (feed, pass 1, pass 6 (~~pass 7~~), pass 9)

Sample name	d (0.1)	d (0.5)	d (0.8)	Residual - weig...	Obscuration
Pass 9	1.514	8.242	20.288	0.486	20.68
Pass 9	1.512	8.208	20.479	0.494	20.73
Pass 9	1.496	8.037	19.913	0.481	20.72
Pass 9 - Average	1.507	8.162	20.224	0.487	20.71
Pass 9	1.497	8.129	19.866	0.474	15.10
Pass 9	1.485	8.012	19.455	0.456	15.08
Pass 9	1.476	7.914	19.090	0.443	15.05
Pass 9 - Average	1.486	8.018	19.466	0.458	15.08
Pass 7	1.881	11.764	29.649	0.529	15.58
Pass 7	1.815	10.912	28.116	0.541	15.92
Pass 7	1.784	10.497	27.497	0.552	16.08
Pass 7 - Average	1.825	11.040	28.448	0.541	15.86
Pass 7	2.068	13.683	35.870	0.512	16.05
Pass 7	1.992	12.696	34.990	0.528	16.47
Pass 7	1.942	12.123	34.094	0.524	16.66
Pass 7 - Average	1.999	12.821	35.009	0.521	16.39
Pass 7	1.937	12.771	36.598	0.526	18.46
Pass 7	1.904	12.357	36.534	0.535	18.65
Pass 7	1.874	11.995	35.884	0.529	18.76
Pass 7 - Average	1.905	12.372	36.341	0.530	18.62
Pass 1	2.231	19.533	108.226	0.451	18.52
Pass 1	2.173	18.395	101.928	0.456	18.71
Pass 1	2.146	17.982	101.184	0.468	18.84
Pass 1 - Average	2.182	18.632	103.728	0.458	18.69
Pass 1	2.555	22.140	116.158	0.434	18.07
Pass 1	2.441	20.426	118.766	0.442	18.74
Pass 1	2.349	19.038	113.781	0.448	19.05
Pass 1 - Average	2.445	20.543	116.209	0.441	18.62
Feed	2.506	51.385	275.284	0.485	15.56
Feed	2.511	52.521	277.445	0.516	15.61
Feed	2.442	47.506	262.391	0.494	15.63
Feed - Average	2.486	50.421	271.747	0.498	15.60
Feed	2.385	52.364	281.740	0.535	16.49
Feed	2.284	44.396	259.599	0.490	16.47
Feed	2.320	47.770	264.232	0.515	16.50
Feed - Average	2.329	48.061	268.685	0.514	16.49

Appendix F Scale-up demonstration study

Appendix F.1 Mill tip speed = 12 m/s, media charge = 35%, media type = CZC

VXP10 mill														
	Density (kg/L)	Flow-rate (L/min)	Speed (rpm)	Current (A)	Power (kW)	Torque (NM)	Temp out (°C)	Temp in(°C)	% solids w/w	Dry (t/h)	kWh/t	Cum kWh/t	P_{80} (µm)	F_{80} (µm)
Pass 1	1.3	13.0	1760	7.8	3.36	15.2	33.8	31.6	36.0	0.36	9.2	9.2	27.7	
Pass 2	1.3	12.1	1760	7.8	3.37	15.2	35.8	33.7	36.0	0.33	10.1	19.3	22.4	
Pass 3	1.3	12.9	1760	7.7	3.30	14.9	37.1	35.0	36.0	0.36	9.1	28.4	20.2	
Pass 4	1.3	12.2	1760	7.7	3.32	15.0	38.5	36.4	36.0	0.34	9.8	38.2	17.6	
Pass 5	1.3	13.2	1760	7.6	3.24	14.6	39.8	37.9	36.0	0.37	8.6	46.8	15.5	40.4

VXP2500 mill														
	Density (kg/L)	Flow-rate (L/min)	Speed (rpm)	Current (A)	Power (kW)	Torque (NM)	Temp out (°C)	Temp in(°C)	% solids w/w	Dry (t/h)	kWh/t	Cum kWh/t	P_{80} (µm)	F_{80} (µm)
7th-Nov,test 1	1.3	1083.3	258	504.0	388.0	14920	30.1	25.2	38.0	32.9	11.8	11.8	40.1	94.5
7th-Nov,test 5	1.3	1083.3	258	596.9	389.6	14931	33.3	28.5	37.0	31.5	12.4	12.4	38.5	103
8th-Nov,test 3	1.4	1083.3	249	503.6	406.2	15096	33.7	28.8	40.0	35.1	11.6	11.6	27.9	58.2
21st-Nov,test 3	1.3	1083.3	241	611.0	469.0	18568	36.6	30.6	36.0	30.2	15.5	15.5	33.3	70.4
23rd-Nov,test 3	1.4	1083.3	241	458.0	357.0	14150	31.0	26.0	44.0	40.0	8.9	8.9	34.0	61.4

Appendix F.2 Mill tip speed = 10 m/s, media charge = 35%, media type = CZC

VXP10 mill														
	Density (kg/L)	Flowrate (L/min)	Speed (rpm)	Current (A)	Power (kW)	Torque (NM)	Temp out (°C)	Temp in(°C)	% solids w/w	Dry (t/h)	kWh/t	Cum kWh/t	P_{80} (µm)	F_{80} (µm)
Pass 1	1.30	8	1500	10	3.02	16	29	26	36	0.2	12.5	12.5	23.1	
Pass 2	1.31	8	1500	10	3.01	16	31	28	36	0.2	12.1	24.6	18.3	
Pass 3	1.31	8	1500	10	3.00	16	33	29	36	0.3	11.9	36.5	15.0	
Pass 4	1.31	8	1500	10	2.99	16	32	29	36	0.3	11.9	48.4	13.7	38.4
VXP10 mill														
	Density (kg/L)	Flowrate (L/min)	Speed (rpm)	Current (A)	Power (kW)	Torque (NM)	Temp out (°C)	Temp in(°C)	% solids w/w	Dry (t/h)	kWh/t	Cum kWh/t	P_{80} (µm)	F_{80} (µm)
Pass 1	1.33	12	1500	9	2.5	13	25	24	37	0.4	6.6	6.6	31.7	
Pass 2	1.28	11	1500	9	2.4	13	27	25	37	0.3	7.3	13.9	25.2	
Pass 3	1.33	13	1500	9	2.5	13	28	27	37	0.4	6.3	20.1	20.7	
Pass 4	1.30	12	1500	9	2.5	13	29	28	37	0.4	6.8	26.9	17.5	
Pass 5	1.33	13	1500	9	2.4	13	30	29	37	0.4	6.1	33.0	16.3	43.6
VXP2500 mill														
	Density (kg/L)	Flowrate (L/min)	Speed (rpm)	Current (A)	Power (kW)	Torque (NM)	Temp out (°C)	Temp in(°C)	% solids w/w	Dry (t/h)	kWh/t	Cum kWh/t	P_{80} (µm)	F_{80} (µm)
07th Nov, test 4	1.29	1666.7	208	522	348	15927	30	27	35	45	8	8	50.19	100.4
8th Nov, test 4	1.35	750.0	208	652	433	19856	37	29	40	24	18	18	22.9	47.9
8th Nov, test 5	1.35	1083.3	208	648	429	19693	35	29	40	35	12	12	25.19	47.2

Appendix F.3 Mill tip speed = 10 m/s, media charge = 40%, media type = CZC

VXP10 mill

	Density (kg/L)	Flow-rate (L/min)	Speed (rpm)	Current (A)	Power (kW)	Torque (NM)	Temp out (°C)	Temp in (°C)	% solids w/w	Dry (t/h)	kWh/t	Cum kWh/t	P_{80} (µm)	F_{80} (µm
PASS 1	1.3	13.4	1472	9.1	2.28	12.2	30.3	28.9	38	0.40	5.6	5.6	34.2	
PASS 2	1.3	12.6	1500	9.0	2.33	12.4	31.6	30.4	38	0.38	6.2	11.8	29.2	
PASS 3	1.3	13.4	1500	9.0	2.34	12.4	32.6	31.3	38	0.40	5.8	17.6	24.9	
PASS 4	1.3	12.6	1500	8.9	2.35	12.5	33.6	32.4	38	0.37	6.3	24.0	23.9	
PASS 5	1.3	13.5	1498	8.9	2.33	12.4	34.6	33.3	38	0.41	5.7	29.6	20.5	45.3

VXP10 mill

	Density (kg/L)	Flow-rate (L/min)	Speed (rpm)	Current (A)	Power (kW)	Torque (NM)	Temp out (°C)	Temp in(°C)	% solids w/w	Dry (t/h)	kWh/t	Cum kWh/t	P_{80} (µm)	F_{80} (µm)
PASS 1	1.2	12.7	1499	9.0	2.06	11.0	27.5	26.3	30	0.28	7.3	7.3	45.45	
PASS 2	1.2	12.1	1500	9.0	2.08	11.0	28.3	27.4	30	0.27	7.8	15.2	38.45	
PASS 3	1.2	12.5	1500	8.9	2.06	10.9	29.2	28.2	30	0.28	7.5	22.7	33.2	
PASS 4	1.2	12.5	1500	8.8	2.06	10.9	29.9	28.9	30	0.28	7.4	30.1	24.2	
PASS 5	1.2	12.3	1500	8.9	2.11	11.2	30.7	29.6	30	0.27	7.9	38.0	22.55	92.1

VXP2500 mill

	Density (kg/L)	Flow-rate (L/min)	Speed (rpm)	Current (A)	Power (kW)	Torque (NM)	Temp out (°C)	Temp in(°C)	% solids w/w	Dry (t/h)	kWh/t	Cum kWh/t	P_{80} (µm)	F_{80} (µm)
17th Oct, test 2	1.3	1250.0	215	493	337	14959	31	26.7	36	35.1	9.6	9.6	41.5	89.2
20th Nov, test 1	1.29	500.0	201	704	457	21708	42.6	29.8	35	13.5	33.7	33.7	20.4	40.8

Appendix F.4 Mill tip speed = 10 m/s, media charge = 65%, media type = CZS

VXP10 mill														
	Density (kg/L)	Flowrate (L/min)	Speed (rpm)	Current (A)	Power (kW)	Torque (NM)	Temp out (°C)	Temp in(°C)	% solids w/w	Dry (t/h)	kWh/t	Cum kWh/t	P_{80} (µm)	F_{80} (µm)
Pass 1	1.32	8.31	1500	9.9	3.3	17.3	33.1	29.4	38	0.25	13.06	13.06	35.1	
Pass 2	1.33	8.57	1500	9.9	3.3	17.6	35.9	32.4	38	0.26	12.72	25.78	23.8	
Pass 3	1.33	8.73	1500	9.9	3.2	16.9	37.9	34.3	38	0.27	12.03	37.81	19.1	
Pass 4	1.34	8.81	1500	9.8	3.2	16.9	39.4	35.6	38	0.27	11.91	49.72	15.4	119
VXP2500 mill														
	Density (kg/L)	Flowrate (L/min)	Speed (rpm)	Current (A)	Power (kW)	Torque (NM)	Temp out (°C)	Temp in(°C)	% solids w/w	Dry (t/h)	kWh/t	Cum kWh/t	P_{80} (µm)	F_{80} (µm)
05th Oct, test 3	1.33	1250.0	215	420	285	12500	31	29	38	37.9	7.5	7.5	29.3	54.2
9th Oct, test 1	1.32	1333.3	215	392	272	12100	28.8	26.1	38	40.1	6.8	6.8	29.6	54.5
19th Oct, test 3	1.35	1250.0	208	434	289	13244	32.9	29.8	38	38.5	7.5	7.5	41.3	106
25th Oct, test 3	1.3	1250.0	208	430	289	13269	28.8	25.8	36	35.1	8.2	8.2	32.24	81.2